IIR modeling of acoustic impulse responses

Derksen, J.P.A.M.

Award date:
1996

TECHNISCHE UNIVERSITEIT EINDHOVEN

FACULTEIT ELEKTROTECHNIEK

LEERSTOEL Signaalverwerking

SIGNAL PROCESSING

IIR modeling of acoustic impulse responses

by

J.P.A.M. Derksen

ESP-18-96

Verslag van een afstudeeronderzoek,
verricht in de vakgroep ESES/ESP, onder
leiding van ir. H.J.W. Belt en
dr.ir. A.C. den Brinker,
in de periode oktober 1995 - oktober 1996.

Eindhoven, 17 oktober 1996.

Abstract

Echo cancellation in hands-free communication has been a widely investigated problem. Rooms in general, have impulse responses of several of thousands samples unequal to zero, when sampled at 8 [kHz]. A FIR (Finite Impulse Response) model of a room would lead to thousands of parameters that would have to be adapted within the sample time when the conditions in a room change (persons walking around etc.)

This report aims to model the room impulse response with an IIR (Infinite Impulse Response) filter bank. One might expect IIR filter banks to approach the physical problem better than FIR filter banks. A special realization of a IIR filter bank, the Kautz filter bank is chosen for this purpose.

The complexity of the problem is researched with the aid of a physical model and the Gabor transform. Several modeling methods are investigated to test their suitability to model these room impulse responses. Also, to the problem dedicated methods have been tested on their performance.

From the investigated method, the Prony method shows the best results. 844 poles were found with a suppression of 14 [dB] (without considering the adaptation process). This in contrast to the FIR, which needed 1200 coefficients.

Acknowledgments

During a year I completed my thesis work in the Signal Processing group of the Department of Electrical Engineering, Eindhoven University of Technology. In this year I have been involved in several different activities. These activities have, especially in the beginning of this year, put a strain on my thesis work. Therefore, first of all, I would like to express my gratitude to my coach, Harm Belt for his patience and conscientious explanations during my thesis work. These explanations helped me to get insight in many aspects of the problem. In addition I would like to thank Bert den Brinker, for correcting and reviewing this report.

During this investigation use has been made of measurements carried out at Philips Research Laboratories, Eindhoven the Netherlands. I would like to express my gratitude to Ing. C.P. Janse for placing these measurements at my disposal.

Furthermore, I like to thank, my parents for their support, my friends and inmates for their companionship and support. Also I like to thank all active members of the IEEE Student Branch Eindhoven, making my board year, but most of all, my thesis work a success.

Sjaak Derksen

Contents

1. Introduction

During several years a lot of research effort has been put into hand free telephoning, teleconferencing and other applications involving communication systems with a microphone and a loudspeaker present in the same room. The old solution, a microphone and loudspeaker acoustically divorced does not longer meet the expectations of modern telecommunication systems.

The general situation for a hand free communication system is sketched in Figure 1-1. In general, a speech signal enters microphone $M1$. This speech signal enters, after passing the channel, via the loudspeaker $L2$ room 2. The same speech signal is then filtered by the transfer characteristics of room 2. The transfer functions concerning the microphones and the loudspeakers are omitted for convenience. The signal is registered by microphone $M2$. After passing a channel again, the signal again reaches room 1 via loudspeaker $L1$.

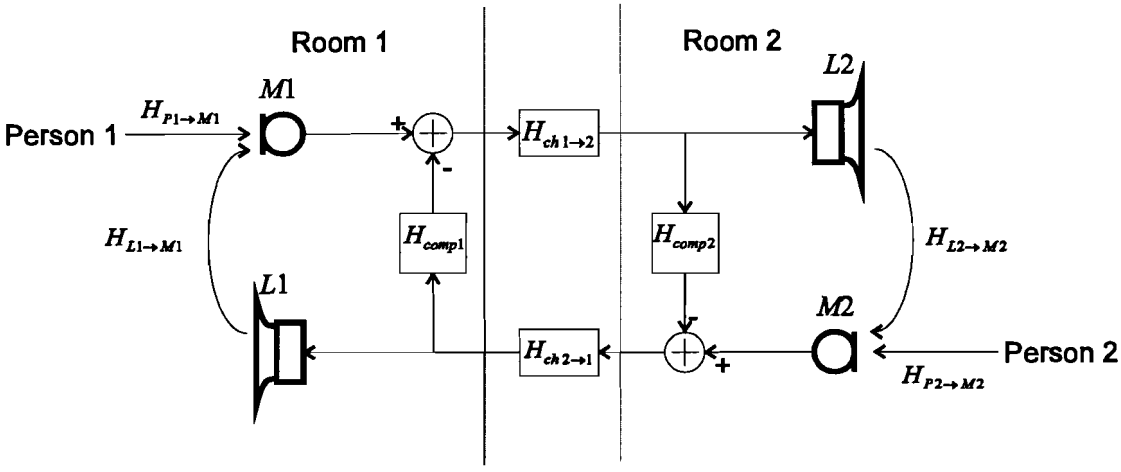

Figure 1-1: *General setup for hand free telecommunication systems*

This has two consequences. Due to the presence of amplifiers in this system, it is possible that the amplification through the whole signal path is greater than one, resulting in the well-known whistling noise. The other annoying property of such a system is the fact that the speaker (in this case Person 1) hears himself with a slight delay. This complicates communication in a severe way.

To avoid these effects, two filters are included in the communication system, one at each side of the system. These filters 'try' to imitate the transfer functions. H_{comp1} 'tries' to approximate $H_{L1\to M1}$ and H_{comp2} 'tries' to approximate $H_{L2\to M2}$. Hence these filters are called compensators. In fact, these compensators are in the most ideal situation, an electric replica of an acoustic system, the room.

$H_{L1\to M1}$ and $H_{L2\to M2}$ are called Room Transfer Functions (RTF's). The RTF is the Fourier transform of the room impulse response. A complete system of loudspeaker,

room and microphone in this configuration is called a LEMS (Loudspeaker Enclosure Microphone System).

Figure 1-2 sketches the situation on one side of the communication system, with nobody speaking in the microphone.

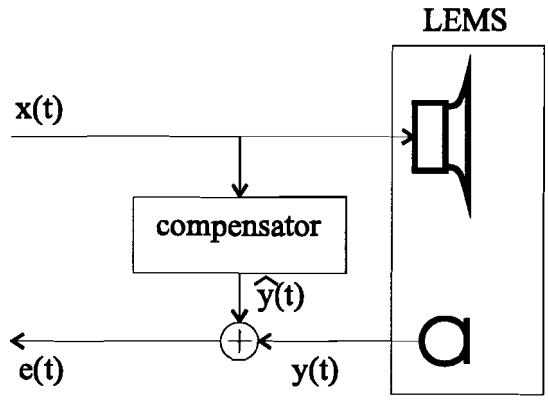

Figure 1-2: *One side of the communication system*

The LEMS also incorporates a person walking around in the room, and for example, other, more slow processes, like temperature variations. These processes in general alter the RTF. The compensator must be able to track these alterations in the RTF, and must therefore be adaptive.

There is a strong relation between the reverberation time of the room and the length of the acoustic impulse response of a room. The reverberation time, the time it takes for an acoustic impulse response to reach a level of -60 [dB] beneath the initial level, may very well be 0.4 [s] long. The signals involved, speech signals, typically sampled at 8 [kHz], forces us to model the impulse response of the room with several thousands samples.

There are other options to solve the above problem, but all involve deficiencies like:
- a studio environment is required
- only half duplex communication is provided
- the speech signal is distorted
- the attenuation between loudspeaker and microphone is insufficient

(see [1]). Therefore, this report concentrates on the alternative, finding an electric model.

[1] And [2] report on several algorithms for the adaptation of the weights in the case of FIR filter banks. However, alternatives for this FIR (Finite Impulse Response) filter bank are not considered in [1] and [2].

[3] Develops a simple acoustic model of a room, and a person walking around in this room (modeled by a sphere). With the aid of acoustic field theory, based on a ray model and stochastic approach, the acoustic pressure $p_{scatt}(t_0, x_0)$ due to the movement of the sphere, at the location of the microphone can be derived. The same can be done for moving the sphere with a speed v to a new location x_0+x' in a time t'.

This expression can be used to find an expression for the autocorrelation function $E\{p_{scatt}(t_0,t_0)p_{scatt}(t_0,t_0+t')\}$. The authors use this expression to evaluate a LMS algorithm. They conclude that the basic LMS algorithm is not capable to track the nonstationarities caused by a person walking at normal speed through a living room if the bandwidth of the system is that of speech or larger, and if the length of the filter is so large that the error due to the nonstationarities is greater than the error due to the finite length of the adaptive filter.

[4] Also reports on other methods for adapting the filter coefficients than the already mentioned (inadequate) LMS algorithm. Examples are :

- NLMS algorithm, which improves the speed of convergence by appointing individual step sizes for the coefficient updates;
- frequency domain algorithms;
- subband methods;
- block LMS structures;
- conjugate gradients algorithms;
- and RLS algorithms.

Perhaps a wrong point of departure is chosen for the modeling of the RTF. The idea of using a tapped-delay line in modeling the problem, arises from the well-known properties of such a filter. Faster adaptation algorithms [4] can be used to bypass the inability of the LMS algorithm to track the highly non-stationary RTF. These kind of solutions do however pass the more fundamental problem if the tapped-delay line is the appropriate model for a RTF. Therefore, faster algorithms are not treated in this report.

In [8] the authors point out by raising the question: "*Does it make any physical sense to fit a pole-zero model to the phenomenon underlying the echo?*" that the properties of a tapped-delay line (FIR filter bank) as model, do not stem from any physical background related to the problem. They suggest an ARMA (Auto Regressive Moving Average) model for the RTF. Such an ARMA model is based on a pole-zero model, instead of an all-zero model and has an impulse response of infinite length. These models can bear a better relation with reality, because damped oscillations do resemble the modes (eigenvibrations) in a room.

The authors of [8] use balanced model reduction to find an ARMA model from a FIR model. The results of their research are encouraging, and hence, they conclude that IIR (Infinite Impulse Response) adaptive filtering must be considered a possible alternative to FIR adaptive filtering for the acoustic cancellation problem.

[6] And [7] tested two criteria for performing system identification in order to find and ARMA model: OE (Output Error) and EE (Equation Error). The EE model structure used was an ARX (Auto Regressive with Exogenous input) structure. The authors concluded that no substantial reduction in coefficients, compared to the MA (Moving Average) FIR model can be made.

[5] Reports a similar finding. The author justifies in first instance the choice for a RF (Recursive Filter) by the fact, every single maximum in the RTF can be simulated by a

general second-order recursive section. One example of a measured RTF is plotted in Figure 1-3.

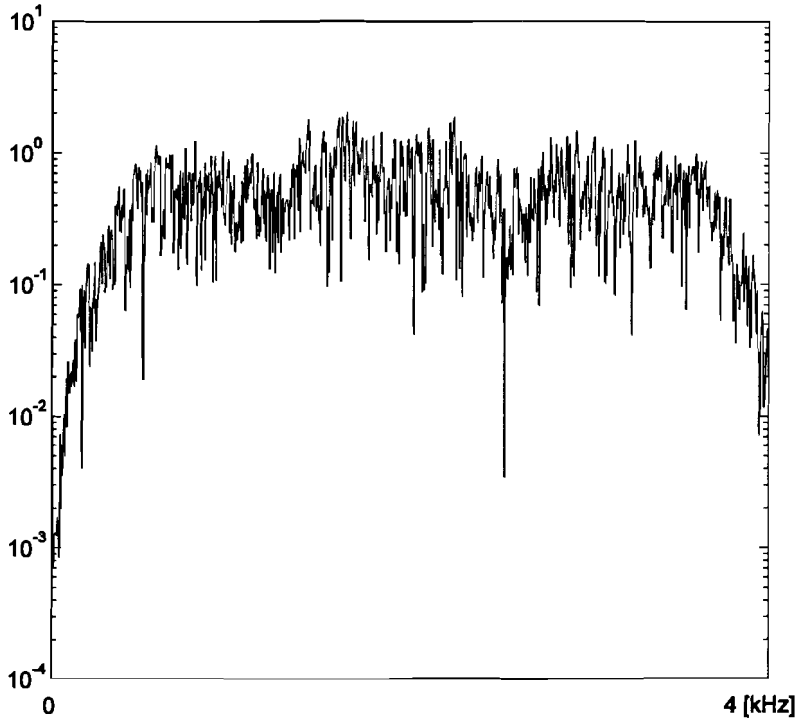

Figure 1-3: *The RTF of a LEMS*

The author found in his measurements around 80 maxima, leading to 4x80=320 free parameters (a second order recursive filter section has four free parameters). This yields a coefficient reduction of 3 to7.

The author used a transversal recursive filter, a tapped-delay line with at some equidistant taps recursive sections. The result is added and forms the filter output. The best results were achieved with 64 recursive sections placed at each 2 taps in a 128 taps long tapped-delay line. The result was comparable to a 200 taps tapped-delay line. From this result the author concluded that nothing was gained, and the tapped-delay line seemed the appropriate choice as filter structure.

Judging on [1] to [8], there is a lot of disagreement if, and how the acoustic echo cancellation problem can be solved satisfactorily. In the time, other new filter structures have evolved based on Kautz functions [9,15]. These filters combine a lot of the nice properties of the tapped-delay line, such as energy conservation along the bank, and orthonormality of the filter outputs, however, the main advantage is the IIR of the Kautz filter. When the poles in the model are kept at a fixed location, the Kautz filter bank enables the use of many of the algorithms previously used in combination with the tapped-delay line. Examples are LMS, RWLS (Recursive Weight Least Square) and NLMS.

The goal of this report is to investigate if Kautz filter banks are applicable in finding a solution for the acoustic echo cancellation problem. In order to do so, it is first necessary to research the complexity of the problem. This research, gives an

impression of the number of free parameters involved by evaluating a simple acoustical model. This is also done with some measurements (impulse responses) of the room. This is carried out in Chapter 2.

In Chapter 3 several methods are investigated to find an ARMA model. These methods can be roughly divided in classical methods like Prony, Steiglitz McBride and an iterative Prony method at one side, and at the other side some methods more dedicated to the problem of modeling the RTF. In this chapter a selection from this modeling methods is made based on partly a synthetic model and the real acoustic impulse responses.

Chapter 4 gives a short description of the Kautz filter bank and its properties.

Chapter 5 discusses the results of applying the selected method to the measured impulse responses. The model is reduced to one of a lower order.

Chapter 6 finally discusses the results.

The data in this report are impulse responses measured at Philips Research Laboratories. Appendix 1 describes under which conditions and how they were measured.

2. Investigating the complexity

2.1 Introduction

There are numerous ways to get an idea of the complexity of the acoustic echo cancellation problem. Some of these ways will be discussed in the next paragraphs,

The problem can be viewed upon as a physical problem. Information present in advance such as physical dimensions, building materials used and decoration and furniture in the room can be used to develop a model. These models are in general very complex. This is shown in the next paragraph, where a model is developed solely based on the room dimensions. Such a 'white box' model cannot be used as an 'electronic model' as in Figure 1-2, to actually suppress the echo, due to it's complexity. The physical model is used to show how many acoustic modes are present in the available bandwidth and how they are distributed along the available bandwidth.

The next strategy is using a Gabor transform to investigate how the signal is distributed in time and frequency. The Gabor transform does have a certain relationship with the 'degrees of freedom' [15] in the model that is searched. How these 'degrees of freedom' map on the model parameters is not investigated, the Gabor transform is only used to make an estimate of the amount of 'degrees of freedom'. Furthermore it can be used as a tool to demonstrate how many time samples certain frequencies in a room impulse response play a role.

To conclude this chapter, a method known from control engineering is used to make an estimate of the amount of parameters in an IIR model. This method is based on the 'black box' assumption. No a-priori knowledge of the system (room) is used. Another similar method on can be found in [14].

2.2 The link to acoustic field theory

IIR models offer, in contrast with FIR models, the possibility to capture some of the 'true' system dynamics of a plant, process or other physical phenomenon. Many authors [5,6,7,8] suggest that there is a possible relation between denominator polynomial in this model and modes (eigenvibrations) in a room. To investigate this for a FIR filter bank, the authors of [3] develop a statistical model and calculate the effect of a person moving through this room on the autocorrelation function of the pressure present at the microphone.

When movement is not taken into consideration it is possible to derive a simple acoustical model. In this model an expression is derived for the sound wave velocity

potential in a rectangular cavity (model for the room). From this quantity, the sound wave velocity and the local pressure as function of time and space coordinates can be derived.

The purpose of this simple model is twofold. The first goal is investigating how many parameters are involved in the modeling of a room transfer function. In order to do so, first the linear wave equation for acoustic airborne waves in a fluid (gas or liquid) is derived. Several neglects are made during this derivation in order to end up with a linear differential equation. This derivation can also be found in [11,12,13]. Secondly a simple room model is developed to investigate how many modes this simple model yields, and how their corresponding frequencies are distributed along the available bandwidth.

The second goal is to show that there is a relation between linear systems and the acoustical problem. There is shown that acoustical systems can be dealt with as linear, but time varying systems. This justifies the use of a linear model.

2.2.1 The acoustic linear wave equation

The Navier-Stokes equation

The first equation to investigate is the Navier-Stokes equation of motion given by:

$$\rho \frac{d}{dt}\underline{\mathbf{U}} = -\underline{\nabla}P + \rho\,\underline{\mathbf{g}} + (\mu_v + \frac{4}{3}\mu)\underline{\nabla}(\underline{\nabla}\cdot\underline{\mathbf{U}}) - \mu\underline{\nabla}\times(\underline{\nabla}\times\underline{\mathbf{U}}) \qquad (2\text{-}1)$$

ρ Fluid density $\left[kg\cdot m^{-3}\right]$
$\underline{\mathbf{U}}$ Velocity vector $\left[m\cdot s^{-1}\right]$
P Pressure $\left[Pa = kg\cdot m^{-1}\cdot s^{-2}\right]$
$\underline{\mathbf{g}}$ Gravitional acceleration vector $\left[m\cdot s^{-2}\right]$
μ Bulk Viscosity for Newtonian Fluids $\left[kg\cdot m^{-1}\cdot s^{-1}\right]$
μ_v Sheer Viscosity for Newtonian Fluids $\left[kg\cdot m^{-1}\cdot s^{-1}\right]$
$\underline{\nabla}$ Laplacian operator $\Rightarrow \underline{\nabla} = \frac{\partial}{\partial x}\hat{x} + \frac{\partial}{\partial x}\hat{y} + \frac{\partial}{\partial x}\hat{z}$ $\left[m^{-1}\right]$

This expression can be derived by taking an infinitesimal volume element of fluid and by taking in account the forces excited on this volume element. This volume element resists being compressed and tries to return to it's original state, just like a spring does when pulled.

Looking at this equation one can immediately see that an acoustic wave is a three dimensional wave. The first part of the equation which is usual neglected are both viscosity's parameters. Air is a fluid with a small viscose behavior when it is

compared for example with water. This neglect is valid for an airborne sound wave but not in the neighborhood of walls (see for example [10] IV.6).

Furthermore the vector U can be separated uniquely into two parts, a longitudinal or irrotational part $\mathbf{U_L}$ and a transverse or rotational part $\mathbf{U_T}$. Fluid motion due to acoustic waves is per definition a longitudinal wave. This means that the transverse part is usually neglected. However air circulation due to room heating can influence this transverse part. In [13] is noticed that in case of sea water the fluid motion due to internal waves is transverse. This can also be said of air circulation due to central heating. If this is not taking into account the Navier-Stokes equation of motion can be simplified to(2-2), which is better known as Euler's equation of motion.

$$\underline{\mathbf{U}} = \underline{\mathbf{U}_T} + \underline{\mathbf{U}_L}, \quad \underline{\mathbf{U}_T} = 0$$
$$\underline{\nabla} \times \underline{\mathbf{U}_L} = 0, \quad \underline{\nabla} \cdot \underline{\mathbf{U}_T} = 0$$
$$\rho \frac{d}{dt}\underline{\mathbf{U}} = -\nabla P + \rho\, \underline{\mathbf{g}} = (\mu_v + \frac{4}{3}\mu)\nabla^2 \underline{\mathbf{U}}$$

With $\nabla^2 = \frac{\partial^2}{\partial x^2} + \frac{\partial^2}{\partial y^2} + \frac{\partial^2}{\partial z^2}$ and $\mu_v = \mu = 0$, Euler's equation of motion is now given by:

$$\rho \frac{\partial}{\partial t}\underline{\mathbf{U}} = -\underline{\nabla} P + \rho \underline{\mathbf{g}} \tag{2-2}$$

The equation of continuity

The next equation of importance is the equation of continuity, better known as the equation of conservation of mass.

$$\frac{\partial}{\partial t}\rho\, dV + \underline{\nabla} \cdot (\rho\, \underline{\mathbf{U}})\, dV = \rho\, Q\, dV \tag{2-3}$$

This equation can again be derived from taking an infinitesimal volume element *dV*. An acoustic wave is by means of compressing and expanding the fluid adding fluid to or respectively extracting fluid from the volume element *dV*.

The term $\frac{\partial}{\partial t}\rho$ reflects the, with time increasing density in the volume element *dV* due to the influx $-\underline{\nabla} \cdot (\rho\, \underline{\mathbf{U}})\, dV$. *Q* is the volume flow rate per unit volume of fluid due to the sound source. Equation (2-3) can be simplified to:

$$\frac{\partial}{\partial t}\rho + \underline{\nabla} \cdot (\rho\, \underline{\mathbf{U}}) = \rho\, Q \tag{2-4}$$

The linear wave equation

Starting from Euler's of motion (2-4) the linear wave equation can now be derived. The velocity of the fluid can be expressed as an ambient fluid velocity $\underline{\mathbf{u}}_0$, which in this case is assumed zero, and a change in this ambient fluid velocity $\underline{\mathbf{u}}$ due to the presence of a sound wave. This leads to:

$$\rho \frac{\partial}{\partial t}\underline{\mathbf{U}} = -\underline{\nabla} P + \rho\, \underline{\mathbf{g}}, \quad \underline{\mathbf{U}} = \underline{\mathbf{u}}_0 + \underline{\mathbf{u}}$$

$$\rho\left(\frac{\partial}{\partial t}\underline{\mathbf{u}} + (\underline{\mathbf{u}}\cdot\underline{\nabla})\underline{\mathbf{u}}\right) = -\underline{\nabla} P + \rho\, \underline{\mathbf{g}}_L$$

Furthermore the condensation s, which is the relative change in density of the fluid due to the presence of an acoustic wave is introduced. p_0 Is the ambient pressure, and p is the pressure due to the acoustic wave.

$$P = p_0 + p, \quad s = \frac{\rho - \rho_0}{\rho}$$

$$p \approx \frac{s}{\kappa_E} \tag{2-5}$$

p Is related to the condensation s by means of the adiabatic compressibility κ_E in the case of air (the entropy remains nearly a constant in the case of a passing sound wave). In this report only sound waves with a relatively small amplitude $s<<1$ are considered. With this knowledge first the equation of continuity can be simplified.

$$\frac{\partial}{\partial t}\rho = \rho_0 \frac{\partial}{\partial t}$$

$$\underline{\nabla}\cdot(\rho\,\underline{\mathbf{u}}) = \underline{\mathbf{u}}\cdot\underline{\nabla}\,\rho + \rho\,\underline{\nabla}\cdot\underline{\mathbf{u}} = \underline{\mathbf{u}}\cdot\underline{\nabla}\left[\rho_0(s+1)\right] + \rho_0(s+1)\underline{\nabla}\cdot\underline{\mathbf{u}} \approx \underline{\mathbf{u}}\cdot\underline{\nabla}\,\rho_0 + \rho_0\underline{\nabla}\cdot\underline{\mathbf{u}}$$

$$\rho\, Q = \rho_0(s+1)Q \approx \rho_0 Q$$

Leading to:

$$\frac{\partial}{\partial t}s + \frac{\nabla\rho_0}{\rho_0}\cdot\underline{\mathbf{u}} + \nabla\cdot\underline{\mathbf{u}} = Q \tag{2-6}$$

The speed of sound is given by the following equation:

$$c = \sqrt{\frac{1}{\kappa_E \rho_0}} = \sqrt{\frac{p_0}{\rho_0}} \tag{2-7}$$

With the aid of the expression derived for the pressure (2-5) the following expression can be derived for the pressure p:

$$c^{2} = \frac{1}{\kappa_E \rho_0} \approx \frac{p}{s\rho_0}$$

$$p \approx \rho_0 s c^2 \tag{2-8}$$

Taking the gradient of (2-8) the following can be derived:

$$\underline{\nabla} p \approx 2\rho_0 s c \underline{\nabla} c + c^2 \underline{\nabla}\left(\rho_0 s\right)$$

This can be substituted in (2-2), Euler's equation of motion leading to:

$$\rho_0 \frac{\partial}{\partial t}\underline{\mathbf{u}} \approx -2\rho_0 s c \underline{\nabla} c - c^2 \underline{\nabla}\left(\rho_0 s\right) + \rho_0 \underline{\mathbf{g}_L} s$$

Differentiating on both sides with respect to *t*:

$$\rho_0 \frac{\partial^2}{\partial t^2}\underline{\mathbf{u}} \approx -2\rho_0 \frac{\partial s}{\partial t} c \underline{\nabla} c - c^2 \underline{\nabla}\left(\rho_0 \frac{\partial s}{\partial t}\right) + \rho_0 \underline{\mathbf{g}_L} \frac{\partial s}{\partial t}$$

$$\underline{\nabla}\left(\rho_0 \frac{\partial s}{\partial t}\right) = \rho_0 \underline{\nabla} \frac{\partial s}{\partial t} + \frac{\partial s}{\partial t} \underline{\nabla} \rho_0$$

$$\Rightarrow \frac{1}{c^2} \frac{\partial^2}{\partial t^2}\underline{\mathbf{u}} \approx \left(-2\frac{\underline{\nabla} c}{c} - \frac{\underline{\nabla}\rho_0}{\rho_0} + \frac{\underline{\mathbf{g}_L}}{c^2}\right)\frac{\partial s}{\partial t} - \underline{\nabla}\frac{\partial s}{\partial t}$$

In case of homogenous fluids like air in a room, c and ρ_0 are constants. Due to this, the two vectors $\frac{\underline{\nabla} c}{c}$ and $\frac{\underline{\nabla}\rho_0}{\rho_0}$ reduce to zero vectors.

The assumption of air being homogenous, is not completely correct. People present in a room, breathe and smoke, and hereby alter the homogenous distribution of the air. However, if the fluid is assumed to be homogenous and the vectors $\frac{\underline{\nabla} c}{c}$ and $\frac{\underline{\nabla}\rho_0}{\rho_0}$ are neglected, the following equation is obtained:

$$\frac{1}{c^2} \frac{\partial^2}{\partial t^2}\underline{\mathbf{u}} \approx \frac{\underline{\mathbf{g}_L}}{c^2} \frac{\partial s}{\partial t} + \underline{\nabla}\frac{\partial s}{\partial t} \tag{2-9}$$

The velocity of sound in air of 293 [K] is 343 [ms^{-1}].

$$\frac{\left|\underline{\mathbf{g}_L}\right|}{c^2} \approx 88.9 \cdot 10^{-6}$$

Let's assume that the wave equation is linear (this will be proven later on), with $\underline{\mathbf{k}}$ the propagation vector and $\underline{\mathbf{r}}$ the position vector:

$$s = \exp(-j\underline{\mathbf{k}}\cdot\underline{\mathbf{r}})\exp(j2\pi f t)$$

The following quantities can then be derived:

$$\left|\frac{\partial s}{\partial t}\right| = kc$$

$$\left|\underline{\nabla}\frac{\partial s}{\partial t}\right| = kc^2$$

With $|\underline{\mathbf{k}}| = \frac{2\pi f}{c}$ is the wave number with units of radians per meter (see 2-15 and 2-16).

Table 2-1 *Approximate values of the terms involving the condensation s in (2-9) several representative frequencies in the case of air.*

f [Hz]	$\lvert\underline{\mathbf{k}}\rvert$	$\frac{\lvert\underline{\mathbf{g}}_L\rvert}{\rho_0}\left\lvert\frac{\partial s}{\partial t}\right\rvert$	$\left\lvert\underline{\nabla}\frac{\partial s}{\partial t}\right\rvert$
1	0.0183183	$558.6*10^{-6}$	$2155*10^{0}$
50	0.9159162	$27.93*10^{-3}$	$107.8*10^{3}$
250	4.5795811	$139.6*10^{-3}$	$538.9*10^{3}$
1000	18.318325	$558.6*10^{-3}$	$2.155*10^{6}$
2500	45.795811	$1.396*10^{0}$	$5.388*10^{6}$
5000	91.591623	$2.792*10^{0}$	$10.78*10^{6}$

As can be seen from Table 2-1, the term $\left|\underline{\nabla}\frac{\partial s}{\partial t}\right| >> \frac{|\underline{\mathbf{g}}_L|}{\rho_0}\left|\frac{\partial s}{\partial t}\right|$. Therefore(2-9) can be reduced to:

$$\frac{1}{c^2}\frac{\partial^2}{\partial t^2}\underline{\mathbf{u}} \approx -\underline{\nabla}\frac{\partial s}{\partial t} \qquad (2\text{-}10)$$

The velocity vector $\underline{\mathbf{u}}$ can be expressed in terms of a velocity potential φ by means of the relation:

$$\underline{\mathbf{u}} = \underline{\nabla}\varphi\,(t,\underline{\mathbf{r}}) \qquad (2\text{-}11)$$

It is further possible to find a similar expression for the pressure. In general, the pressure is viewed as the 'effort' variable, and the propagation speed and direction is considered the 'flow' variable. It is also possible to define an characteristic impedance, reflection and transmission coefficients similar like the behavior of electromagnetic waves upon entering a different medium. To be complete, the expression for the pressure is given by:

$$p(t,\underline{\mathbf{r}}) \approx \rho_0(\underline{\mathbf{r}})\frac{\partial}{\partial t}\varphi\,(t,\underline{\mathbf{r}}) \tag{2-12}$$

For more details see [13]. Substituting (2-6) in (2-10), and using (2-11) leads to the following:

$$\frac{1}{c^2}\frac{\partial^2}{\partial t^2}\underline{\mathbf{u}} \approx -\underline{\nabla}\left[Q - \frac{\underline{\nabla}\rho_0}{\rho_0}\cdot\underline{\mathbf{u}} - \underline{\nabla}\cdot\underline{\mathbf{u}}\right]$$

$$\underline{\nabla}(\underline{\nabla}\cdot\underline{\mathbf{u}}) + \underline{\nabla}\left(\frac{\underline{\nabla}\rho_0}{\rho_0}\cdot\underline{\mathbf{u}}\right) - \frac{1}{c^2}\frac{\partial^2}{\partial t^2}\underline{\mathbf{u}} \approx \underline{\nabla}Q$$

$$\underline{\nabla}(\nabla^2\varphi) + \underline{\nabla}\left(\frac{\underline{\nabla}\rho_0}{\rho_0}\cdot\underline{\nabla}\varphi\right) - \frac{1}{c^2}\frac{\partial^2}{\partial t^2}\underline{\nabla}\varphi \approx \underline{\nabla}Q$$

$$\underline{\nabla}\left(\nabla^2\varphi + \frac{\underline{\nabla}\rho_0}{\rho_0}\cdot\underline{\nabla}\varphi - \frac{1}{c^2}\frac{\partial^2}{\partial t^2}\varphi\right) \approx \underline{\nabla}Q$$

Assuming the air is homogenous in a room, the term $\frac{\underline{\nabla}\rho_0}{\rho_0}$ can again be set equal the zero vector. This results in the following equation:

$$\nabla^2\varphi\,(t,\underline{\mathbf{r}}) - \frac{1}{c\,(\underline{\mathbf{r}})^2}\frac{\partial^2}{\partial t^2}\varphi\,(t,\underline{\mathbf{r}}) \approx Q(t,\underline{\mathbf{r}})$$

Take $x_M(t,\underline{\mathbf{r}}) = Q(t,\underline{\mathbf{r}})$ [s^{-1}], the acoustic source to the fluid medium. The linear wave equation for acoustic signals is now given by:

$$\nabla^2\varphi\,(t,\underline{\mathbf{r}}) - \frac{1}{c\,(\underline{\mathbf{r}})^2}\frac{\partial^2}{\partial t^2}\varphi\,(t,\underline{\mathbf{r}}) \approx x_M(t,\underline{\mathbf{r}}) \tag{2-13}$$

2.2.2 The solution of the homogenous linear wave equation

The solution of the homogenous ($x_M(t,\underline{\mathbf{r}}) = 0$) linear wave equation in a rectangular coordinate system can be derived by means of separation of variables. But first it is assumed that the velocity potential $\varphi\,(t,\underline{\mathbf{r}})$, $\underline{\mathbf{r}} = x\underline{\hat{\mathbf{x}}} + y\underline{\hat{\mathbf{y}}} + z\underline{\hat{\mathbf{z}}}$, can be separated in a time dependent part and a place dependent part.

$$\varphi\,(t,\underline{\mathbf{r}}) = \varphi_f\,(\underline{\mathbf{r}})\exp(j2\pi f\,t)$$

When this is substituted in the time-dependent wave (2-13), this yields:

$$\nabla^2\varphi_f\,(\underline{\mathbf{r}}) - k^2\varphi_f\,(\underline{\mathbf{r}}) = 0$$

which is known as the time-independent Helmholtz equation. The solution of this equation can be found by separation of variables:

$$\varphi_f(x,y,z) = \left[A_x e^{-jk_x x} + B_x e^{jk_x x}\right]\left[A_y e^{-jk_y y} + B_y e^{jk_y y}\right]\left[A_z e^{-jk_z z} + B_z e^{jk_z z}\right] \quad (2\text{-}14)$$

$$\underline{\mathbf{k}} = k_x \underline{\hat{\mathbf{x}}} + k_y \underline{\hat{\mathbf{y}}} + k_z \underline{\hat{\mathbf{z}}} \quad (2\text{-}15)$$

$$|\underline{\mathbf{k}}| = k = \sqrt{k_x^2 + k_y^2 + k_z^2} \quad (2\text{-}16)$$

The factors A_i correspond with waves traveling in the positive direction and the factors B_i correspond with waves traveling in the negative direction. When the wave propagation is present in an unbounded medium, where no reflections are present the solution of the Helmholtz equation can also be written as:

$$\varphi_f(\underline{\mathbf{r}}) = A\exp(-j\underline{\mathbf{k}}\cdot\underline{\mathbf{r}})$$

where

$$A = A_x A_y A_z$$

making the total solution:

$$\varphi_f(t,\underline{\mathbf{r}}) = A\exp(-j\underline{\mathbf{k}}\cdot\underline{\mathbf{r}})\exp(+j2\pi f\, t)$$

2.2.3 The rectangular cavity as room model

In first approximation a room can be modeled as a rectangular cavity with ideal rigid boundaries as pictured in Figure 2-1. This is however a very crude approximation. A rectangular cavity is in general not a good approximation for a room, but it can be used as an 'building block' to make better approximations. In this particular case it is used to demonstrate the large amount of 'mathematical degrees of freedom' which a simple model leads to.

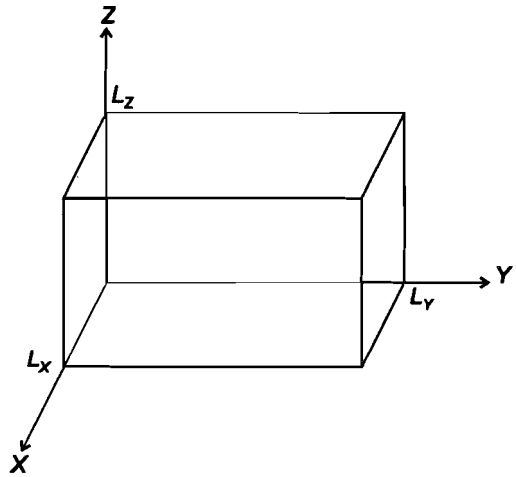

Figure 2-1: *Rectangular cavity*

Also the assumption that all the materials are (acoustically) rigid is a very crude assumption. A wide range of materials are used, like bricks, plaster work, curtains, windows etc. Some materials have some 'nasty' resonating properties. Examples are windows and wall panels. These materials do not only reflect sound waves local on the place where the sound wave is incident, but also global. The vibrations travel over the whole surface of for example a window and set air in motion over the whole surface of the window. Other materials have a rough surface, which diffracts the sound waves in various directions. In general, rooms do have furniture and other objects which scatter sound waves.

Now lets start again with the solution of the linear wave equation:

$$\varphi_f(x,y,z) = X(x)Y(y)Z(z)$$
$$X(x) = A_x e^{-jk_x x} + B_x e^{jk_x x}$$
$$Y(y) = A_y e^{-jk_y y} + B_y e^{jk_y y}$$
$$Z(z) = A_z e^{-jk_z z} + B_z e^{jk_z z}$$

$$\varphi(t,\underline{\mathbf{r}}) = \varphi_f(\underline{\mathbf{r}})\exp(+2\pi f t)$$
$$u_{f,n}(\underline{\mathbf{r}}) = \hat{\underline{\mathbf{n}}}\cdot\underline{\nabla}\varphi_f(\underline{\mathbf{r}})\exp(+j2\pi f t)$$

With $\hat{\underline{\mathbf{n}}}$ is the unit normal vector perpendicular to the boundary surfaces, pointing outward on every boundary surface.

$$u_{f,n}(x,y,z) = \hat{\underline{\mathbf{n}}}\cdot\left[Y(y)Z(z)\frac{d}{dx}X(x)\hat{\underline{\mathbf{x}}} + X(x)Z(z)\frac{d}{dy}Y(y)\hat{\underline{\mathbf{y}}} + X(x)Y(y)\frac{d}{dz}Z(z)\hat{\underline{\mathbf{z}}}\right] \tag{2-17}$$

The first boundary condition is at $x=0$, which corresponds to the YZ plane (Figure 2-1). The unit vector $\hat{\underline{\mathbf{n}}}$ points to the negative x direction: $\hat{\underline{\mathbf{n}}} = -\hat{\underline{\mathbf{x}}}$. With the use of this, and since the normal component of the acoustic fluid velocity vector must be equal to zero on a rigid boundary (2-17) reduces to:

$$u_{f,n}(0,y,z) = -Y(y)Z(z)\frac{d}{dx}X(x)\Big|_{x=0} = 0$$

Substituting the component for $X(x)$ in this equation leads to the following equation:

$$jk_x Y(y)Z(z)\left(A_x - B_x\right) = 0$$

and since this expression must hold for all allowed values of y and z at $x=0$,

$$B_x = A_x \tag{2-18}$$

At the other side, at L_X, of the cavity a similar derivation can be made. The normal vector here is pointing in the positive x-direction: $\underline{\hat{\mathbf{n}}} = \underline{\hat{\mathbf{x}}}$.

$$u_{f,n}(0,y,z) = -Y(y)Z(z)\frac{d}{dx}X(x)\Big|_{x=L_X} = 0$$

With the aid of the expression for $X(x)$ and (2-18) the following equations can be found:

$$2A_X k_X Y(y)Z(z)\sin(k_X L_X) = 0$$
$$\sin(k_X L_X) = 0$$
$$k_X L_X = l\pi, \qquad l = 0,1,2,.....$$

or:

$$k_x = \frac{l\pi}{L_x}, \qquad l = 0,1,2,.....$$

In order to satisfy the boundary conditions, the propagation component is only allowed at certain discrete values. Similar expressions can be found for k_Y and k_Z:

$$k_X = \frac{l\pi}{L_X}, \qquad l = 0,1,2,.....$$
$$k_Y = \frac{m\pi}{L_Y}, \qquad m = 0,1,2,.....$$
$$k_Z = \frac{n\pi}{L_Z}, \qquad n = 0,1,2,.....$$

Substituting these wave numbers and the amplitudes A_X, A_Y, A_Z, B_X, B_Y and B_Z back into the expression for the wave equation 2-14, the following expression can be found:

$$\varphi_{f,lmn}(x,y,z) = A_{lmn}\cos(\frac{l\pi}{L_X}x)\cos(\frac{l\pi}{L_Y}y)\cos(\frac{l\pi}{L_Z}z), \qquad l,m,n = 0,1,2,....$$
$$A_{lmn} = 8A_X A_Y A_Z$$

where the subscript *lmn* corresponds with the (l,m,n) eigenfunction or normal mode of the cavity. This solution is of the solutions of the homogenous solution for the time independent Helmholtz equation. The total solution is given by the summation of this solution over all values of (lmn).

$$\varphi_f(t,\mathbf{r}) = \sum_{l=0}^{\infty}\sum_{m=0}^{\infty}\sum_{n=0}^{\infty}\varphi_{f,lmn}(\mathbf{r})\exp(+2\pi f_{lmn}t)$$

$$\varphi(t,x,y,z) = \sum_{l=0}^{\infty}\sum_{m=0}^{\infty}\sum_{n=0}^{\infty}A_{lmn}\cos(\frac{l\pi}{L_X}x)\cos(\frac{l\pi}{L_Y}y)\cos(\frac{l\pi}{L_Z}z)\exp(+2\pi f_{lmn}t) \qquad (2\text{-}19)$$

With f_{lmn} equal to:

$$f = \frac{c}{2\pi}\sqrt{k_X^2 + k_Y^2 + k_Z^2}$$

$$f = f_{lmn} = \frac{c}{2}\sqrt{\left(\frac{l}{L_X}\right)^2 + \left(\frac{m}{L_Y}\right)^2 + \left(\frac{n}{L_Z}\right)^2}$$

This is the solution for the homogenous case.

The amount of eigenvibrations (modes) and the distribution of the modes present in a room, can be demonstrated in a small calculation example, take for example the measurements of the room which is used in this report. f_{max}=4 [kHz], L_X=7.80 [m], L_Y=3.60 [m], L_Z=3.45 [m] and c=343 [m/s] (at 293 °K);

$$f_{lmn} = \frac{c}{2}\sqrt{\left(\frac{l}{L_X}\right)^2 + \left(\frac{m}{L_Y}\right)^2 + \left(\frac{n}{L_Z}\right)^2} < f_{\max}$$

Each combination of *lmn* fulfilling this inequality is a candidate for an eigenvibration. It can be verified that 658,047 combinations of *lmn* fulfill this inequality. This simple calculation example shows how many modes are possible in the worst case. However, there always will be a smaller set of dominating modes. Therefore the set of necessary modes can perhaps be smaller in practice.

The result can be plotted in a figure. This can for obvious reasons not be done for all 658.047 combinations. In order to demonstrate the distribution of the modes over the frequency range 0 - 4000 [Hz], the original 658.047 combinations can decimated by sorting the modes in ascending order, taking the median value over sets of 6000 modes and plotting them in Figure 2-2.

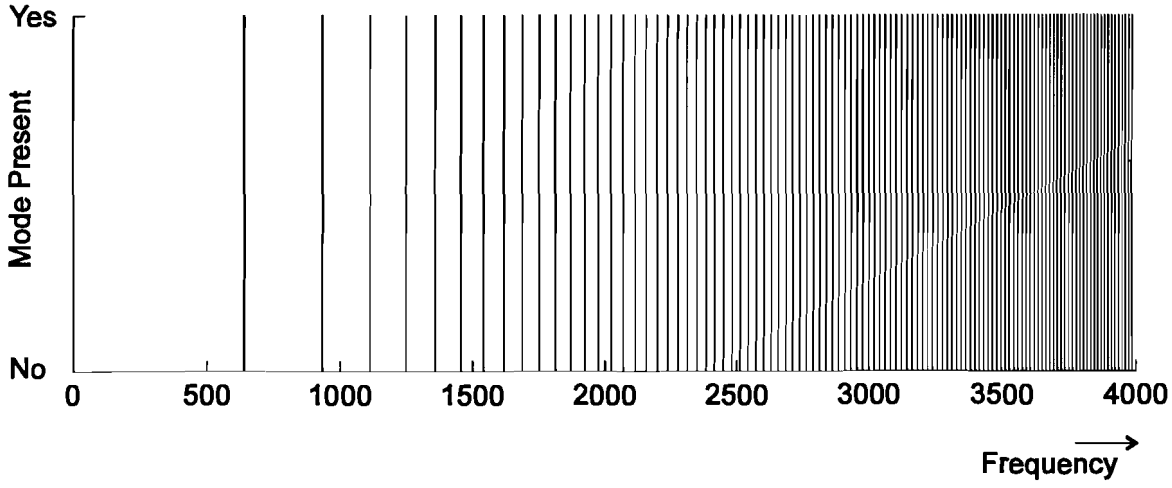

Figure 2-2: *Decimated modes present in the measurement room*

From Figure 2-2 can be concluded that the modes become more dense, when the frequencies are higher. In reality, the walls could absorb these higher modes more than

the lower modes. However, the effect is so clearly present that after modeling the room transfer function, a similar effect should found and even dominate the model.

In real cases however a loudspeaker (source) is present, which forces sound waves into the cavity. Assume a point source $\delta(\mathbf{r}-\mathbf{r}_0)$ is taken as a source. When neglecting the time dependent part, this gives rise to the following expression [13]:

$$\varphi_f(\mathbf{r}) = \int_{V_0} x_{f,M}(\mathbf{r}_0)\, g_f\left(\mathbf{r}\middle|\mathbf{r}_0\right) dV_0 - \oint_{S_0}\left[g_f\left(\underline{\mathbf{r}}\middle|\underline{\mathbf{r}_0}\right)\frac{\partial}{\partial n_0}\varphi_f(\underline{\mathbf{r}_0}) - \varphi_f(\underline{\mathbf{r}_0})\frac{\partial}{\partial n_0} g_f\left(\underline{\mathbf{r}}\middle|\underline{\mathbf{r}_0}\right)\frac{\partial}{\partial n_0}\right] dS_0$$

The function g is a Green function (see next paragraph). S_0 is the surface of the enclosed volume and n_0 is the normal vector pointing outwards on this surface. The first integral on the right hand side can be associated with the homogenous solution.

2.2.4 The description of an acoustical system with linear filter theory

A sound source can in first instance be modeled as a point source $\delta(\underline{\mathbf{r}}-\underline{\mathbf{r}_0})$. This is a omnidirectional unit-amplitude source, which is only present at $\underline{\mathbf{r}} = \underline{\mathbf{r}_0}$. The solution of the inhomogenous Helmholtz equation (2-13) with $X_M(\underline{\mathbf{r}}) = \delta(\underline{\mathbf{r}}-\underline{\mathbf{r}_0})$ and c, the speed of sound, independent of the position $\underline{\mathbf{r}}$. The solution of this equation is a so called Green function defined by:

$$g_f\left(\underline{\mathbf{r}}\middle|\underline{\mathbf{r}_0}\right) \equiv -\frac{\exp\left(-jk\left|\underline{\mathbf{r}}-\underline{\mathbf{r}_0}\right|\right)}{4\pi\left|\underline{\mathbf{r}}-\underline{\mathbf{r}_0}\right|}$$

In general, an acoustical system can be described with Fourier transform techniques. A three dimensional Fourier transform can be defined for the space dependent part of the Helmholtz equation and because the space and time part of the Helmholtz equation are completely separable, a 'normal' time Fourier transform can be applied to the time dependent part. In this way, an arbitrary sound source can be modeled.

$$\Phi(\eta, \underline{\mathbf{r}}) = F_t\left\{\varphi(t,\underline{\mathbf{r}})\right\} = \int_{\infty}^{\infty} \varphi(t,\underline{\mathbf{r}}) \exp(-j2\pi\eta t)dt$$

$$\Phi(\eta, \underline{\beta}) = F_{\mathbf{r}}\left\{\Phi(\eta, \underline{\mathbf{r}})\right\} = \int_{\infty}^{\infty} \Phi(\eta, \underline{\mathbf{r}}) \exp(j2\pi\, \underline{\beta}\cdot\underline{\mathbf{r}})\underline{d\mathbf{r}}$$

The variable η corresponds with the frequency and $\underline{\beta}$ corresponds with the spatial frequency. The frequency and angular spectrum $\Phi(\eta, \underline{\beta})$ corresponds with the

direction of the harmonics in the signal and the frequency of the signal. The time dependent Helmholtz equation can be Fourier transformed in respect to time. This leads to the following expression.

$$\nabla^2\Phi(\eta,\underline{\mathbf{r}})+\left(\frac{2\pi\eta}{c}\right)^2\Phi(\eta,\underline{\mathbf{r}})=X_M(\eta,\underline{\mathbf{r}})$$

When this expression is Fourier transformed with respect to position, a product form can be derived for example in the case of free space propagation in an unbounded medium.

$$\nabla^2\Phi(\eta\,\underline{\mathbf{r}})+\left(\frac{2\pi\eta}{c}\right)^2\Phi(\eta,\underline{\mathbf{r}})=X_M(\eta,\underline{\mathbf{r}})=\exp(-2\pi\eta\,t_0)\delta\,(\underline{\mathbf{r}}-\underline{\mathbf{r}_0})$$

$$\xrightarrow{F_{\mathbf{r}}}$$

$$-\left(\left(2\pi\beta_X\right)^2+\left(2\pi\beta_Y\right)^2+\left(2\pi\beta_Z\right)^2\right)\Phi(\eta,\underline{\boldsymbol{\beta}})+\left(\frac{2\pi\eta}{c}\right)^2\Phi(\eta,\underline{\boldsymbol{\beta}})=\exp(-2\pi\eta\,t_0)\exp(+2\pi\,\underline{\boldsymbol{\beta}}\cdot\underline{\mathbf{r}_0})$$

$$\Rightarrow\Phi(\eta,\underline{\boldsymbol{\beta}})=\frac{1}{\left(\frac{2\pi\eta}{c}\right)^2-\left(\left(2\pi\beta_X\right)^2+\left(2\pi\beta_Y\right)^2+\left(2\pi\beta_Z\right)^2\right)}\exp(-2\pi\eta\,t_0)\exp(+2\pi\,\underline{\boldsymbol{\beta}}\cdot\underline{\mathbf{r}_0})$$

$$\Rightarrow\Phi(\eta,\underline{\boldsymbol{\beta}})=H_M(\eta,\underline{\boldsymbol{\beta}})X_M(\eta,\underline{\boldsymbol{\beta}})$$

with

$$H_M(\eta,\underline{\boldsymbol{\beta}})=\frac{1}{\left(\frac{2\pi\eta}{c}\right)^2-\left(\left(2\pi\beta_X\right)^2+\left(2\pi\beta_Y\right)^2+\left(2\pi\beta_Z\right)^2\right)}$$

the transfer function of free space propagation. In the time - space domain this can be described as an convolution integral:

$$\varphi\,(t,\underline{\mathbf{r}})=\int_{-\infty}^{\infty}\int_{-\infty}^{\infty}x_M(t_0,\underline{\mathbf{r}_0})h_m(t,\underline{\mathbf{r}}\,;t_0,\underline{\mathbf{r}_0})dt_0d\underline{\mathbf{r}_0}\qquad(2\text{-}20)$$

The one-integral-sign over the space vector $\underline{\mathbf{r}}$ is substituting three integral signs. Because an arbitrary steady (not moving) point source X_m in an unbounded medium leads to a time and space invariant expression, h_m can be written as:

$$h_m(t,\underline{\mathbf{r}}\,;t_0,\underline{\mathbf{r}_0})=h_m(t-t_0,\underline{\mathbf{r}}-\underline{\mathbf{r}_0})$$

The solution of the wave equation in the case of a not moving sound source in an unbounded medium degenerates the problem to a time-invariant respectively space-invariant filter problem. For example, a moving source implicates a Doppler shift. In the case of applying a sound source to the problem of the rectangular cavity, where is

dealt with a bounded medium the problem is however time variant, and dependent on the position of the listener.

In the case of a LEMS, the microphone is not moving. Persons in the room however are moving. Assuming there is no movement, it should be possible to construct a transfer function. Such a transfer function, can when coupled with the transfer functions of the apertures (microphone and loudspeaker) be associated with the compensating device. In such a place dependent transfer function $H_M(\underline{r},\eta,\underline{\beta})$ the position can be eliminated for example by setting this position equal to the position of the receiving aperture (loudspeaker) and this result should be equal to the compensating device transfer function.

2.2.5 Conclusions from an acoustical point of view

As one can see, several neglects are made in the derivation of the linear wave equation. Let's start from the beginning, the derivation of the Euler equation of motion. In this derivation the fluid is considered homogenous. This implies that the air has the same composition over the room. This is however not always true. For example, people can smoke in a room and must be able to breath (exhaling a more carbon dioxide rich air) and so on. Further, a homogenous composition means also that there is no density gradient in the equilibrium density, that is, in the absence of a sound wave, examples of this are open windows. The effects of this however, are minimal and the neglects made in this matter are justified.

Also the neglecting of the transverse part is justified. Central heating can locally disturb the solution of the differential equation. Air circulation due to heating, moving of people, wind trough an opened window are relatively slow when compared with the speed of sound.

Temperature gradients due to central heating can also influence the expression for the speed of sound (2-7). The density of air is of course also a function of the temperature. This expression can be made linear, when assumed we are dealing with a perfect diatomic gas [11].

Other, until now not considered neglects, are the thermal conductivity and the viscose behavior of gas. These processes tend to transform the organized motion of sound into the disorganized motion of heat. Both, the viscosity and the thermal conductivity of air are small. Although it can be useful to look at a first order-approximation, the energy transfer takes place so slowly that it's probably not or barely noticeable in a room with relatively small dimensions. For a sound wave of 1000 [Hz] must travel around 10 [km] in open for its intensity to be reduced by a factor 3. In the neighborhood of walls however, these problems play a more important part [10,12].

All of these effects separately, play a minor role, but together they can add a noisy component to the sound wave.

If the room is modeled as a simple rectangular cavity, one can easily see that there are a lot of possible combinations of wave numbers present in the solution for the homogenous problem. Each permutation of *lmn* givers rise to a new mode and thus, to one complex degree of freedom. It can be shown that the number of degrees of freedom increases rapidly with increasing frequency (Figure 2-2).

The problem's complexity increases when a more real model is used as a model for the room, and for example, when the damping of the walls is incorporated in the model. This damping is much larger than the free-space damping. This means that jumps in amplitude take place when a sound wave 'hits' the wall.

Another important conclusion is that there can be established a link between the acoustical transfer function and the compensator model. This relation is complex and of high order, but it should be possible to associate a mode with a complex pole pair. This is based on the fact that linear techniques can be applied in order to derive the acoustic transfer function. These are essentially the same techniques which are used in network theory.

The damping of an acoustic wave in free space is small, and probably negligible when compared with the dimension of a room. The damping caused by the walls however, is not negligible. This damping also takes places in the form of discontinuities when the time-dependency of the signal entering the microphone is considered. This makes it virtually impossible to associate a damping factor with one oscillation. To bypass this problem, there is also the possibility to delay some exponential sequences, and 'start' them when a sound wave 'hits' the wall in order to model the discontinuity in the damping.

When the movement of persons and objects is taken into consideration one could only hope that the variations in the room which take place in tree dimensions could be modeled with an adaptive model in one dimension.

2.3 'Degrees of freedom' and the Gabor signal expansion.

2.3.1 Introduction, the Gabor signal expansion

To get an impression of the number of degrees of freedom a Gabor signal expansion can be useful. This Gabor signal expansion is a mathematical 'tool' to describe the signal in the time domain and the frequency domain simultaneously. The available data are measured impulse response data of a certain room. This data, is a set of samples, sampled with a certain period T. Therefore the impulse response data is a function of the time only.

The Gabor transform, is not simply a transform from one domain to another. It is also a transform which has one 'source' dimension, and two 'destination' dimensions. This implies that there are more possibilities for the inverse transformation.

The Gabor transform also introduces a certain conflict. Time has the unit of seconds and frequency has a unit of Hertz (seconds^{-1}). As a consequence of this, the Gabor signal expansion must satisfy certain restrictions. These restrictions are similar to 'Heisenberg's uncertainty principle' in mechanics. This principle states that it's impossible to determine accurately the position and velocity of a particle at the same instance of time. Time is necessary to determine the direction and the velocity. The position of the particle changes during this time. In case of a local frequency distribution function at certain infinitely small interval of time, the same problem arises. A time interval which is *not* indefinitely small is required to determine a Fourier transform and hence, to measure a 'spectogram'.

Gabor originally restricted himself to an elementary signal. He saw the simultaneous description of a signal in time and frequency as an 'information diagram'. Furthermore he found that there exist 'elementary signals' which occupy the smallest possible area in both domains simultaneous and therefore in his 'information diagram'. Each elementary signal can be considered as conveying exactly one 'quantum of information', in other words, one (complex) degree of freedom. Gabor restricted himself to Gaussian shaped elementary signal. Therefore the time signal can be expanded into a set of properly shifted and modulated (shift in the frequency domain) Gaussian signals [25,26,27].

2.3.2 The Gabor signal expansion

As pointed out in the previous section, Gabor restricted himself to an elementary Gaussian shaped signal (2-21).

$$g(t) = 2^{\frac{1}{4}} e^{-\pi(\frac{t}{T})^2} \tag{2-21}$$

$$\frac{1}{T}\int |g(t)|^2 dt \tag{2-22}$$

Where the factor $2^{\frac{1}{4}}$ is added to normalize the integral (2-22) to unity. The signal $\varphi(t)$ can be written as a set of shifted and modulated versions of the elementary signal $g(t)$ (2-23).

$$g_{mk}(t) = g(t - mT)e^{jk\Omega t} \tag{2-23}$$

Gabor states that a signal $\varphi(t)$ can be extended to a linear combination of shifted and modulated elementary signals. In the expression for $g_{mk}(t)$ T equals the time-shift and Ω equals the frequency shift. Both must satisfy the relationship $\Omega T = 2\pi$.

$$\varphi(t) = \sum_m \sum_k a_{mk} g_{mk}(t)$$

Because the elementary functions $g_{mk}(t)$ are not orthogonal to each other, a window function $w(t)$ has to be defined to establish orthogonality. This is expressed in the inner product definition for Hilbert spaces. If the functions $g_{nl}(t)$ and $g_{mk}(t)$ orthogonal to each other than this inner product must imply the Kronecker delta functions.

$$\int g_{nl}^{*}(t) g_{mk}(t) dt = d_{m-n} d_{l-k}$$

The integral above however, does not yield this Kronecker delta function, when a Gaussian shaped function is used.

Orthogonality is necessary to define a inverse transform from the Gabor signal expansion to the signal again. With the aid of the bi-orthogonality condition 2-24 a transformation pair 2-25 and 2-26 can be defined (see [15]).

$$\int w_{nl}^{*}(t) g_{mk}(t) = \delta_{n-m} \delta_{l-k} \tag{2-24}$$

$$a_{mk} = \int \varphi(t) w_{mk}^{*}(t) dt \quad \text{transform} \tag{2-25}$$

$$\varphi(t) = \sum \sum a_{mk} g_{mk}(t) \quad \text{inverse - transform} \tag{2-26}$$

To determine the coefficients, a Zak transform can be applied [15]. The Zak transform of a signal is defined by $\tilde{\varphi}(t,\omega;\tau)$. Please note the tilde on top of the function, stating that the function is a Zak transform. The Zak transform is defined as a Fourier transform of the sequence $\varphi(t+m\tau)$.

$$\tilde{\varphi}(t,\omega;\tau) = \sum_{m} \varphi(t+m\tau) e^{-jm\omega\tau} \quad \text{Zak transform}$$

$$\varphi(t+m\tau) = \frac{\tau}{2\pi} \int_{2\pi/\tau} \tilde{\varphi}(t,\omega;\tau) e^{jm\omega t} dt \quad \text{Inverse Zak transform}$$

This Inverse Zak transform is *periodic* in the frequency variable ω with period $2\pi/\tau$ and *quasi-periodic* in the time variable t with *quasi-period* τ.

This Zak transform can be used to rewrite the bi-orthogonality condition 2-24 into a product form.

$$T \cdot \tilde{g}(t,\omega;\tau) \cdot \tilde{w}(t,\omega;\tau) = 1 \tag{2-27}$$

The Zak transform can also be used to rewrite the Gabor transform 2-25 in a product form. This reads [25]:

$$\bar{a}\ (t,\omega;\tau) = T \cdot \tilde{\varphi}\ (t,\omega;\tau) \cdot \tilde{w}^{*}\ (t,\omega;\tau) \tag{2-28}$$

The dash above the function $\bar{a}\ (t,\omega;\tau)$ indicates that $\bar{a}\ (t,\omega;\tau)$ is a Fourier transform in two dimensions. This is related to the coefficients a_{mk} through the following Fourier transform:

$$\bar{a}\ (t,\omega;\tau) = \sum_{m}\sum_{k} a_{mk} e^{-j(m\omega T - k\Omega t)}$$

When this bi-orthogonality condition in product form 2-27 is used to determine the window function $\tilde{w}(t,\omega;\tau)$, care must be taken for zeros in the function $\tilde{g}\ (t,\omega;\tau)$ because $\tilde{g}\ (t,\omega;\tau)$ forms the numerator in $\tilde{w}(t,\omega;\tau)$. These zeros become delta functions in a zero function $\tilde{z}\ (t,\omega;\tau)$.

$$\tilde{w}(t,\omega;\tau) = \left.\frac{1}{T \cdot \tilde{g}\ (t,\omega;\tau)}\right|_{\tilde{g}\ (t,\omega;\tau)\neq 0} + \tilde{z}\ (t,\omega;\tau)$$

2.3.3 Implementation of a discrete Gabor signal expansion

To successfully implement a Gabor signal expansion, a discrete Gabor transform has to be defined, equivalently to the discrete Fourier transform (DFT).

Analogous to the Fourier transform for time discrete signals (FTD) there is also a Gabor transform for discrete time signals. When a FTD is applied to a discrete time signal, replicas of the frequency spectrum are repeated along the frequency axes with period $\Omega = 2\pi/T$. Care has to be taken that the signal is sufficiently band-limited, in order to avoid aliasing problems. The same problem occurs with the Gabor transform. Sampling of the time axes leads to repetition on the frequency axes. In the case of Gabor, the Gabor lattice is repeated in the frequency dimension.

When this is taken one step further, and also the frequency axes is sampled, periodicity occurs in the time direction also. Square brackets [] and the variable n (short for nT) are used to illustrate the discrete time nature of the signals. The discrete Zak transform can then be defined as:

$$\tilde{\varphi}\ [n,l;N,M] = \varphi\ (n,\frac{\Theta}{M}l;N) = \sum_{m}\varphi\ [n+mN] e^{-jm(\frac{2\pi}{M})l} \tag{2-29}$$

The following strategy can be applied:

1. Determine from the window $w[n]$ the Zak transform $\tilde{w}\ [n,l;N,M]$
   Determine from the signal $\varphi[n]$ the function $\tilde{\varphi}\ [n,l;N,M]$
2. With the aid of the bi-orthogonality relation for discrete signals $\bar{a}\ [n,l;N,M] = N\tilde{\varphi}\ [n,l;N,M] \cdot \tilde{w}\ [n,l;N,M]$ the Fourier transform of the array A_{mk} can be found.

3. With the aid of a fast inverse Fourier transform algorithm the coefficients A_{mk} can be found. A_{mk} is however periodic in both frequency and time.
4. a_{mk} can be found by taking one period of A_{mk}.

In a vector manipulating environment like MatLab, The Zak transform can easily be defined as a vector product. Care has to be taken that the signal is zero outside the elementary interval, that is for every n<0 and n>MN. In this case, the transform can be limited to the elementary interval.

$$\underline{\mathbf{e}}[l]=\begin{pmatrix}1 & e^{-\frac{2\pi}{M}l} & \cdots & e^{-\frac{2\pi}{M}(M-1)l}\end{pmatrix}^T$$

$$\underline{\varphi}[n]=\begin{pmatrix}\varphi[n] & \varphi[n+N] & \cdots & \varphi[n+(M-1)N]\end{pmatrix}^T$$

$$\tilde{\varphi}[n,l\,;N,M]=\tilde{\varphi}_{n,l}=\underline{\mathbf{e}}^T[l]\underline{\varphi}[n],\quad n\in[0,(N-1)],\ l\in[0,(M-1)]$$

$$PSI=\begin{pmatrix}\tilde{\varphi}_{0,0} & \tilde{\varphi}_{0,1} & \tilde{\varphi}_{0,2} & \cdots & \tilde{\varphi}_{0,M-1}\\ \tilde{\varphi}_{1,0} & \tilde{\varphi}_{1,1} & & & \vdots\\ \tilde{\varphi}_{2,0} & & & & \vdots\\ \vdots & & & \ddots & \vdots\\ \tilde{\varphi}_{N-1,0} & \cdots & \cdots & \cdots & \tilde{\varphi}_{N-1,M-1}\end{pmatrix}$$

With n, the variable associated with time down columns, and m associated with the frequency across rows.

The Fourier transform of the coefficient matrix A_{mk}, can be obtained by multiplying the elements of W, the ZAK transform (obtained in a similar way as *PSI*) of the window function element wise with *PSI*.

In the case of the Gaussian elementary signal $g(t)$, the window function can be derived by means of , the bi-orthogonallity condition, the discrete version of 2-27.

$$g(t)=2^{\frac{1}{4}}e^{-\pi(\frac{t}{T})^2}\xrightarrow{ZAK}\tilde{g}(t,\omega)=2^{\frac{1}{4}}e^{-\pi(\frac{t}{T})^2}\theta_3(\pi\xi^*)$$

θ_3 is the theta function with $\xi = \omega/\Omega + j\, t/T$.

$$T\,\tilde{w}(t,\omega)=2^{-\frac{1}{4}}e^{\pi(\frac{1}{T})^2}\frac{1}{\theta_3(\pi\xi)}$$

The function $\theta_3^{-1}(\pi\xi)$ can be written as a Fourier series. The constant K_0 = 1.86407468 represents the complete elliptic integral for the modulus $\frac{1}{2}\sqrt{2}$.

$$\frac{1}{\theta_3(\pi\xi^*)} = \left(\frac{K_0}{\pi}\right)^{\frac{3}{2}}\left(c_0 + 2\sum_{m=1}^{\infty}(-1)^m c_m \cos(2\pi m\xi)\right)$$

with

$$c_m = \sum_{n=0}^{\infty}(-1)^m e^{-\pi(n+\frac{1}{2})(2m+n+\frac{1}{2})}$$

The window function can be derived from it's ZAK transform by means the inverse ZAK transform. This leads to the following expression for *w(t)* in the elementary interval -½T < t ≤ ½T:

$$T\,w(t) = \frac{1}{\sqrt[4]{2}}\left(\frac{K_0}{\pi}\right)^{-\frac{3}{2}} e^{\pi(\frac{t}{T})^2} \sum_{n+\frac{1}{2}\geq\left|\frac{t}{T}\right|}(-1)^n e^{=\pi(n+\frac{1}{2})^2} \equiv \frac{1}{\sqrt[4]{2}}\left(\frac{K_0}{\pi}\right)^{-\frac{3}{2}}(-1)^m e^{\pi\left((\frac{t}{T})^2-(m+\frac{1}{2})^2\right)}$$

The approximation is valid in a interval $(m-\frac{1}{2})T \leq |T| < (m+\frac{1}{2})T$. It should be noticed that for the discrete versions of this function, the symmetry of the function in respect to the raster is important. Therefor it is necessary to determine whether an odd or an even amount of samples N will be used. The total number of samples in a measured impulse response is 2048. The number of samples N in the determination of the ZAK transform is set to 64 and the number of samples in the frequency direction M is set to 32. This is done because M*N=2048. As limit case, all 2048 entries in the Gabor transform matrix A are necessary. This equals the case when an FIR model is used. Furthermore, in the case of MxN=2048 no aliasing is present.

The implementation of the inverse Fourier transform to obtain A_{mk}, is quite simple. First perform a M-points IFFT across rows. After this action, perform a N-point IFFT down columns. Transpose the result.

2.3.4 Results

A typical measured impulse response has a length of 2048 samples. The sample frequency is 10 [kHz] for the impulse responses "direct" and "diffuus". The other impulse responses are various impulse responses, measured with a person at different locations in the room (Table A-1, Appendix 1) sampled at 8 [kHz]. The room is a laboratory room with a typical reverberation time of 0.4 a 0.5 [s].

To model the impulse responses with a FIR model, 2048 coefficients are needed. These 2048 coefficients (degrees of freedom) can be considered as a limit case, at most 2048 coefficients are needed to model the signal.

Starting with the impulse response, a Gabor expansion of each impulse response is derived with the aid of Matlab (see for example Figure 2-3). This Gabor expansion

should, according to the previous paragraphs, represent the number of degrees of freedom.

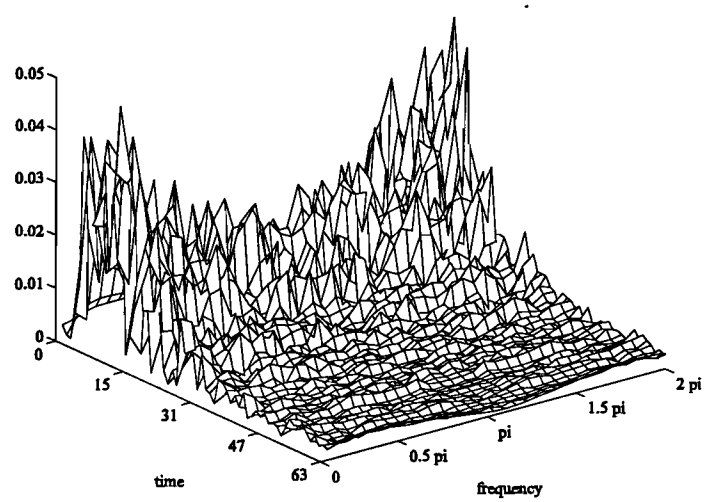

Figure 2-3: *Gabor transformed impulse response "diffuus"*

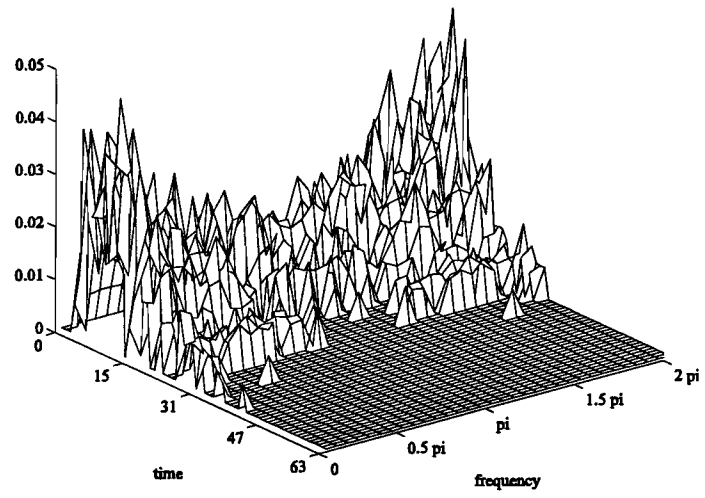

Figure 2-4: *Gabor transformed impulse response "diffuus", and clamped at -20 [dB]*

Because no coefficient is actually zero, a threshold is applied. Beneath this threshold, Gabor coefficients are clamped to zero. A good measure for this threshold can be the absolute value of the largest Gabor coefficient. Every Gabor coefficient beneath a certain dB level below this absolute value will be suppressed (Figure 2-4). Note the time axes is reversed. This is done deliberately, because an reverberation typically damps exponentially. This means that the first reflection is the loudest and the following reflections are less loud.

The Gabor plots in Figure 2-3 and Figure 2-4 are symmetrical around π. Except for the value at f=0. This should be repeated at f=2π. These values correspond with the dc or mean component in the signal at a certain time, yielding one degree of freedom. The other entries up to f=π yield a complex degree of freedom, meaning two degrees of freedom, but they are symmetrical positioned around f=π. The most convenient way to count the 'degrees of freedom', is counting the matrix entries unequal to zero in the clamped Gabor lattice. Each entry unequal to zero yields 'one degree of freedom'.

To determine how 'well' the clamped Gabor lattices describes the corresponding impulse responses, an objective measure is necessary. This can be done by taking first the absolute value of these Gabor lattice entries, and at the other hand, taking the difference between the clamped Gabor entries and the original Gabor lattice entries. It is then convenient to take the percentage of this difference relative to the original energy. The measure called Relative Modeled Energy in the Gabor Lattice (RME_{GL}) can be found in the last column of Table 2-2.

$$RME_{GL} = \frac{\sum_{M,K}\left(\left|a_{nk}\right| - \left|a_{clamped,nk}\right|\right)^2}{\sum_{M,K}\left|a_{nk}\right|^2} * 100\%$$

It is important to realize that the entries in the Gabor lattice are dependent. Hence it is impossible to relate the percentage RME_{GL} obtained directly to the Relative Modeled Energy (RME). To do this correctly, the signal must first be reconstructed from the Gabor lattice. The RME_{GL} however, gives a good impression, especially when the absolute values of the coefficients are small.

A first conclusion can be drawn from this table. The clamped Gabor transforms of -18 [dB] yields between 567 and 1159 degrees of freedom and an energy coverage higher than 90% (except 'direct') . This is a reduction of a factor 2 compared with the FIR model, in which 2048 coefficients are necessary. Also can be seen that the energy coverage of impulse response 'direct' increases faster at low dB levels, with a small increase in degrees of freedom compared to the other impulse responses. This impulse response has a direct path with a lot of energy, compared to its own the reverberations. This 'direct path' can be modeled with a relatively small amount of Gabor entries. This effect is compensated later at lower thresholds.

An interesting question is: "which entries change in the Gabor lattice when the test subject walks trough the room?". In other words, is there a possibility to appoint an sub area of entries which can be used to describe all impulse responses. If this is the case, an adaptive filter can be created with a smaller set of coefficients than in the FIR case of 2048 coefficients.

Let's assume that the measurements imp01, imp02, imp03, imp04, imp05 and imp06 are representative for the majority of possible impulse responses. It should again be possible to define a threshold. Above this threshold, coefficients are considered

necessary, below this threshold, coefficients are considered obsolete. The coefficients considered necessary can be represented with a one. Coefficients which are considered obsolete can be represented with a zero. A good value for this threshold is given by -18 [dB]. In Table 2-2 at a threshold of -18 [dB] all the above mentioned signals have an RME_{GL} of 90 % or above.

Table 2-2: *Clamped Gabor transforms of the measured impulse responses and their degrees of freedom, dgf means # degrees of freedom and sec means signal energy covered in percents.*

	dgf	RME_{GL}	dgf	RME_{GL}	dgf	RME_{GL}	dgf	RME_{GL}	dgf	RME_{GL}
	-3 [dB]		-6 [dB]		-9 [dB]		-12 [dB]		-15 [dB]	
diffuse	20	18	65	40	162	64	306	82	429	90
direct	10	29	18	39	45	57	81	67	143	76
imp01	10	7	78	30	197	51	392	69	733	84
imp01b	8	7	52	26	157	49	307	67	574	82
imp02	14	9	83	32	213	55	401	72	763	88
imp02b	14	9	83	32	222	56	411	72	757	88
imp03	14	10	82	35	191	55	377	72	671	86
imp04	10	10	48	26	139	49	275	66	501	80
imp05	10	9	59	28	184	56	333	72	570	85
imp06	42	20	135	44	289	64	543	80	840	90
	-18 [dB]		-21 [dB]		-24 [dB]		-27 [dB]		-30 [dB]	
diffuse	567	94	734	97	920	98	1108	99	1362	100
direct	244	84	400	90	655	95	941	97	1283	99
imp01	1143	94	1485	98	1738	99	1854	100	1958	100
imp01b	940	93	1209	97	1470	99	1692	100	1822	100
imp02	1076	95	1326	98	1559	99	1702	100	1862	100
imp02b	1066	95	1328	98	1559	99	1724	100	1857	100
imp03	970	93	1274	97	1604	99	1801	100	1906	100
imp04	857	91	1186	96	1474	99	1701	100	1863	100
imp05	846	92	1119	96	1450	99	1710	100	1871	100
imp06	1159	96	1453	98	1731	100	1880	100	1950	100

The resulting matrices with entries zero or one for each impulse response can be added over all impulse responses. The resulting matrix is a kind of histogram. The value of each entry represents the amount of times an entry was present in a Gabor transform of an impulse response. The results are displayed in Figure 2-5. The darkest color represents no 'hits' and the lightest colors represent 6 'hits'.

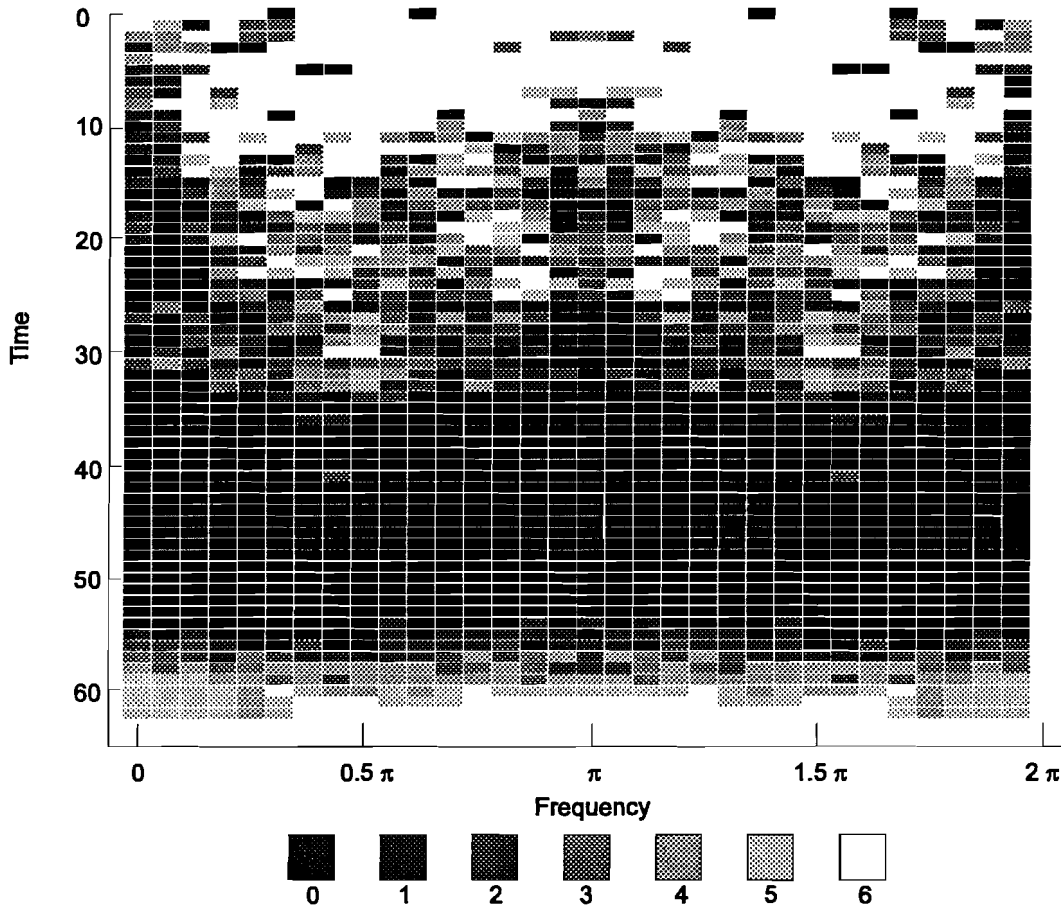

Figure 2-5: *Histogram, 'entry hits' for the impulse responses imp01, imp02 ... imp06*

Table 2-3: *hits versus amounts*

hits	amount
0	600
1	235
2	156
3	115
4	172
5	149
6	630

Looking at these numbers, there is assumed that with 2 hits or more, a coefficient is likely to be necessary for the model. This leads to 156+115+172+149+630=1222 coefficients.

Furthermore here should be pointed out that when a higher RME_{GL} is desired, more coefficients are probably necessary. This is not sure, because it might just be that the coefficients with hits 2 and 3 change into 5 or 6 hits. This means that the total amount of coefficients remains the same.

The Gabor transform shows us that almost all frequencies are contained in the impulse responses over the complete time range. Although a threshold was applied to the Gabor lattice, it can be argued that this threshold is not strict enough. The Gabor lattice demonstrates that room impulse responses are complicated signals.

2.4 Order estimation based on Hankel matrices and SVD

Another way to get an impression of the order of the number of poles, needed to model the impulse response is by means of the Hankel matrix and singular value decomposition. This first estimate can be used as start order later on. Model reduction methods can be used to decrease the order further. The method here is also described in [14].

To obtain this impression, consider the room impulse response as a process which can be perfectly modeled. The output of this process, $y[n]$, is superimposed with Gaussian white noise, which together form the measured room impulse response. Thus, the measured room impulse response $h[n]$ can be written as:

$$h[n] = y[n] + n_\sigma[n]$$

The impulse responses are all of length N (N=2048). This means the impulse response can be perfectly modeled with a ARMA model of order N/2. For simplicity reasons, take N even. The model impulse response can now be expressed in the Auto Regressive (AR) parameters a_p and the room impulse response $h[n]$:

$$y[n] + n_\sigma[n] = \begin{cases} h[n] & 0 < n \le \frac{N}{2} - 1 \\ -\sum_{p=\frac{N}{2}}^{N-1} a_p y[n] = h[n] & \frac{N}{2} \le n \le N-1 \end{cases}$$

The latter expression can be solved perfectly to obtain a_p. If the ARMA order is not chosen equal to N/2, the expression can be solved in least square sense. The energy transfer from past inputs to future outputs can be investigated in order to find out how many AR parameters are needed. The future outputs are entries in a vector:

$$\underline{\mathbf{y}_f}[n] = \left(y\left[\frac{N}{2}\right] \quad y\left[\frac{N}{2}+1\right] \quad \cdots \quad y[N-1] \right)^T$$

The from the past inputs to the future outputs transferred energy $y_f[n]$ can be written as:

$$E_t = \sum_{n=\frac{N}{2}}^{N-1} y_f^2[n] = trace\left(\underline{\mathbf{y}_f^T \mathbf{y}_f}\right)$$

The Hankel matrix is given by:

$$\mathbf{H} = \begin{pmatrix} h[1] & h[2] & \cdots & h\left[\frac{N}{2}-1\right] \\ h[2] & h[3] & & \vdots \\ \vdots & & \ddots & \vdots \\ h\left[\frac{N}{2}-1\right] & h\left[\frac{N}{2}\right] & \cdots & h[N-1] \end{pmatrix}$$

H can be separated in a Hankel matrix due to the model $y[k]$, and a Hankel matrix due to the additive noise $n[k]$.

$$\mathbf{H} = \mathbf{H}_y + \mathbf{H}_n$$

E_t is now given by the following expression:

$$trace\left(\underline{\mathbf{y}_f^T \mathbf{y}_f}\right) = trace\left(\underline{\mathbf{u}_p^T} \mathbf{H}^T \mathbf{H} \underline{\mathbf{u}_p}\right)$$
$$\Leftrightarrow trace\left(\underline{\mathbf{u}_p^T}\left(\mathbf{H}_y + \mathbf{H}_n\right)^T\left(\mathbf{H}_y + \mathbf{H}_n\right)\underline{\mathbf{u}_p}\right),$$

with

$$\underline{\mathbf{u}_p} = \left(u(1) \quad u(2) \quad \cdots \quad u\left(\frac{N}{2}-1\right)\right)^T.$$

The above expresses how long energy passed to the system by the excitation $\underline{\mathbf{u}_p}$ remains in the system formed by **H**.

Using singular value decomposition, the Hankel matrix can be written as a product of three new matrices, The unitary matrices **U** and **V**, and the diagonal matrix **S** with nonnegative elements in decreasing order so that:

$$\mathbf{H} = \mathbf{U}\mathbf{S}\mathbf{V}^T$$

This can be applied to the

$$trace\left(\underline{\mathbf{y}_f^T \mathbf{y}_f}\right) = trace\left(\underline{\mathbf{u}_p^T}\left(\mathbf{U}\mathbf{S}\mathbf{V}^T\right)^T\left(\mathbf{U}\mathbf{S}\mathbf{V}^T\right)\underline{\mathbf{u}_p}\right)$$
$$\Leftrightarrow trace\left(\underline{\mathbf{u}_p^T}\mathbf{V}\mathbf{S}^T\mathbf{U}^T\mathbf{U}\mathbf{S}\mathbf{V}^T\underline{\mathbf{u}_p}\right)$$
$$\Leftrightarrow trace\left(\underline{\mathbf{u}_p^T}\mathbf{V}\mathbf{S}\mathbf{I}\mathbf{S}\mathbf{V}^T\underline{\mathbf{u}_p}\right)$$
$$\Leftrightarrow trace\left(\underline{\mathbf{u}_p^T}\mathbf{V}\mathbf{S}^2\mathbf{V}^T\underline{\mathbf{u}_p}\right)$$

The diagonal matrix $\mathbf{S}^2$ is given by:

$$\mathbf{S}^2 = \mathbf{S}_y^2 + \sigma_n^2 \mathbf{I} + 2\mathbf{S}_y\mathbf{S}_n \cos(\chi)$$

In this expression only the first *P* samples of $\mathbf{S}_y^2$, with *P* the true order are unequal to zero. These P parameters cannot be retrieved from $\mathbf{S}^2$ however, because they are biased with the σ_n^2, the noise energy and a disturbance caused by the cross products of the true system and the imposed noise: $2\mathbf{S}_y\mathbf{S}_n \cos(\chi)$. For not too high noise levels, most of the energy from past inputs to future outputs is transferred over the true systems singular values.

This can be done for the measured room impulse responses. The result, of applying this method to imp01, is plotted in Figure 2-6. The order can now be estimated and is given by the number of squared singular values at which the squared singular values approach the noise level. Normally a sharp decrease to a certain level (the noise level) can be observed.

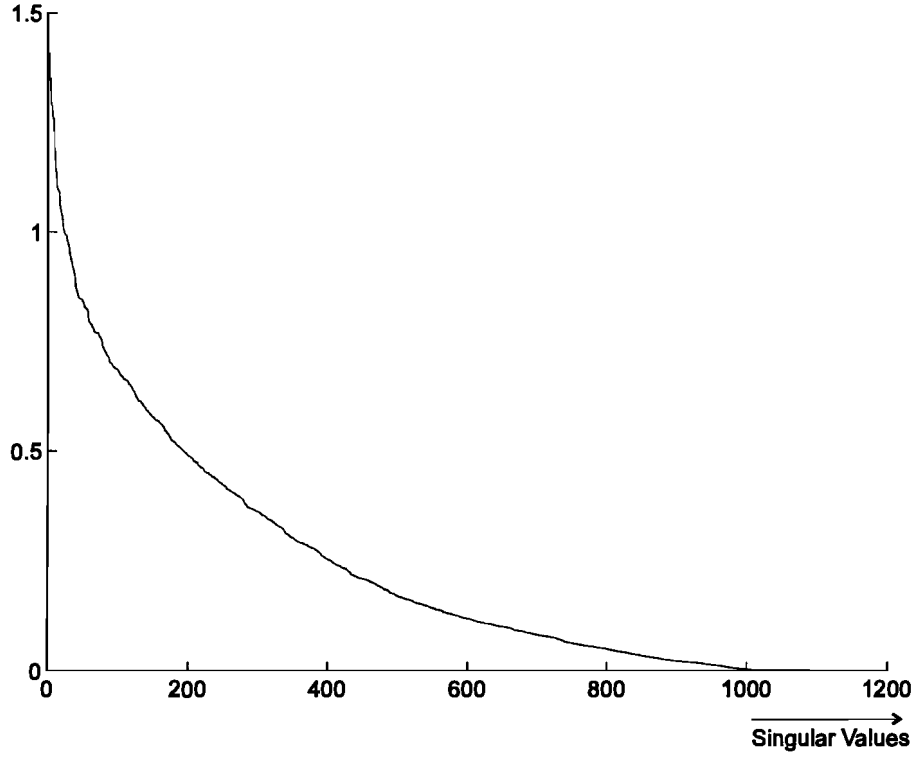

Figure 2-6: *Square singular values of the Hankel matrix*

From impulse response 2 and impulse response 2b (the latter is a repeated version of measurement 2) the noise level can be estimated. It should be pointed out that this is a very crude estimate of the noise level. More measurements have to be carried out to find a more exact noise level. The noise level and the squared singular values are plotted in Figure 2-7.

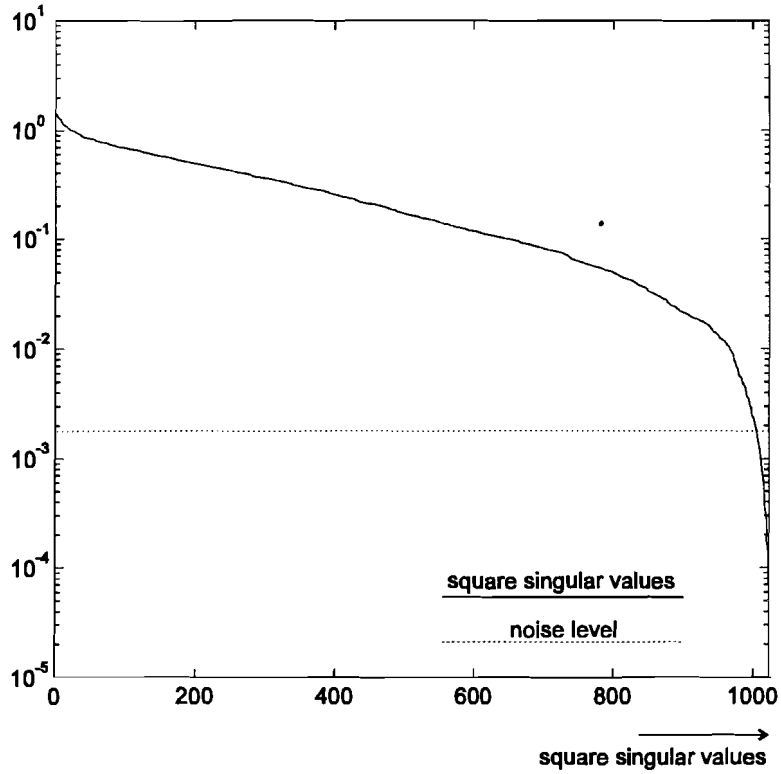

Figure 2-7: *Squared singular values and noise level*

Looking at Figure 2-7, around 1000 coefficients are needed in the initial model.

3. Modeling the impulse responses with an IIR model.

3.1 Introduction

To model a room transfer function, there are a number of options. The first option is a MA model. This model can be easily obtained from the room impulse response of a room, and is associated with a tapped-delay line (Figure 3-1).

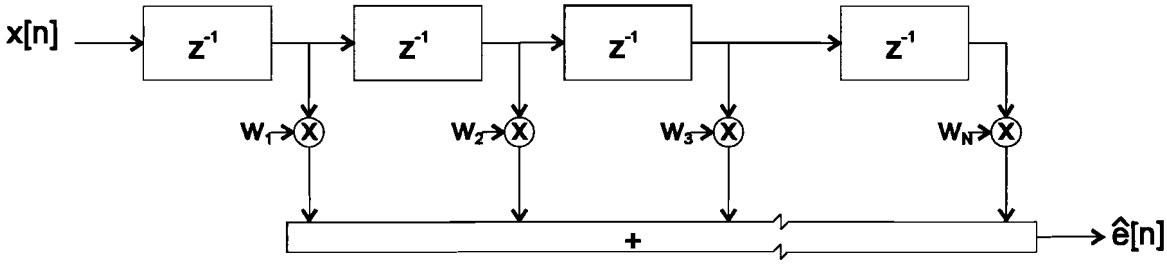

Figure 3-1: *The tapped-delay line*

In the case of 'no direct speech' entering the microphone, an estimation $\hat{y}[n]$ of the signal from the microphone is made on the basis of the signal which enters the 'loudspeaker' $x[n]$. This estimation is subtracted from the undesired echo signal $y[n]$ coming out of the microphone (Figure 1-2).

In the case of a 'direct speech' signal $s[n]$ entering the microphone, the signal coming out of the microphone $\tilde{e}[n]$ will be the sum of the unwanted echo $e[n]$ and the speech signal $s[n]$. The compensator now has to subtract the estimation of the unwanted echo $\hat{e}[n]$ from $\tilde{e}[n]$ (Figure 3-2).

Several thousands of coefficients w_1 - w_N are necessary when a reasonable attenuation of the signal $e[n]$ entering the microphone is desired, considering the small amount of time (sample time) available for the algorithm used to adapt these coefficients.

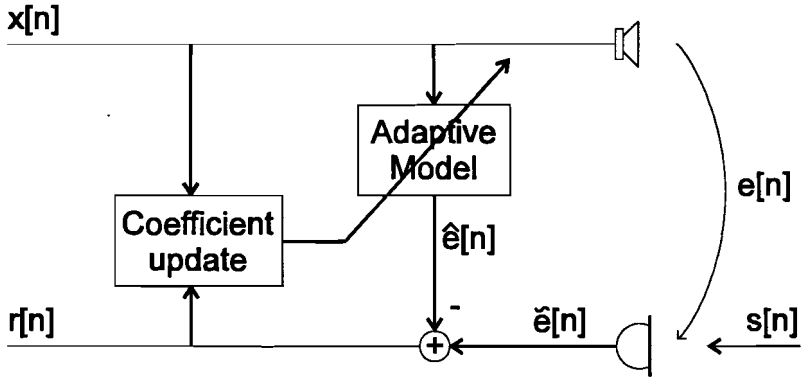

Figure 3-2: *model of the adaptive echo canceller*

As already suggested in the introduction, a reduction in the amount of model parameters may be achieved when using an IIR model instead of a FIR model. This reduction can not be achieved with a echo cancellation device based on a FIR filter bank as shown in Figure 3-1.

The IIR model can be divided in a Moving Average (MA) part and a Auto Regressive (AR) part. The MA part describes how the current output relates to the past input values, the AR part describes how the current output relates to the past outputs.

$$\begin{aligned} y[n] = b_0 x[n] + b_1 x[n-1] + b_2 x[n-2] \cdots + b_Q x[n-Q] \\ -a_1 y[n-1] - a_2 y[n-2] \cdots - a_P y[n-P] \end{aligned} \tag{3-1}$$

The transfer function of the IIR model can in general be described in the Z-domain with a nominator polynomial and a denominator polynomial, and in the form of the summation of first order sections.

$$\frac{b_0 + b_1 z^{-1} + b_2 z^{-2} \cdots + b_Q z^{-Q}}{1 + a_1 z^{-1} + a_2 z^{-2} \cdots + a_P z^{-P}} = \frac{c_1}{1 - z_1 z^{-1}} + \frac{c_2}{1 - z_2 z^{-1}} \cdots \frac{c_P}{1 - z_P z^{-1}}$$

In this expression P has to be greater than Q. The poles z_i can be found by searching the roots of the denominator polynomial, for example with a Newton method. Because the model describes a real model, the poles are real valued or complex conjugated. The impulse response is infinite.

There are several procedures to find an IIR model from an FIR model. For example: Prony, Iterative methods based on Prony and Steiglitz-McBride. These will be discussed in paragraph 3.3.

To test these methods a synthetic model, from which the poles are known can be generated. This model can be used as input for the different procedures. After using the method, the poles found by the procedure can be compared with the poles from the generated model. This will be discussed in the next paragraph.

Most of the procedures for finding the pole locations find their origin in the (industrial) system/process identification. Most of the systems/processes in this area are of relatively low order, compared to this acoustical problem. The available system identification methods present in for example MatLab are not well equipped for these kind of orders.

The amount of poles and the length of the impulse response lead to numerical difficulties. For example, if we try to model the room transfer function with 800 poles (400 complex conjugated pairs) (see Gabor transform) and the impulse response is 2048 samples long the iterative Prony method produces a 800 x 2048 Van der Monde matrix. This leads to a very ill-conditioned matrix which has to be inverted.

For the method of Steiglitz-McBride we need to find the roots of a 800^{th} order polynomial. This leads to numerical problems when for example a Newton method is used. Paragraph 3.5 discusses a 'divide and conquer strategy'. 'Divide and conquer' in this context, is reducing the problem by means of 'cutting' the impulse response in smaller components. Three alternatives have been investigated, all based on the assumption that the room impulse response can be divided in subbands.

The last paragraph in this chapter deals with the results of using the synthetic model with the methods described above. A selection of a procedure is made on the basis of the results.

3.2 Constructing a synthetic model

The need for a synthetic model is obvious. In the measured room impulse responses the exact locations of the poles are unknown. If we want to find out how well an algorithm performs, the location of the poles must be known in advance. After running the algorithm the resulting poles can be compared with the ones in the generated model. To make it more 'difficult' for the algorithm, noise can be added.

The noise level cannot be of a constant level. Because the impulse responses are decaying exponentially, the addition of a noise floor of constant power would destroy the small amplitude information in the tail of the impulse response. The addition of a noise with constant power is also not related to a physical phenomenon. The noise is for example related to scattering effects and small (not worth modeling) amplitude interfering vibrations. Hence, the power of the noise is dependent on the amplitude of the reverberations, which is exponentially decaying. The noise itself is chosen Gaussian with a standard deviation equal to root of the energy in the signal (RMS value). The dead time is not modeled (see Appendix I).

Half of the total amount of poles of the model can be chosen randomly on a positive half circle in the complex Z domain (imaginary part greater than zero). The other half can be calculated, taking the complex conjugated versions of the first half. The radius of this circle can be calculated from the reverberation time, which was known during the measurements. This reverberation time is 0.4 - 0.5 [s]. This reverberation time is defined as the time τ_r, which it takes the impulse response to decay 60 [dB]. This means that within one elementary time (sample time T) the signal is decayed by:

$$\frac{60}{\tau_r f_s} \; [dB]$$

with f_s the sample frequency. A pole can be represented in the time domain by the decaying sequence:

$$H(z) = \frac{1}{1 - a e^{j\phi} z^{-1}} \xrightarrow{\text{inverse Z transform}} h[n] = a^n e^{jn\phi}$$

The radius is now given by:

$$20\log\left(\frac{a^n}{a^{n+1}}\right)=\frac{60}{\tau_r f_s} \Rightarrow a=10^{-\frac{3}{\tau_r f_s}}$$

For a sample frequency f_s=8 [kHz] and τ_s=0.5 this leads to a=0.99827 (see Appendix I).

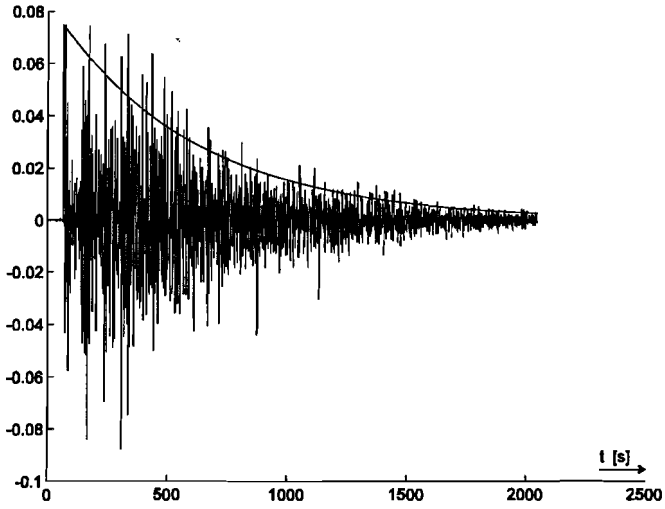

Figure 3-3: *Envelope a=0.99827*

The physical poles are probably not perfectly located on a circle. This because the attenuation mainly depends on the walls and not on the free space attenuation. The distance to the walls and the microphone is not in all directions the same. So to make the synthetic model more realistic the poles are located with a random small deviation from the circle 0.99827.

With this set of poles, a denominator polynomial can be constructed. The construction of such a denominator polynomial however, involves the multiplication of a large amount of factors:

$$A(z)=\prod_{i=1}^{N}(1-z^{-1}z_i)$$

This multiplication can lead to numerical problems, and is therefore not preferable.

Better is the usage of a Kautz filter bank (see the next chapter) the poles are placed in a Kautz filter bank. The energy conservation property through the all-pass sections assures that the effect of all poles is present in the impulse response. This Kautz bank, now being a synthetic model of the room, can be fed with a Dirac pulse. The weights w_ϕ and w_φ can be set to equal one. The impulse response of the synthetic model is now given by:

$$h_s[n]=h_{rp}[n]+N_l\cdot G\left(0,\frac{1}{N}\sqrt{\sum_{n=0}^{N-1}h_{rp}^2[n]}\right)\cdot a^n$$

With $G(\mu,\sigma)$ a Gaussian distributed stochastic variable with mean μ and standard deviation σ, N_l the noise level and $h_{rp}[n]$ the impulse response from the Kautz bank with the random poles chosen according the above procedure. Thus, this model can now be used to test the properties of modeling procedures. The roots of the denominator polynomial are known and can be compared with the ones found by the modeling procedures.

3.3 Some methods to determine an IIR model

3.3.1 Prony's method

Assume that the room impulse response is of length N. The Prony algorithm tries to approximate $h[n]$ on this N-point interval with $\hat{h}[n]$. Thus, the impulse response $h[n]$ is defined as:

$$h[n]=\begin{cases} h[n] & 0\le n\le N-1 \\ 0 & n<0 \vee n\ge N \end{cases} \tag{3-2}$$

The solution in the Prony algorithm involves a separation of the moving average (MA) part and the auto regressive (AR) part (3-1). In the (discrete) time, the model can be written as:

$$\begin{aligned}&\hat{h}[n]+a_1\hat{h}[n-1]+a_2\hat{h}[n-2]+\cdots+a_P\hat{h}[n-P]\\ &\quad=b_0\delta[n]+b_1\delta[n-1]+b_2\delta[n-2]+\cdots b_Q\delta[n-Q]\end{aligned}$$

Now, use can be made of the property of the MA part. This MA part is zero in this case for $n>Q$, i.e. only when an impulse is present at the input of the model. The model is then only dependent on the AR part of the model:

$$\hat{h}[n]=-a_1\hat{h}[n-1]-a_2\hat{h}[n-2]-\cdots-a_P\hat{h}[n-P] \qquad Q<n\le N-1$$

The estimation $\hat{h}[n]$ can of course also be based on past values of $h[n]$:

$$\hat{h}[n]\approx -a_1h[n-1]-a_2h[n-2]-\cdots-a_Ph[n-P] \qquad Q<n\le N-1$$

This expression can also be written as a (overdetermined) matrix equation:

$$\begin{pmatrix}\hat{h}[Q+1]\\ \hat{h}[Q+2]\\ \vdots\\ \hat{h}[N-2]\\ \hat{h}[N-1]\end{pmatrix}=-\begin{pmatrix}h[Q] & h[Q-1] & \cdots & h[Q-P+1]\\ h[Q+1] & h[Q] & \cdots & h[Q-P+2]\\ \vdots & & & \vdots\\ h[N-3] & \cdots & \cdots & h[N-P]\\ h[N-2] & h[N-3] & \cdots & h[N-P+1]\end{pmatrix}\cdot\begin{pmatrix}a_1\\ a_2\\ \vdots\\ a_P\end{pmatrix}$$

$$\underline{\mathbf{h}} = -\mathbf{H}\underline{\mathbf{a}}$$
$$\underline{\mathbf{a}} = -\left(\mathbf{H}^{-1}_{pseudo}\right)\underline{\mathbf{h}}$$

There are several ways to determine the pseudo inverse ($\mathbf{H}^{-1}_{pseudo}$). One of the better methods involves using a singular value decomposition of the matrix:

$$\mathbf{H} = \mathbf{U}\mathbf{S}\mathbf{V}^T \quad \text{with} \quad \mathbf{U}^T\mathbf{U} = \mathbf{V}\mathbf{V}^T = \mathbf{I}$$
$$\mathbf{H}^{-1}_{pseudo} = \mathbf{V}\mathbf{S}^{-1}\mathbf{T}$$

The MatLab 'left slash' routine gives a is the solution in the least squares sense to the this overdetermined system of equations.

The MA parameters can be found in a similar way. Using (3-2) ($h[n]$ is zero for n<0), the values at $n=0$, to $n=Q$ can be determined:

$$\hat{h}[n]+a_1\hat{h}[n-1]+a_2\hat{h}[n-2]+\cdots+a_P\hat{h}[n-P]\Big|_{n=0} = \hat{h}[0] = h[0]$$
$$\hat{h}[n]+a_1\hat{h}[n-1]+a_2\hat{h}[n-2]+\cdots+a_P\hat{h}[n-P]\Big|_{n=1} = h[1]+a_1h[0]$$
$$\vdots$$
$$\hat{h}[n]+a_1\hat{h}[n-1]+a_2\hat{h}[n-2]+\cdots+a_P\hat{h}[n-P]\Big|_{n=P} = a_Ph[P]+a_{P-1}h[P-1]+\cdots+h[0]$$

and

$$b_0\delta[n]+b_1\delta[n-1]+b_2\delta[n-1]+\cdots b_Q\delta[n-Q]\Big|_{n=0} = b_0$$
$$b_0\delta[n]+b_1\delta[n-1]+b_2\delta[n-1]+\cdots b_Q\delta[n-Q]\Big|_{n=1} = b_1$$
$$\vdots$$
$$b_0\delta[n]+b_1\delta[n-1]+b_2\delta[n-1]+\cdots b_Q\delta[n-Q]\Big|_{n=Q} = b_Q$$

Concluding, these 2 expressions could be reformulated in a matrix expression, and the coefficients from the nominator polynomial could be calculated:

$$\begin{pmatrix} b_0 \\ b_1 \\ \vdots \\ b_P \end{pmatrix} = \begin{pmatrix} h[0] & 0 & \cdots & 0 \\ h[1] & h[0] & & 0 \\ \vdots & \vdots & \ddots & 0 \\ h[P] & h[P-1] & \cdots & h[0] \end{pmatrix} \begin{pmatrix} 1 \\ a_1 \\ \vdots \\ a_P \end{pmatrix}$$

$$\underline{\mathbf{b}} = \mathbf{K}\underline{\mathbf{a}}$$

The Prony algorithm is quite simple, but has some disadvantages. The approximation of the denominator polynomial is based on the 'tail', the last N-Q samples of the measured room impulse responses. In our case, 2/3 of the total amount of degrees of freedom are necessary and therefore Q is around 1/3 of the length of the impulse response. This means that this tail is 2/3 of the total length of the impulse response. 1/3 of the total available information is simply 'thrown away'. Hence, it is desirable that a lot of dynamically behavior of the unknown system (the room) is still present after 1/3 of this impulse response. This is no problem for poles located near the unity circle. Poles present in the measured room impulse response, located to far from this unity circle will due to this method, not be modeled.

Furthermore, to extract the poles from the denominator polynomial leads (probably) to numerical problems due to the high order of this polynomial (see 3.5.1).

3.3.2 An iterative Prony method

The discussed iterative Prony procedure [17] starts with a set of initial poles. These initial poles can be obtained by the 'normal' Prony procedure. An IIR model can be expressed in the Z-domain as:

$$\hat{H}(z)=\frac{\hat{B}(z)}{\hat{A}(z)}=\frac{\hat{b}_0+\hat{b}_1z^{-1}+\cdots+\hat{b}_Qz^{-Q}}{1+\hat{a}_1z^{-1}+\cdots+\hat{a}_Pz^{-P}}=\frac{c_1}{1-z_1z^{-1}}+\frac{c_2}{1-z_2z^{-1}}\cdots\frac{c_P}{1-z_Pz^{-1}}\quad\text{with}\quad P>Q$$

This expression can be transformed in order to obtain the impulse response of the model:

$$\hat{h}[n]=c_1z_1^n+c_2z_2^n+c_3z_3^n+\cdots c_Pz_P^n$$

The poles of the system can be found by taking the roots of the polynomial This expression can be cast into a matrix expression.

$$\begin{pmatrix}1 & 1 & \cdots & 1\\ z_1 & z_2 & \cdots & z_P\\ z_1^2 & z_2^2 & \cdots & z_P^2\\ z_1^3 & \vdots & & \vdots\\ \vdots & \vdots & & \vdots\\ z_1^{N-1} & z_2^{N-1} & \cdots & z_P^{N-1}\end{pmatrix}\cdot\begin{pmatrix}c_1\\ c_2\\ \vdots\\ c_P\end{pmatrix}=\begin{pmatrix}\hat{h}[0]\\ \hat{h}[1]\\ \hat{h}[2]\\ \hat{h}[3]\\ \vdots\\ \hat{h}[N-1]\end{pmatrix}$$

$$\mathbf{R}\,\underline{\mathbf{c}}=\underline{\hat{\mathbf{h}}}$$

Where R is called a Van der Monde matrix. In the first iteration, the coefficient vector $\underline{\mathbf{c}}$ can be resolved in least square sense:

$$\underline{\hat{\mathbf{h}}} = \left(\mathbf{R}^{-1}_{pseudo}\right)\underline{\mathbf{c}}$$

In this expression, $\mathbf{R}^{-1}_{pseudo}$ is again a pseudo inverse.

The measured room impulse response vector $\underline{\mathbf{h}}$ can now be written as a sum of an equation error vector and the approximated impulse response $\underline{\hat{\mathbf{h}}}$.

$$\underline{\mathbf{h}} = \underline{\hat{\mathbf{h}}} + \underline{\mathbf{e}}$$
$$\mathbf{R}\,\underline{\mathbf{c}} = \underline{\hat{\mathbf{h}}}$$

The matrix $\mathbf{R}$ is a function of a root vector $\underline{\mathbf{r}}$.

$$\underline{\mathbf{r}} = \left(\Re\{z_1\} \;\; \Re\{z_2\} \;\; \cdots \;\; \Re\{z_P\} \;\; \Im\{z_1\} \;\; \Im\{z_2\} \;\; \cdots \;\; \Im\{z_P\}\right)^t$$

The error can be minimized. A scalar function Q can be introduced, depending on the vector $\underline{\mathbf{r}}$. This scalar expresses the error in *one* quantity Q. In order to do so, the above expression can be rewritten as:

$$\underline{\mathbf{e}} = \underline{\mathbf{h}} - \mathbf{R}\,\underline{\mathbf{c}}$$
$$Q(\underline{\mathbf{r}}) = \underline{\mathbf{e}}^h\underline{\mathbf{e}} = \left(\underline{\mathbf{h}} - \mathbf{R}\,\underline{\mathbf{c}}\right)^h\left(\underline{\mathbf{h}} - \mathbf{R}\,\underline{\mathbf{c}}\right)$$

To minimize this function an expression as function of $\underline{\mathbf{r}}$ has to be found, i.e. in the neighborhood of $\underline{\mathbf{r}}$. Hence, the behavior of the function $Q\left(\underline{\mathbf{r}} + \underline{\boldsymbol{\delta}}\right)$ is approximated by a kind of power series. This is the first step in the Marquardt algorithm. The expression for the approximation in the k^{th} iteration is given by:

$$Q\left(\underline{\mathbf{r}}^{(k)} + \underline{\boldsymbol{\delta}}\right) \approx q^{(k)}\left(\underline{\boldsymbol{\delta}}\right) = Q\left(\underline{\mathbf{r}}^{(k)}\right) + \underline{\mathbf{g}}^{(k)T}\underline{\boldsymbol{\delta}} + \frac{1}{2}\underline{\boldsymbol{\delta}}^T\mathbf{H}^{(k)}\underline{\boldsymbol{\delta}} \qquad (3\text{-}3)$$

In this expression, $\underline{\mathbf{g}}^{(k)}$ and $\mathbf{H}^{(k)}$ are respectively the gradient and Hessian matrix. The expressions for these matrices can be found in Appendix III. Because it is also possible to evaluate $Q\left(\underline{\mathbf{r}}^{(k)} + \underline{\boldsymbol{\delta}}\right)$, it is simply possible to verify whether the approximation is accurate enough.

The step $\underline{\boldsymbol{\delta}}$ can be determined by a modified Newton algorithm:

$$\left(\mathbf{H}^{(k)} + \upsilon^{(k)}\mathbf{I}\right)\underline{\boldsymbol{\delta}} = -\underline{\mathbf{g}}^{(k)}$$

In this expression, $\upsilon^{(k)}$ is a small positive constant determined by the accurateness of the approximation $q^{(k)}\left(\underline{\boldsymbol{\delta}}\right)$. The step $\underline{\boldsymbol{\delta}}$ has to point in the direction of the minimum,

that is, against the gradient. Hence, the inner product $\langle \underline{\mathbf{g}}^{(k)}, \underline{\delta} \rangle$ must satisfy the following relation:

$$\langle \underline{\mathbf{g}}^{(k)}, \underline{\delta} \rangle < 0$$
$$\Leftrightarrow \underline{\delta}^t \left(-\underline{\mathbf{g}}\right) > 0$$
$$\Leftrightarrow \underline{\delta}^t \left(\mathbf{H}^{(k)} + \upsilon^{(k)}\mathbf{I}\right)\underline{\delta} > 0$$

This implies that $\left(H^{(k)} + \upsilon^{(k)}\mathbf{I}\right)$ has to be positive definite.

The accurateness can be expressed in a quantity $\rho^{(k)}$.

$$\rho^{(k)} = \frac{Q\left(\underline{\mathbf{r}}^{(k)}\right) - Q\left(\underline{\mathbf{r}}^{(k)} + \underline{\delta}^{(k)}\right)}{Q\left(\underline{\mathbf{r}}^{(k)}\right) - q^{(k)}\left(\underline{\delta}^{(k)}\right)}$$

The approximation is accurate when $\rho^{(k)}$ is in the neighborhood of one.

The Marquardt algorithm can now be summarized:

1. Determine initial value of r.
2. Calculate $\left(H^{(k)} + \upsilon^{(k)}\mathbf{I}\right)$, if this is not positive definite, increase $\upsilon^{(k)}$ (for example: $\upsilon^{(k)} = 4\upsilon^{(k)}$).
3. Calculate the step $\underline{\delta}$: $\underline{\delta} = -\left(\mathbf{H}^{(k)} + \upsilon^{(k)}\mathbf{I}\right)^{-1}\underline{\mathbf{g}}^{(k)}$
4. Evaluate the approximation of (3-3)
5. If $\rho^{(k)} < \alpha$ then $\upsilon^{(k+1)} = 4\upsilon^{(k)}$,
   if $\alpha \le \rho^{(k)} < \beta$ then $\upsilon^{(k+1)} = \upsilon^{(k)}$,
   if $\rho^{(k)} \ge \beta$ then $\upsilon^{(k+1)} = \frac{\upsilon^{(k)}}{2}$
   (for example: $\alpha = 0.25$ $\beta = 0.75$).
6. If $\rho^{(k)} < \alpha$, then $\underline{\mathbf{r}}^{(k+1)} = \underline{\mathbf{r}}^{(k)}$,
   else: $\underline{\mathbf{r}}^{(k+1)} = \underline{\mathbf{r}}^{(k)} + \underline{\delta}^{(k)}$.
7. Make an update step in the coefficients $\underline{\mathbf{c}}$, $\underline{\mathbf{c}} = \left(\mathbf{R}^{-1}\right)\underline{\mathbf{h}}$

3.3.3 The Steiglitz-McBride algorithm

In 1965 Steiglitz and McBride suggested an algorithm based on an equation error, to perform system identification [18]. This algorithm can be used to construct an ARMA model of the system, when a impulse response of the unknown system is available. The following figure depicts the calculation scheme for the Steiglitz-McBride. In this scheme, the variable q is the unit advance operator.

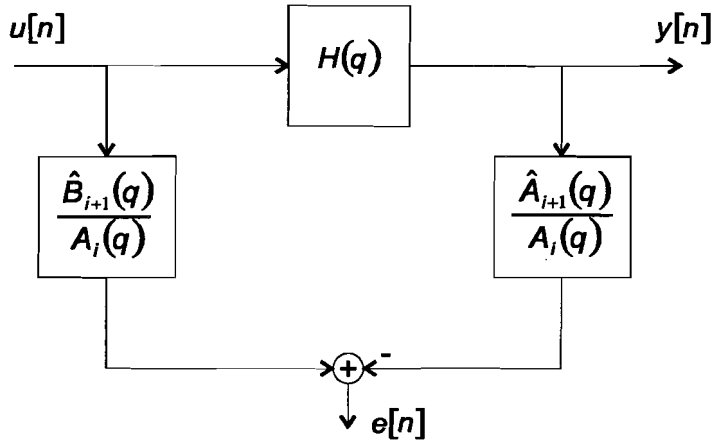

Figure 3-4: *The Steiglitz-McBride calculation scheme (time domain)*

In the iteration procedure the equation

$$\frac{\hat{A}_{i+1}(q)}{\hat{A}_i(q)} = \frac{a_{1i+1}q + a_{2i+1}q^2 + \cdots + a_{Pi+1}q^P}{a_{1i}q + a_{2i}q^2 + \cdots + a_{Pi}q^P}$$

will tend to 1. After some iterations, when this equation tends to 1, $e[n]$ is approximately equal to the output error. During the iteration process, the progress can be indicated by the following expression:

$$e_{eq\,i+1} = \sum_{p=1}^{P}\left(a_{p\,i+1} - a_{p\,i}\right)^2$$

If this $e_{eq\,i+1}$ is small enough, the model satisfies the output error model.

The expression for the output error is given by:

$$\sum_{n=0}^{N-1} e^2[n] = \sum_{n=0}^{N-1}\left(\hat{B}_{i+1}(q)\frac{u[n]}{\hat{A}_i(q)} + \hat{A}_{i+1}(q)\frac{y[n]}{\hat{A}_i(q)}\right) = \sum_{n=0}^{N-1}\left(\hat{B}_{i+1}(q)u_i[n] + \hat{A}_{i+1}(q)y_i[n]\right)^2$$

With $u_i[n]$ and $y_i[n]$ filtered versions $u[n]$ and $y[n]$. This expression can be written as a vector equation.

$$\underline{\theta}_{i+1} = \begin{pmatrix} a_{1,i+1} & a_{2,i+1} & \cdots & a_{P,i+1} & b_{0,i+1} & b_{1,i+1} & \cdots & b_{Q,i+1} \end{pmatrix}^T$$

$$\underline{\varphi}_i[n] = \begin{pmatrix} -y_i[n-1] & -y_i[n-2] & \cdots & -y_i[n-P] & u_i[n] & u_i[n-1] & \cdots & u_i[n-Q] \end{pmatrix}^T$$

$$J = \sum_{n=0}^{N-1} e^2[n] = \sum_{n=0}^{N-1} \left(y[n] - \underline{\varphi}_i^T[n]\, \underline{\theta}_{i+1} \right)^2$$

This expression can be simplified:

$$J = \sum_{n=0}^{N-1} \left(y[n] - \underline{\theta}_{i+1}^T\, \underline{\varphi}_i[n] \right) \left(y[n] - \underline{\varphi}_i^T[n]\, \underline{\theta}_{i+1} \right)$$

$$J = \sum_{n=0}^{N-1} y^2[n] - \underline{\theta}_{i+1}^T \left\{ \sum_{n=0}^{N-1} \underline{\varphi}_i[n] y[n] \right\} + \left\{ \sum_{n=0}^{N-1} \underline{\varphi}_i^T[n] y[n] \right\} \underline{\theta}_{i+1} + \underline{\theta}_{i+1}^T \left\{ \sum_{n=0}^{N-1} \varphi_i[n] \underline{\varphi}_i^T[n] \right\} \underline{\theta}_{i+1}$$

$$J = \sum_{n=0}^{N-1} y^2[n] - \underline{\theta}_{i+1}^T\, \underline{\mathbf{R}}_{\varphi y} - \underline{\mathbf{R}}_{\varphi y}^T\, \underline{\theta}_{i+1} + \underline{\theta}_{i+1}^T\, \mathbf{R}_{\varphi\varphi}\, \underline{\theta}_{i+1}$$

$$J = \sum_{n=0}^{N-1} y^2[n] - 2\, \underline{\theta}_{i+1}^T\, \underline{\mathbf{R}}_{\varphi y} + \underline{\theta}_{i+1}^T\, \mathbf{R}_{\varphi\varphi}\, \underline{\theta}_{i+1}$$

In this expression the matrix $\mathbf{R}_{\varphi\varphi}$ and the vector $\underline{\mathbf{R}}_{\varphi y}$ are given by:

$$\mathbf{R}_{\varphi\varphi} = \sum_{n=0}^{N-1} \underline{\varphi}_i[n] \underline{\varphi}_i^T[n] = \begin{pmatrix} \sum_{n=0}^{N-1} \varphi_{i,1}[n]\varphi_{i,1}[n] & \sum_{n=0}^{N-1} \varphi_{i,1}[n]\varphi_{i,2}[n] & \cdots & \sum_{n=0}^{N-1} \varphi_{i,1}[n]\varphi_{i,P+Q+1}[n] \\ \sum_{n=0}^{N-1} \varphi_{i,2}[n]\varphi_{i,1}[n] & \sum_{n=0}^{N-1} \varphi_{i,1}[n]\varphi_{i,1}[n] & & \vdots \\ \vdots & & \ddots & \vdots \\ \sum_{n=0}^{N-1} \varphi_{i,P+Q+1}[n]\varphi_{i,1}[n] & \cdots & \cdots & \sum_{n=0}^{N-1} \varphi_{i,1}[n]\varphi_{i,1}[n] \end{pmatrix} \tag{3-4a}$$

$$\underline{\mathbf{R}}_{\varphi y} = \sum_{n=0}^{N-1} \underline{\varphi}_i[n] y[n] = \begin{pmatrix} \sum_{n=0}^{N-1} \varphi_{i,1}[n] y[n] \\ \sum_{n=0}^{N-1} \varphi_{i,2}[n] y[n] \\ \vdots \\ \sum_{n=0}^{N-1} \varphi_{i,P+Q+1}[n] y[n] \end{pmatrix} \tag{3-4b}$$

The parameter vector $\underline{\theta}_{i+1}$, at which J is minimal, are given by the normal equation. The normal equation can be obtained by taking the derivative of the above expression.

$$\frac{\partial J}{\partial\, \underline{\theta}_{i+1}} = -2\, \underline{\mathbf{R}}_{\varphi y} + 2\, \mathbf{R}_{\varphi\varphi}\, \underline{\theta}_{i+1} = \mathbf{0}$$

Leading to:

$$\underline{\theta}_{i+1} = \mathbf{R}_{\varphi\varphi}^{-1}\, \underline{\mathbf{R}}_{\varphi y} \tag{3-5}$$

The matrix $\mathbf{R}_{\varphi\varphi}$ and the vector $\underline{\mathbf{R}}_{\varphi y}$ can be calculated each iteration. After that the new $u_{i+1}[n]$ and $y_{i+1}[n]$ can be obtained by filtering $u_i[n]$ and $y_i[n]$.

3.4 Comparing the modeling methods.

Now three modeling methods are discussed, and a synthetic model of a room is available, the opportunity arises to compare the performance of the modeling methods. The impulse response of the synthetic model is called $h_s[n]$.

When a denominator polynomial is found with the aid of a certain method x out of this synthetic impulse response $h_s[n]$, the roots can be taken to find the model pole set. With these poles, a Kautz filter bank can be constructed. Each Kautz function is generated by each pole in the model pole set (see chapter 4).

The weights $w_{1\Phi}$ - $w_{N\Phi}$ and $w_{1\Psi}$ - $w_{2\Psi}$ (Figure 4-1) can be found by taking the inner product between the corresponding Kautz function and the impulse response from the synthetic model $h_s[n]$:

$$w_{i\Phi} = \left\langle \Phi_i[n], h_s[n] \right\rangle \text{ and } w_{i\Psi} = \left\langle \Psi_i[n], h_s[n] \right\rangle \quad i = 1.....P$$

For simplicity reasons, the Kautz functions are now not longer separated into complex pairs. This results in:

$$\Theta_{2i}[n] = \Phi_i[n] \text{ and } \Theta_{2i+1}[n] = \Psi_i[n] \quad i = 1.....2P$$
$$\Rightarrow w_{2i} = w_{i\Phi} \text{ and } w_{2i+1} = w_{i\Psi} \quad i = 1.....2P$$
$$\Rightarrow w_i = \left\langle \Theta_i[n], h_s[n] \right\rangle$$

The Kautz filter bank functions now as a model belonging to method x. The impulse response of this Kautz filter bank is called $h_x[n]$ and is an approximation for the impulse response of the synthetic model $h_s[n]$.

$$h_x[n] = \sum_{i=1}^{P} w_i \Theta_i[n]$$

Assume that an indefinite number of Kautz functions form a complete basis, with the aid of which it is possible to describe arbitrary decaying signals on the positive time axis. The impulse response of the synthetic model can now be written as a truncated summation of weighted Kautz functions $h_x[n]$ and the remainder, an indefinite summation of weighted Kautz functions.

$$h_s[n] = h_x[n] + h_{un}[n] = \sum_{i=1}^{2P} w_i \Theta_i[n] + \sum_{i=2P+1}^{\infty} w_i \Theta_i[n]$$

With $h_{un}[n]$ the unmodeled part. The performance of an algorithm can now be expressed as:

$$RME = \left(1 - \frac{\sum_{n=0}^{N-1} \left(h_{un}[n]\right)^2}{\sum_{n=0}^{N-1} \left(h_s[n]\right)^2} \right) \cdot 100\ \%$$

with *RME,* the Relative Modeled Energy. This expression can be written out:

$$RME = \frac{\sum_{n=0}^{\infty} \left(h_s[n]\right)^2 - \sum_{n=0}^{\infty} \left(h_s[n] - h_x[n]\right)^2}{\sum_{n=0}^{\infty} \left(h_s[n]\right)^2} 100\% = \frac{2\sum_{n=0}^{\infty} h_s[n]h_x[n] - \sum_{n=0}^{\infty} h_x[n]}{\sum_{n=0}^{\infty} \left(h_s[n]\right)^2} 100\%$$

Replacing the approximation by the Kautz series:

$$RME = \frac{2\sum_{i=1}^{2P} w_i \sum_{n=0}^{\infty} h_s[n]\Theta_i[n] - \sum_{i=1}^{2P}\sum_{j=1}^{2P} w_j w_i \sum_{n=0}^{\infty} \Theta_i[n]\Theta_j[n]}{\sum_{n=0}^{\infty} \left(h_s[n]\right)^2} 100\%$$

And now recognizing the inner product and making use of the orthonormality of the Kautz functions:

$$\sum_{n=0}^{\infty} h_s[n]\Theta_i[n] = \left\langle h_s[n], \Theta_i[n] \right\rangle = w_i \Rightarrow 2\sum_{n=0}^{\infty} h_s[n] \sum_{i=1}^{2P} w_i \Theta_i[n] = 2\sum_{n=0}^{\infty} w_i^2$$

$$\sum_{n=0}^{\infty} \Theta_i[n]\Theta_j[n] = \delta_{ij} \Rightarrow \sum_{n=0}^{\infty} h_x^2[n] = \sum_{i=1}^{2P}\sum_{j=1}^{2P} w_j w_i \sum_{n=0}^{\infty} \Theta_i[n]\Theta_j[n] = \sum_{i=1}^{2P} w_i^2$$

leads to:

$$RME = \frac{\sum_{i=1}^{2P} w_i^2}{\sum_{n=0}^{N-1} h_s^2[n]} 100\ \%$$

where use has been made that a limited impulse response of N samples is generated. Outside this interval $h_s[n]$ is zero.

To test the modeling methods, each run a 20th order model is generated. Without the addition of noise, all methods are capable of finding the exact poles. By subsequently adding more noise to the generated model (see paragraph 3.2), it is possible to notice some differences between the three methods.

To start the modeling methods in a fair and comparable way, the denominator polynomial of the Prony method is used as initial denominator for the Steiglitz-McBride method.

The performance of the algorithms differs significantly for each generated model, although the same noise level is used. Hence, each noise level is tested five times (with new models), for all three modeling methods. Figure 3-5 displays the standard deviations for each test method. The results can be found in [Appendix II B].

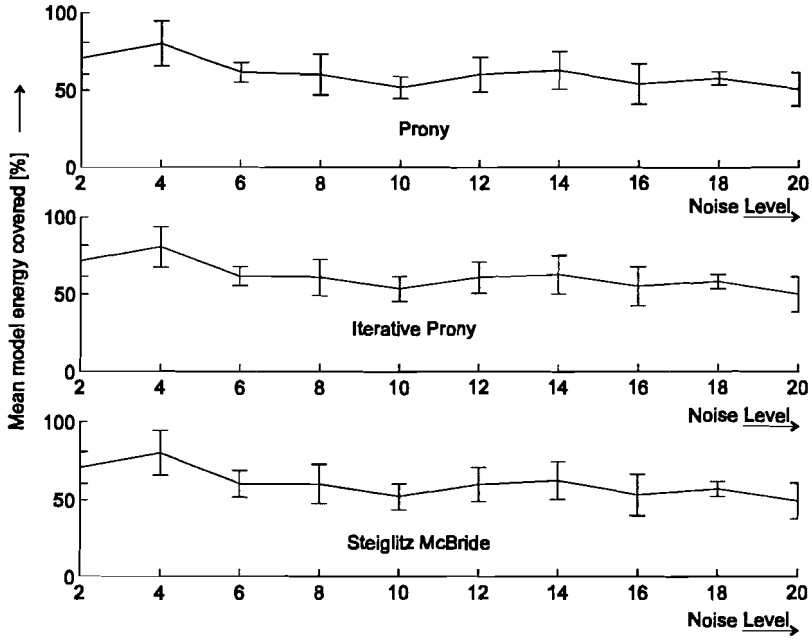

Figure 3-5: *The mean performance and standard deviations for 3 tested methods*

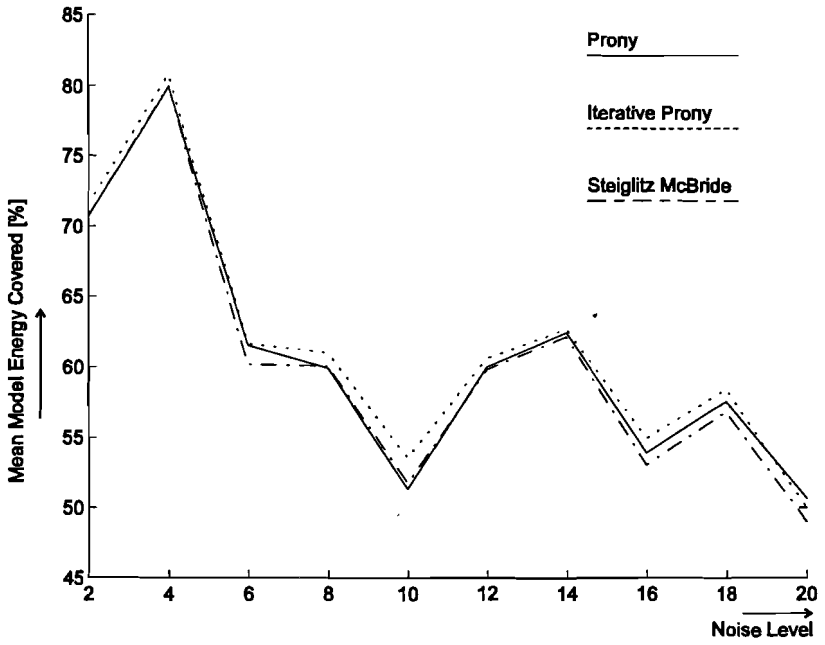

Figure 3-6: *Mean Relative modeled energy [%] for three tested methods*

From Figure 3-6 can be concluded that the Iterative Prony method performs slightly better than the Steiglitz-McBride and Prony methods. This can perhaps better be concluded from Appendix II B, where in almost every calculation, the Iterative Prony method performs better. Curious in this respect is the Steiglitz-McBride algorithm. This algorithm performs slightly worse than the 'ordinary' Prony method. Especially when one considers that this method starts with the Prony denominator polynomial. Assumed is that one of the major cause contributing to this effect is the 'head', i.e. the first samples of the model are responsible for this effect.

A higher order model does not automatically contribute to a better relative modeled energy percentage. This is demonstrated in Appendix II A, where models are used based on 20 poles and a noise addition of a factor N 2 to 20 [see paragraph 3.2]. For each order and each noise level, a new model is generated and the three methods are tested. A higher order model can contribute to a higher signal energy covered, see for example table entries 'noise level 4' and 'approximation order 26', but this is not necessary, table entries 'noise level 4' and 'approximation order 28'.

The question arises if this error criterion (relative modeled energy) is correct. Most of the energy in the model is present in the 'head' i.e. the first samples of the impulse response. This suggests that a Prony method would perform better, simply because the (MA) parameters model this 'head' perfectly.

The question: 'Is this error criterion correct?' is difficult to answer. It depends heavily on the implementation of the application. Until more investigation is carried out on this subject, it is the best criterion available. Therefore this criterion is maintained during the remainder of this report.

The Steiglitz-McBride algorithm performs in general a bit worse than the other methods. Because it is a well documented method and because the ability to reformulate this method, it is used to compare the subband methods discussed in the following paragraph.

3.5 Reducing the calculation requirements with a subband method.

3.5.1 Introduction

As discussed in the introduction, the mentioned methods to find an IIR model, depend either on a large Van der Monde matrix or a numerical procedure to find the roots of a polynomial. This means, that large bad conditioned matrices are created or a 'roots command' is used to calculate roots from polynomials order six hundred or higher. Therefore, in first instance, an attempt has been made to split up the problem in smaller ones. This cannot be done in the time domain, because 'the information' for exponentially damped oscillations is present over the complete time range of 2048 samples.

To calculate the roots of a polynomial, use can be made of the Newton method. A Newton method (or similar method) is based on successive substitution in a polynomial $p(x_i)$. This implies that each iteration, a new value for x_i has to be calculated. The calculation scheme is given by:

$$x_{i+1} = x_i + \frac{p(x_i)}{p'(x_i)}$$

This means that this polynomial has to be evaluated each iteration. The polynomial $p(x_i)$ is given by:

$$p(x_i) = c_N x_i^N + c_{N-1} x_i^{N-1} + \cdots + c_i x_1 + c_0$$

If $|x_i| << 1$ then x_i^N could well be exceeding the floating point resolution. For example, $0.75^{600} = 1.088\ 10^{-75}$.

In this case, where the radius of the roots is expected to be around 0.9983 (Paragraph 3.2) it might be possible that a root location procedure is accurate enough. This deserves attention, however, it is not certain that the majority of the poles is located around this radius. Besides, root finding algorithms are computer power demanding. It is therefore desirable to investigate other methods, which are less computer power demanding.

When a time domain solution doesn't satisfy our requirements, it is perhaps a logic step to switch to the frequency domain for a solution. In Figure 3-7 one can notice the effect of a pole with radius 0.95 and angle 0.25π.

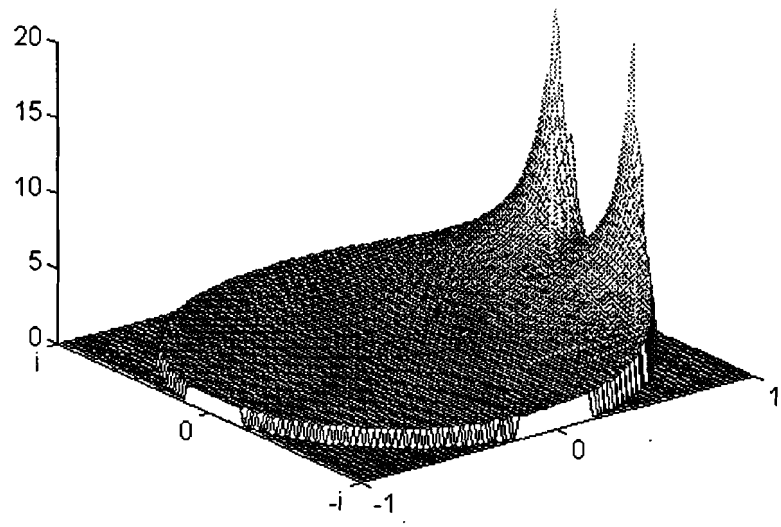

Figure 3-7: $|H(z)|^2$ *With poles at* $0.95e^{j0.25\pi}$ *and* $0.95e^{-j0.25\pi}$

The unit circle represents the Fourier transform and should be evaluated from 0 (corresponding to 0) to π (corresponding to 0.5 f_s). If the majority of the effect of the pole can be appointed to one small frequency band, it should be possible to split the signal in frequency bands.

Assume a pole is located at $a = |a|e^{j\varphi_a}$, with $|a|$ the modulus of the pole, and φ_a the argument of the pole. The effect of the pole on the frequency behavior can perhaps best be described by the characteristics of a band pass filter. Thus, the transfer function is evaluated at $|z| = 1$.

$$H(z) = \frac{b}{1 - az^{-1}}\bigg|_{|z|=1} = \frac{b}{1 - |a|e^{j\varphi_a}e^{-j\Omega}}$$

Now the transfer function is evaluated on the unity circle, the 3 [dB] bandwidth can be determined.

$$\left|H\left(e^{j\Theta_{3dB}}\right)\right| = \frac{1}{2}\left|H\left(e^{j\varphi_a}\right)\right|$$

The modulus of the transfer function at $\Omega = \varphi_a$ is given by:

$$\left|H\left(e^{j\varphi_a}\right)\right| = \frac{|b|}{\left|1 - |a|e^{j\varphi_a}e^{-j\varphi_a}\right|} = \frac{|b|}{1 - |a|}$$

Take $B = 2\left(\varphi_a - \Theta_{3dB}\right)$. The above expression can then be rewritten as:

$$\frac{|b|}{\left|1 - |a|e^{j\varphi_a}e^{-j\Theta_{3dB}}\right|} = \frac{|b|}{\left|1 - |a|e^{j\frac{B}{2}}\right|} = \frac{1}{2}\frac{|b|}{1 - |a|}$$

$$\Leftrightarrow \left|1 - |a|e^{j\frac{B}{2}}\right| = \left|1 - |a|\cos\left(\tfrac{1}{2}B\right) - j|a|\sin\left(\tfrac{1}{2}B\right)\right| = 2\left(1 - |a|\right)$$

$$\Leftrightarrow \sqrt{\left(1 - |a|\cos\left(\tfrac{1}{2}B\right)\right)^2 + |a|^2\sin^2\left(\tfrac{1}{2}B\right)} = 2\left(1 - |a|\right)$$

$$\Leftrightarrow 1 - 2|a|\cos\left(\tfrac{1}{2}B\right) + |a|^2 = 4\left(1 - |a|\right)^2$$

$$\cos(B) \approx 1 - \tfrac{1}{2}\left(\tfrac{1}{2}B\right)^2 \quad \text{when } |a| \approx 1$$

$$\Rightarrow |a|\left(\tfrac{1}{2}B\right)^2 = 4\left(1 - |a|\right)^2 - \left(1 - 2|a| + |a|\right) = 3\left(1 - |a|\right)^2$$

$$\Leftrightarrow B = \sqrt{\frac{12}{|a|}}\left(1 - |a|\right)$$

This demonstrates that a if the modulus $|a|$ is close enough to 1, the effect of the pole is confined to a limited band of width B. In the modeling of an acoustic impulse

response in a room with a reverberation time of 0.5 [s], the average modulus will be in the neighborhood of $|a| = 0.9983$. This is close enough to one for the above approximation. Thus, the average bandwidth $B = 5.98\ 10^{-3}$, and hence 525x2poles.

3.5.2 Subband method I: filtering

Assume the impulse response is Fourier transformed and divided in S subbands of R samples. The total length of the signal is N samples.

Consider the low pass band. This can be written as:

$$x_{LP}[n] = \frac{1}{N}\sum_{k=-N/2}^{N/2} X[k]U[k]e^{j\left(\frac{2\pi}{N}\right)kn} = \frac{1}{N}\sum_{k=-R/2}^{R/2} X[k]e^{j\left(\frac{2\pi}{N}\right)kn}$$

$$U[k] = \begin{cases} 1 & |k| \le R/2 \\ 0 & |k| > R/2 \end{cases}$$

With $X[k]$, $U[k]$ the N-point discrete Fourier transforms of $u[n]$ and $x[n]$. After this operation, the signal is decimated by a factor S. This can be achieved by defining a sequence $C_S[n]$ which is only equal to one, when S is a multiplication of n. This sequence can be written as a Fourier series, because it is periodic with S samples. This leads to the following expression:

$$C_S[n] = \frac{1}{S}\sum_{l=0}^{S-1} e^{j\frac{2\pi}{S}ln}$$

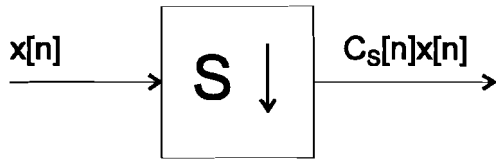

Figure 3-8: *Down sampler*

The decimated sequence $x_{LP}[n]\downarrow_S$ can then be written as follows:

$$x_{LP}[n]\downarrow_S = \frac{1}{N}\sum_{k=-R/2}^{R/2} X[k]e^{j\left(\frac{2\pi}{N}\right)kn}\frac{1}{S}\sum_{l=0}^{S-1} e^{j\left(\frac{2\pi}{S}\right)ln} = \frac{1}{NS}\sum_{k=-R/2}^{R/2}\sum_{l=0}^{S-1} X[k]e^{j2\pi\left(\frac{l}{N}+\frac{R}{S}\right)n}$$

This only leads to a solution only if:

$$\frac{k}{N} = -\frac{l}{S} \Leftrightarrow l = -\frac{kS}{N} = -\frac{k}{R}$$

Leading to the following expression for $x_{LP}[n]\downarrow_S$:

$$x_{LP}[n]\downarrow_S = \frac{1}{NS}\sum_{k=-R/2}^{R/2} X[k]e^{j2\pi\left(\frac{k}{R}\right)n} \tag{3-6}$$

Which is the R-point discrete Fourier transform. In the case of pass band signals, a demodulation has to be included to shift the pass band back to the low pass band. Concluding, this leads to the following operation:

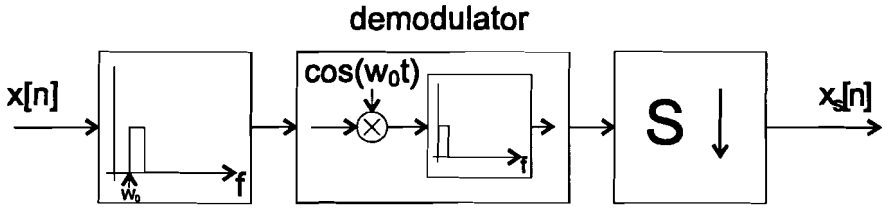

Figure 3-9: *Filter bandwidth R samples, S bands*

If we are able to reconstruct $x[n]$ from all $x_s[n]$ perfectly, it is possible to insert a (reduced) models in the reconstruction. A problem which arises is 'how to translate the model to the output'. Assume an up sampling is used to reconstruct the complete model.

The up sampling process can be described. This is done by first introducing the Z-transform of $x[n]$.

$$X_{up}(z) = \sum_{n=-\infty}^{\infty} x_{up}[n]z^{-n}$$

$$x_{up}[n] = \begin{cases} 0, & \text{if } n \neq kL \\ x[n], & \text{if } n = kL \end{cases}$$

$$\Leftrightarrow X_{up}(z) = \sum_{k=-\infty}^{\infty} x_{up}[kL]z^{-kL} = \sum_{k=-\infty}^{\infty} x[k]z^{-kL} = X(z^L)$$

De Steiglitz-McBride algorithm offers us the possibility to represent the signal as a polynomial. This polynomial is on it's turn can be written as a summation of first order sections.

$$X_u(z) = \frac{B(z)}{A(z)} = \frac{b_Q z^Q + b_{Q-1}z^{Q-1} + \cdots + b_1 z + b_0}{a_P z^P + a_{P-1}z^{P-1} + \cdots + a_1 z + 1} = \sum_{i=1}^{P} \frac{c_i}{1 - z_i z^{-1}}$$

When up-sampling, the signal then can be written as:

$$X_u(z^L) = \sum_{i=1}^{P} \frac{c_i}{1 - z_i z^{-L}} = \sum_{i=1}^{P} \sum_{j=1}^{L} \frac{c_{ij}}{1 - z_i j z^{-1}}$$

$$\text{with} \quad \frac{c_i}{1 - z_i z^{-L}} = \sum_{j=1}^{L} \frac{c_{ij}}{1 - z_{ij} z^{-1}}$$

The location of the new poles z_{ij} can now be calculated:

$$1 - z_i z^{-L} = 0, \quad z_i = a_i e^{j\phi_i}$$
$$\Rightarrow a_i e^{j\phi_i} z^{-L} = 1, \quad z^{-L} = a_i^{-1} e^{-j\phi_i + k*2\pi}$$
$$z_{ik} = a_i^{\frac{1}{L}} e^{j\left(\frac{\phi_i}{L} - \frac{k*2\pi}{L}\right)}$$

The summation in the previous leads to a repetition of 'pie-slices' in the Z-plane. Over the radius, a power operation is performed.

$$g(z) = f(z^L) = f\left(|a|^L e^{j\varphi L}\right) \tag{3-7}$$

The function $e^{j\varphi L}$ takes on the same values L times as $e^{j\varphi}$ traveling around a circle in the Z-plane. This is demonstrated in Figure 3-10,where a pole is located at $0.95e^{j0.25\pi}$, and it's complex conjugated value. The spectrum is sampled up a factor L=4. The result is depicted in Figure 3-11.

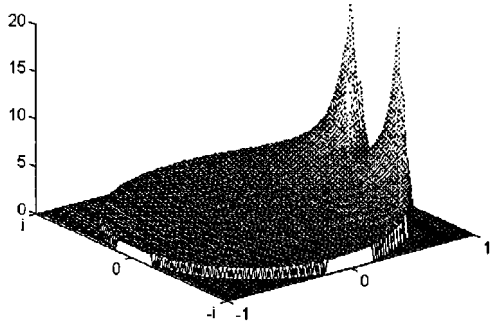

Figure 3-10

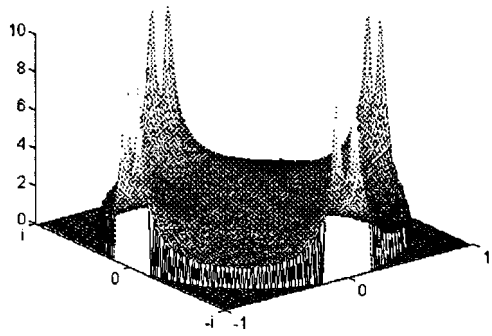

Figure 3-11

In general, the down sampling process expands the influence of a 'low pass pole' over the whole Z-plane. The up sampling process, compresses this result again to one low pass 'pie-slice', and repeats this 'pie-slice' over the whole Z-plane. Selecting the appropriate band is now simply a matter of selecting the matching 'pie-slice'. Thus, reconstruction is possible by means of up-sampling and selecting the appropriate band.

Implementation

To realize a subband method with the Steiglitz-McBride algorithm, a filter for selecting the s^{th} subband has to be designed. The filter must be FIR, because an IIR filter would add poles to the impulse response. If the FIR filter is designed with the aid of the 'windowing method' [19] the following problems are encountered:

1. In realizing such a filter we are bound to a limited time interval. Hence, the filter function has be windowed. When a window function is used, oscillations occur in the amplitude transfer function, and will be present in the stop and pass band. These oscillations are dependent on the size of the filter kernel (Gibbs phenomenon), and the window function. The amplitude of the oscillations can be reduced by choosing another window function. For example a Bartlett-, Hanning-, Kaiser-, Blackman- or Hamming window. These windows lead all to a broader transition from pass to stop band when compared with the step window. Therefore, using these windows will allways be a trade-off.

2. The filter function has to be made causal. This means, including a delay in the impulse response of the transfer function. This delay causes a filtered measured acoustic impulse response to have a delay. This can cause problems when modeling this signal with an ARMA model. The (non orthogonal) basis functions have to cancel each other at the start of the impulse response.

Figure 3-12 depicts the constructing of a band pass filter and the demodulating of this pass band.

Figure 3-12a depicts the transfer function of the band pass filter. This function was obtained by taking a 128 points DFT of the 128 points impulse response of the band pass filter. Sample 128 corresponds to 2π.

In the demodulation process, this function is multiplied by a cosine function. This multiplication invokes a mirror image of the band pass function to shift in the range. Figure 3-12b depicts this effect. The transfer function is obtained by demodulating the (256 points) impulse response of the band pass filter, and taking a 256 point DFT. Sample 256 corresponds to 2π.

In Figure 3-12d the result filter transfer function is depicted, after low pass filtering with Figure 3-12c.

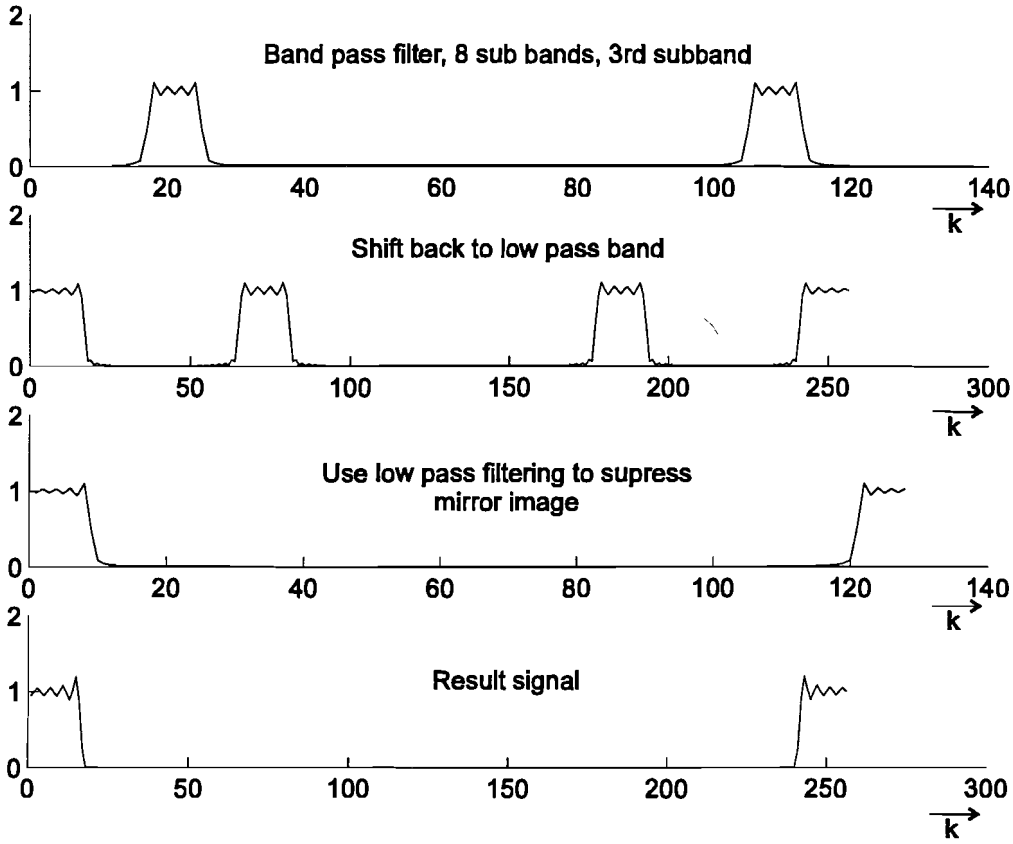

Figure 3-12: *Constructing a filter bank. From above to beneath: figure 5a - 5d*

To test the 'effectiveness' of the algorithm, a impulse response of the synthetic model (see Paragraph 3.2) from which the poles are known can be applied to the algorithm. This impulse response is of order 51 (50 poles, 25 complex conjugated pairs) and *not* distorted by noise. This model room impulse response is depicted in Figure 3-13.

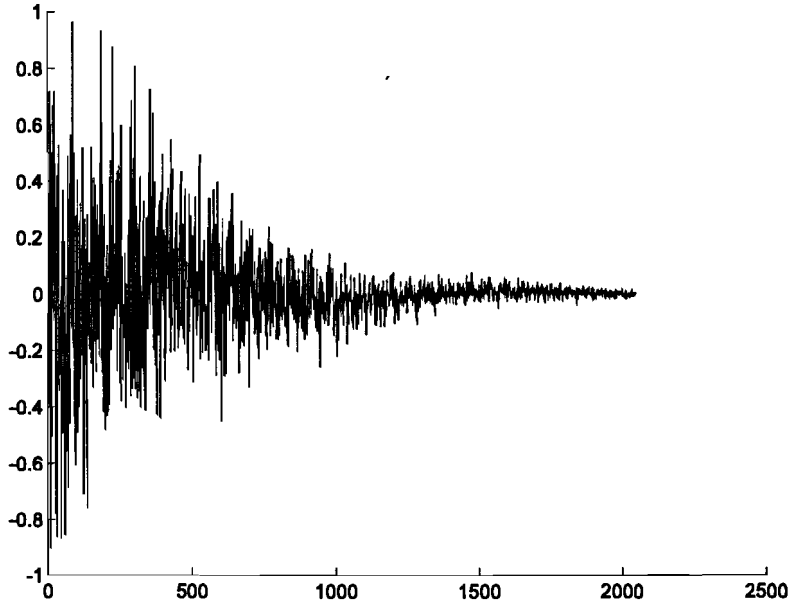

Figure 3-13: *Modeled impulse response*

To demonstrate the algorithm, 8 subbands are used. and Figure 3-13 depicts the down sampled impulse response of the third subband.

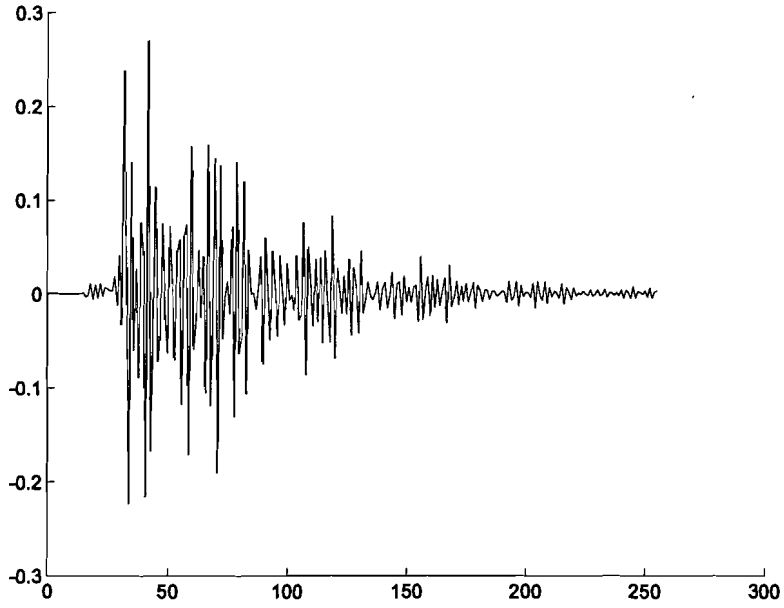

Figure 3-14: *Decimated signal, subband 3*

On each demodulated subband, the Steiglitz-McBride (10 iterations) algorithm is performed. After transforming the poles back according to (3-7) the found poles should approximate the poles in the model. The result (pole location of the original and of the approximation) is depicted in Figure 3-15.

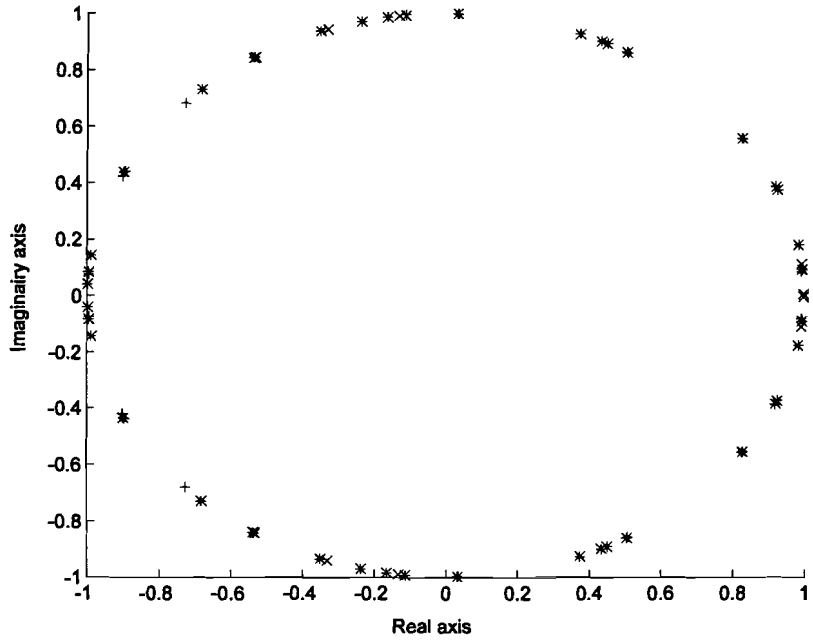

Figure 3-15: *Pole location, x - original and + - approximation*

The algorithm is capable of covering 64,19 % (*RME*) of the energy in the original impulse response. This is not enough, certainly not considering the fact that no noise was added to the model. A part of the impulse responses of both the model and the approximation are plot in Figure 3-16.

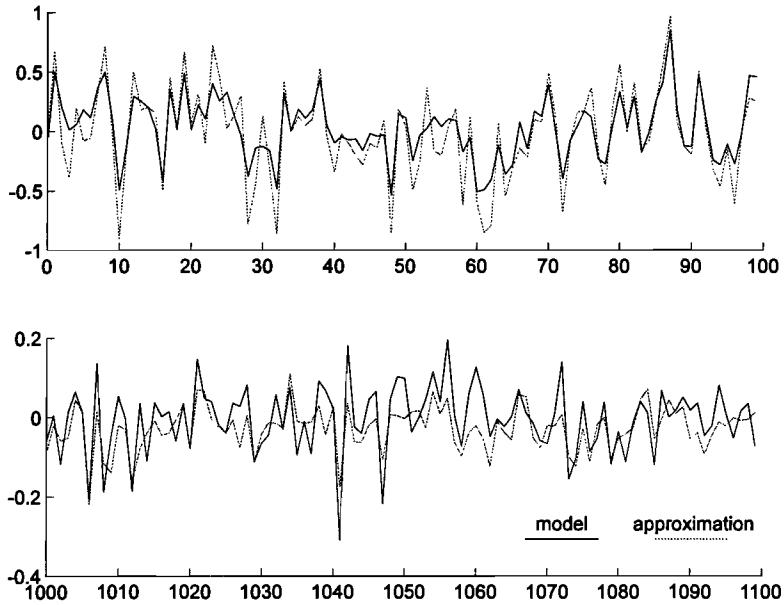

Figure 3-16: *Some samples of the impulse responses of the original and approximation*

This algorithm, based on a subband method in the time domain, does not suffice the requirements. This can be blamed on several causes. Possible causes are:

1. The Gibbs-effect. Oscillations in the pass band invoke non allowable distortions in the signal. The Steiglitz-McBride algorithm tries to model these distortions, resulting in deviating pole locations.

2. Insufficient suppression in the stop bands. Information from near subbands enters the current subband.

3. The Steiglitz-McBride algorithm is not capable of placing poles just outside the subband, although this may yield a better solution. These poles can later on be disposed, because they are most likely also found in one of the surrounding subbands.

4. The algorithm has problems with the delay introduced to make the filter causal.

3.5.3 Subband method II: Approximating integrals in the frequency domain

Considering the Steiglitz-McBride algorithm it is also possible to define a equation error criterion in the frequency domain. Depicted in Figure 3-4 is the calculation scheme. The Steiglitz-McBride algorithm is an iterative algorithm which tries to

minimize the an error criterion. In the regular Steiglitz-McBride algorithm this equation error is defined as:

$$\sum_{n=0}^{N-1} e^2[n]$$

with N the length of the measured impulse response. This equation error criterion can be written as an integral in the (continuous) frequency domain, minimizing the amplitude of the transformed error signal. Note that the phase is not taken into consideration. Thus, this new criterion can be defined as:

$$\int_{\Omega_0}^{\Omega_1} \left| E\left(e^{j\Omega}\right) \right|^2 d\Omega$$

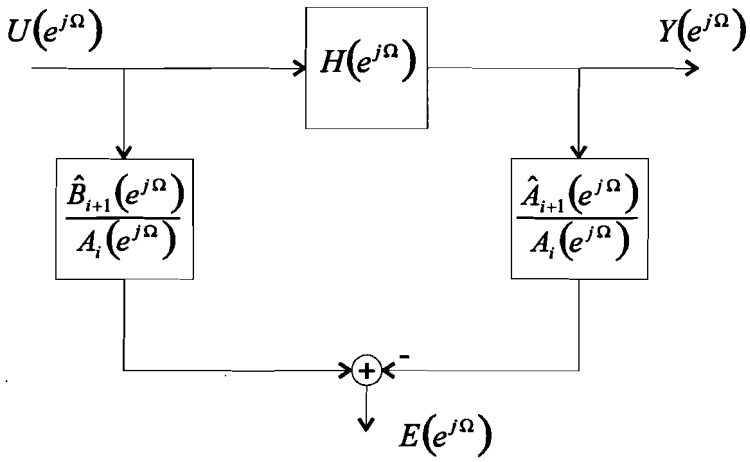

Figure 3-17: *The Steiglitz-McBride calculation scheme*

This enables us to optimize the estimate for H, for a small frequency band. The problem can now be reduced with a divide and conquer strategy, where the error criterion is divided in subband problems. The estimate for the transfer function is now given by the following expression:

$$\hat{H}_{i+1}\left(e^{j\Omega}\right) = \frac{\hat{B}_{i+1}\left(e^{j\Omega}\right)}{\hat{A}_{i+1}\left(e^{j\Omega}\right)}$$

This error criterion can be written out. This leads to the following expression:

$$\int_{\Omega_0}^{\Omega_1} \left| \hat{A}_{i+1}\left(e^{j\Omega}\right) \frac{Y\left(e^{j\Omega}\right)}{\hat{A}_i\left(e^{j\Omega}\right)} - \hat{B}_{i+1}\left(e^{j\Omega}\right) \frac{U\left(e^{j\Omega}\right)}{\hat{A}_i\left(e^{j\Omega}\right)} \right|^2 d\Omega$$

with the subscript *i* denoting the previous iteration and *i+1* denoting the current iteration. Because the each quotient in this expression can be considered as one function, dependent on the previous iteration, the equation can be written as:

$$\int_{\Omega_0}^{\Omega_1} \left| \hat{A}_{i+1}(e^{j\Omega}) Y_i(e^{j\Omega}) - \hat{B}_{i+1}(e^{j\Omega}) U_i(e^{j\Omega}) \right|^2 d\Omega$$

Now introducing the following vectors:

$$\underline{\theta}_{i+1} = \begin{pmatrix} a_{1,i+1} & a_{2,i+1} & \cdots & a_{P,i+1} & b_{0,i+1} & b_{1,i+1} & \cdots & b_{Q,i+1} \end{pmatrix}^T$$

$$\underline{\varphi}_i(e^{j\Omega}) = \begin{pmatrix} -e^{-j\Omega} Y_i(e^{j\Omega}) & -e^{-j2\Omega} Y_i(e^{j\Omega}) & \cdots & -e^{-jP\Omega} Y_i(e^{j\Omega}) & U_i(e^{j\Omega}) \\ e^{-j\Omega} U_i(e^{j\Omega}) & \cdots & e^{-jQ\Omega} U_i(e^{j\Omega}) \end{pmatrix}^T$$

the expression can be re-written as a vector expression:

$$\int_{\Omega_0}^{\Omega_1} \left| E(e^{j\Omega}) \right|^2 d\Omega = \int_{\Omega_0}^{\Omega_1} \left| Y_i(e^{j\Omega}) - \underline{\theta}_{n+1}^T \underline{\varphi}_i(e^{j\Omega}) \right|^2 d\Omega$$

The constants P and Q represent respectively the denominator and nominator polynomial order.

With some effort, the absolute signs can be eliminated, also $\underline{\theta}_{i+1}^T$ equals $\underline{\theta}_{i+1}^h$ because the elements in $\underline{\theta}_{i+1}^T$ are estimates for the nominator and denominator polynomial coefficients from a physical system. These coefficients are real valued.

$$\int_{\Omega_0}^{\Omega_1} \left| E(e^{j\Omega}) \right|^2 d\Omega = \int_{\Omega_0}^{\Omega_1} \left(Y_i(e^{j\Omega}) - \underline{\theta}_{i+1}^T \underline{\varphi}_i(e^{j\Omega}) \right) \left(Y_i(e^{j\Omega}) - \underline{\theta}_{i+1}^T \underline{\varphi}_n(e^{j\Omega}) \right)^* d\Omega$$

Now, it is possible to minimize this expression with respect to the parameter vector $\underline{\theta}_{i+1}$. This is done by taking the derivative of the above expression with respect to $\underline{\theta}_{i+1}$ and setting this to zero.

$$\frac{d}{d\underline{\theta}} \int_{\Omega_0}^{\Omega_1} \left(Y_i(e^{j\Omega}) - \underline{\theta}_{i+1}^T \underline{\varphi}_i(e^{j\Omega}) \right) \left(Y_i(e^{j\Omega}) - \underline{\theta}_{i+1}^T \underline{\varphi}_i(e^{j\Omega}) \right)^* d\Omega = 0$$

Assuming the argument of the integral is continuous on the interval Ω_1 - Ω_2, the derivative may be taken from the argument of the integral leading to:

$$\int_{\Omega_0}^{\Omega_1} \frac{d}{d\underline{\theta}} \left\{ Y_i^2(e^{j\Omega}) - \underline{\theta}_{i+1}^T \underline{\varphi}_i(e^{j\Omega}) Y_i(e^{j\Omega}) - \left(\underline{\theta}_{i+1}^T \underline{\varphi}_i(e^{j\Omega}) Y_i(e^{j\Omega}) \right)^* + \underline{\theta}_{i+1}^T \underline{\varphi}_i(e^{j\Omega}) \underline{\varphi}_i^h(e^{j\Omega}) \underline{\theta}_{i+1} \right\} d\Omega = 0$$

This can be simplified:

$$\left\{\int_{\Omega_0}^{\Omega_1}\underline{\varphi}_i\left(e^{-j\Omega}\right)\underline{\varphi}_i^T\left(e^{j\Omega}\right)d\Omega+\int_{\Omega_0}^{\Omega_1}\underline{\varphi}_i\left(e^{j\Omega}\right)\underline{\varphi}_i^T\left(e^{-j\Omega}\right)d\Omega\right\}\underline{\theta}_{i+1}$$
$$=\int_{\Omega_0}^{\Omega_1}Y_i\left(e^{j\Omega}\right)\underline{\varphi}_i\left(e^{-j\Omega}\right)d\Omega+\int_{\Omega_0}^{\Omega_1}Y_i\left(e^{-j\Omega}\right)\underline{\varphi}_i\left(e^{j\Omega}\right)d\Omega$$

This expression can be cast into a matrix expression:

$$\left(\mathbf{R}_{\varphi\varphi}+\mathbf{R}_{\varphi\varphi}^{*}\right)\underline{\theta}_{i+1}=\left(\underline{\mathbf{R}}_{Y\varphi}+\underline{\mathbf{R}}_{Y\varphi}^{*}\right)^{T}$$

leading to:

$$\underline{\theta}_{i+1}=\left(\Re\left\{\mathbf{R}_{\varphi\varphi}\right\}\right)^{-1}\Re\left\{\underline{\mathbf{R}}_{Y\varphi}\right\}=\mathbf{R}_{\varphi\varphi}^{-1}\underline{\mathbf{R}}_{Y\varphi}$$

with:

$$\underline{\mathbf{R}}_{Y\varphi}=\begin{pmatrix}\int_{\Omega_2}^{\Omega_1}Y_i\left(e^{-j\Omega}\right)\varphi_1 d\Omega\\ \int_{\Omega_2}^{\Omega_1}Y_i\left(e^{-j\Omega}\right)\varphi_2 d\Omega\\ \vdots\\ \int_{\Omega_2}^{\Omega_1}Y_i\left(e^{-j\Omega}\right)\varphi_{P+Q} d\Omega\end{pmatrix}$$

$$\mathbf{R}_{\varphi\varphi}=\mathbf{R}_{\varphi\varphi}^{h}=\begin{pmatrix}\int_{\Omega_2}^{\Omega_1}\varphi_1\varphi_1^{*}d\Omega & \int_{\Omega_2}^{\Omega_1}\varphi_1\varphi_2^{*}d\Omega & \cdots & \int_{\Omega_2}^{\Omega_1}\varphi_1\varphi_{P+Q}^{*}d\Omega\\ \int_{\Omega_2}^{\Omega_1}\varphi_2\varphi_1^{*}d\Omega & \int_{\Omega_2}^{\Omega_1}\varphi_2\varphi_2^{*}d\Omega & & \vdots\\ \vdots & & \ddots & \vdots\\ \int_{\Omega_2}^{\Omega_1}\varphi_{P+Q}\varphi_1^{*}d\Omega & \cdots & \cdots & \int_{\Omega_2}^{\Omega_1}\varphi_{P+Q}\varphi_{P+Q}^{*}d\Omega\end{pmatrix}$$

Lets first look at the expression for the vector $\underline{\varphi}_i$. The Fourier transform $Y\left(e^{j\Omega}\right)$ can be determined easily.

$$Y\left(e^{j\Omega}\right)=\sum_{n=-\infty}^{\infty}y[n]e^{-jn\Omega}$$

Since the data (room impulse response) has a limited length of N samples, and can be considered zero outside this interval, the Fourier transformation can be written as:

$$Y(e^{j\Omega}) = \sum_{n=0}^{N-1} y[n]e^{-jn\Omega}$$

The input signal *U[n]* is a delta function. Therefore its transform equals 1.

$$U(e^{j\Omega}) = 1$$

With the aid of these equations, an expression for $Y_i(e^{j\Omega})$ and $U_i(e^{j\Omega})$

$$Y_i(e^{j\Omega}) = \frac{Y(e^{j\Omega})}{\hat{A}_i(e^{j\Omega})} = \frac{\sum_{n=0}^{N-1}\{y[n]e^{-jn\Omega}\}}{\sum_{p=0}^{P} a_{p,i}e^{-jp\Omega}}$$

$$U_i(e^{j\Omega}) = \frac{U(e^{j\Omega})}{\hat{A}_i(e^{j\Omega})} = \frac{1}{\sum_{p=0}^{P} a_{p,i}e^{-jp\Omega}}$$

Now, having the expressions for $Y_i(e^{j\Omega})$ and $U_i(e^{j\Omega})$, the vector $\underline{\varphi}$ can be constructed, and consequently the vector $\underline{\mathbf{R}}_{Y\varphi}$ and the matrix $\mathbf{R}_{\varphi\varphi}$. The matrix $\mathbf{R}_{\varphi\varphi}$ can be built of 4 sub matrices, matrix $\mathbf{R}_{\varphi\varphi}^{(1)}$ dimensions PxP, matrix $\mathbf{R}_{\varphi\varphi}^{(2)}$ dimensions PxQ, matrix $\mathbf{R}_{\varphi\varphi}^{(3)}$ dimensions QxP and matrix $\mathbf{R}_{\varphi\varphi}^{(4)}$ dimensions QxQ. These can be found in Appendix IV.

There are several ways to perform the integration in both the vector $\underline{\mathbf{R}}_{Y\varphi}$ and the matrix $\mathbf{R}_{\varphi\varphi}$. To perform a numerical integration procedure would mean performing this procedure over N terms with P terms in the denominator, for the vector P+Q times, and for the matrix (P+Q)*(P+Q) times for R subbands. Although use could be made of the Hermittian properties of the matrix $R_{\varphi\varphi}$, and the amount of calculations could be divided roughly by two, this still would mean a lot of calculating.

However, there are simple algorithms to calculate the integrals in both the matrix and the vector. For example, the trapezium rule uses frequency discrete values of the functions in the nominator and denominator. These discrete values can of course be calculated with fast Fourier algorithms. In fact, when more points are used in the Fourier transform, it should be possible to use higher order polynomials in the approximation process. The approximation can then be made more accurate using the Newton Cotes formulas. More points can be acquired by adding trailing zeros to *y[n]*.

As mentioned, there are several methods to approximate an integral. Let's first look at the trapezium rule. To demonstrate this, take an arbitrary coefficient from matrix $\mathbf{R}_{\varphi\varphi}^{(1)}$ (see Appendix IV). The parameter *s* in the exponential in the expression under the

integral sign takes in account each coefficient in the matrix. The integral from Ω_1-Ω_2 can be represented by a sum.

$$I^{(1)} = \int_{\Omega_0}^{\Omega_1} \left| \frac{\sum_{r=0}^{N-1} y[r] e^{-jr\Omega}}{\sum_{p=0}^{P} a_{p,i} e^{-jp\Omega}} \right|^2 e^{js\Omega} d\Omega = \sum_{k=0}^{M-1} \left\{ \int_{\Omega_0+k\delta}^{\Omega_0+(k+1)\delta} \left| \frac{\sum_{r=0}^{N-1} y[r] e^{-jr\Omega}}{\sum_{p=0}^{P} a_{p,i} e^{-jp\Omega}} \right|^2 e^{js\Omega} d\Omega \right\}$$

With $M\delta = \Omega_1 - \Omega_0$. Now, an attempt can be made to approximate the integral in this summation. To achieve this, use can be made of the trapezium rule.

$$\int_{\Omega_0+k\delta}^{\Omega_0+(k+1)\delta} \left| \frac{\sum_{r=0}^{N-1} y[r] e^{-jr\Omega}}{\sum_{p=0}^{P} a_{p,n} e^{-jp\Omega}} \right|^2 e^{js\Omega} d\Omega \approx \frac{1}{2}\delta \left| \frac{\sum_{r=0}^{N-1} y[r] e^{-jr(\Omega_0+k\delta)}}{\sum_{p=0}^{P} a_{p,n} e^{-jp(\Omega_0+k\delta)}} \right|^2 e^{js(\Omega_0+k\delta)} +$$

$$\frac{1}{2}\delta \left| \frac{\sum_{r=0}^{N-1} y[r] e^{-jr(\Omega_0+(k+1)\delta)}}{\sum_{p=0}^{P} a_{p,n} e^{-jp(\Omega_0+(k+1)\delta)}} \right|^2 e^{js(\Omega_0+(k+1)\delta)}$$

The summation in the denominator could be extend to the same length as the summation in the numerator. Doing this, the following coefficients are set to zero:

$$a_{p,i} = \begin{cases} 0, & p > P \\ a_{p,n}, & 0 \le p \le P \end{cases}$$

Furthermore, the step size δ, can be chosen according to the length of the impulse response N. The Fourier transform for time discrete signals FTD [19] is periodic with 2π. If this FTD is sampled at frequencies $\frac{2\pi}{N}$ this finally results in taking the DFT [19], the Discrete Fourier Transform.

$$\left| \frac{\sum_{r=0}^{N-1} y[r] e^{-jr\Omega}}{\sum_{p=0}^{P} a_{p,i} e^{-jp\Omega}} \right|^2 = \left| \frac{\sum_{r=0}^{N-1} y[r] e^{-jr\Omega}}{\sum_{p=0}^{N-1} a_{i,n} e^{-jp\Omega}} \right|^2 \xrightarrow{\Omega = k\frac{2\pi}{N}} \left| \frac{\sum_{r=0}^{N-1} y[r] e^{-jrk\frac{2\pi}{N}}}{\sum_{p=0}^{N-1} a_{i,n} e^{-jpk\frac{2\pi}{N}}} \right|^2 = \left| \frac{Y[k]}{A_i[k]} \right|^2$$

Using this results, the integral can be approximated, the borders of the integral must then be multiplied with $\frac{N}{2\pi}$, to scale them to the new scale.

$$\int_{\Omega_0+k\delta}^{\Omega_0+(k+1)\delta} \left| \frac{\sum_{r=0}^{N-1} y[r]e^{-jr\Omega}}{\sum_{p=0}^{P} a_{p,i}e^{-jp\Omega}} \right|^2 e^{js\Omega} d\Omega$$

$$\approx \frac{1}{2}\frac{2\pi}{N}\left(\left| \frac{Y\left[\frac{N}{2\pi}\left(\Omega_0 + k\frac{2\pi}{N}\right)\right]}{A_i\left[\frac{N}{2\pi}\left(\Omega_0 + k\frac{2\pi}{N}\right)\right]} \right|^2 e^{js\left(\Omega_0 + k\frac{2\pi}{N}\right)} + \left| \frac{Y\left[\frac{N}{2\pi}\left(\Omega_0 + (k+1)\frac{2\pi}{N}\right)\right]}{A_i\left[\frac{N}{2\pi}\left(\Omega_0 + (k+1)\frac{2\pi}{N}\right)\right]} \right|^2 e^{js\left(\Omega_0 + (k+1)\frac{2\pi}{N}\right)} \right)$$

$$= \frac{1}{2}\frac{2\pi}{N}\left(\left| \frac{Y\left[\frac{N\Omega_0}{2\pi} + k\right]}{A_i\left[\frac{N\Omega_0}{2\pi} + k\right]} \right|^2 e^{js\left(\Omega_0 + k\frac{2\pi}{N}\right)} + \left| \frac{Y\left[\frac{N\Omega_0}{2\pi} + k + 1\right]}{A_i\left[\frac{N\Omega_0}{2\pi} + k + 1\right]} \right|^2 e^{js\left(\Omega_0 + (k+1)\frac{2\pi}{N}\right)} \right)$$

Resulting in the following approximation:

$$I^{(1)} = \int_{\Omega_0}^{\Omega_1} \left| \frac{\sum_{r=0}^{N-1} y[r]e^{-jr\Omega}}{\sum_{p=1}^{P} a_{p,n}e^{-jp\Omega}} \right|^2 e^{js\Omega} d\Omega$$

$$\approx \sum_{k=0}^{M-1} \left\{ \frac{1}{2}\frac{2\pi}{N}\left(\left| \frac{Y\left[\frac{N\Omega_0}{2\pi} + k\right]}{A_n\left[\frac{N\Omega_0}{2\pi} + k\right]} \right|^2 e^{js\left(\Omega_0 + k\frac{2\pi}{N}\right)} + \left| \frac{Y\left[\frac{N\Omega_0}{2\pi} + k + 1\right]}{A_n\left[\frac{N\Omega_0}{2\pi} + k + 1\right]} \right|^2 e^{js\left(\Omega_0 + (k+1)\frac{2\pi}{N}\right)} \right) \right\}$$

For evaluating the integral over the complete range (one frequency band), it is important to note that the signal values at the frequencies between π and 2π are the complex conjugated from those between 0 and π. Therefore it is sufficient if the integral is only evaluated between 0 and π.

Approach

In order to compare the performance of this modeling method with the previous one, it is necessary to use a similar model. Thus, a synthetic model is created of 50 poles and 2048 samples with no noise added to the impulse response of the synthetic model.

In this case, the expressions for the approximations of the parameter vectors of the Steiglitz-McBride algorithm in the frequency domain are quite easy to interpret. The frequency range is again divided into 8 subbands.

The Steiglitz-McBride algorithm is performed on each subband. The initial order of the denominator and nominator polynomial were set to 14. The algorithm reduces the

order until a matrix is found which is not rank deficient. Apparently, when the matrix is rank deficient, the system is overdetermined. This rank deficiency is checked by means of the condition number. This condition number is the ratio between the smallest singular value and the largest. The threshold for reduction is set to condition number smaller than 10^{-16}.

The algorithm is able to find solutions which lie outside the current subband. These solutions are used in finding the optimal solution for the current subband. However, only the poles in the subband are selected at the end of the iterations. Real poles are only allowed in the first and the last subband.

The amount of iterations was set to 14. This amount was necessary for the error criterion to reach values below the 0.1 (3.3.3).

Table 3-1: *Subbands versus initial amount of poles and eventually selected poles*

Subband nr.	1	2	3	4	5	6	7	8
# of poles reduced to:	5	7	8	8	10	9	6	4
# poles inside subband:	2	6	8	6	6	8	8	2

Starting with 14 initial poles in a subband, i.e. a total amount of 112 poles, the amount of poles is reduced to 57. From these 57 poles, 46 are selected because 11 poles were located outside the subband under treatment.

Figure 3-18 shows how the impulse response of the model generated by this subband method approximates the synthetic model impulse response. A total energy coverage of 91.64 [%] was reached.

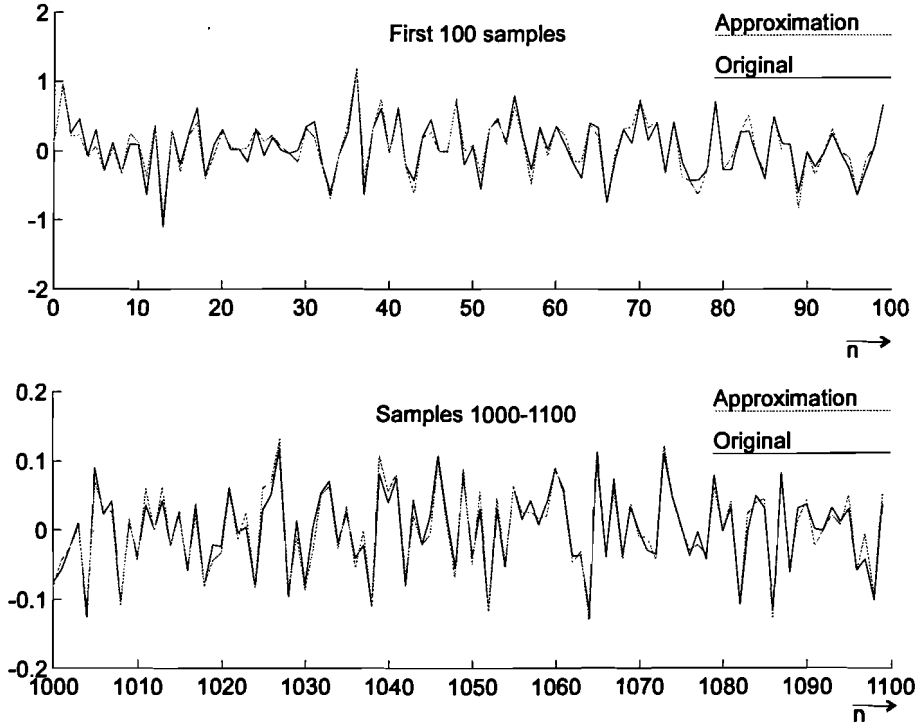

Figure 3-18: *impulse responses of the synthetic model and the approximation.*

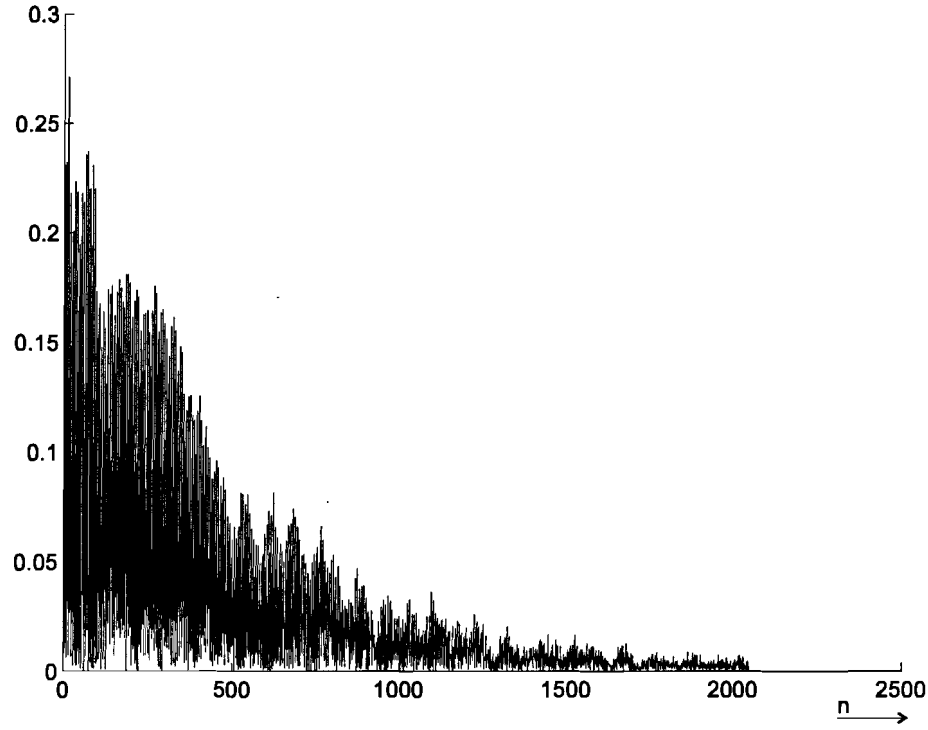

Figure 3-19: *Absolute error:* $\left|h_s - \hat{h}\right|$

From Figure 3-19 can be concluded that the error decreases with time. This is obvious. The energy in the synthetic model decreases also with the time.

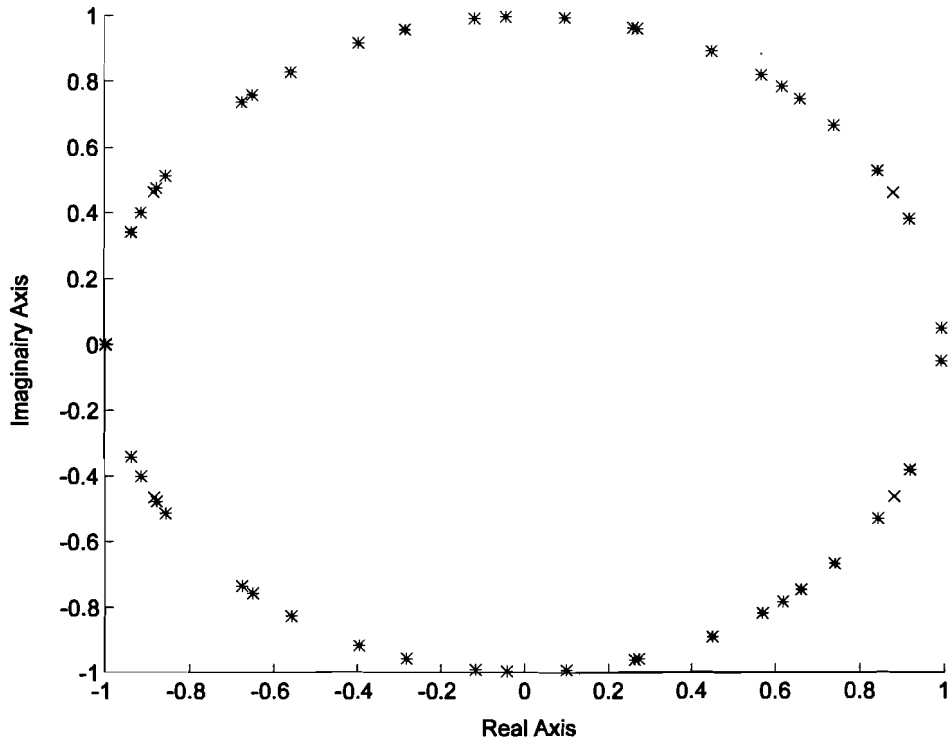

Figure 3-20: *Location of the poles, x synthetic model and + approximation*

Although the modeling method is capable to find many of the poles present in the synthetic model, not all poles were found. This means that the approximation is not accurate enough, especially when one considers the fact that no noise was added to the impulse response of the synthetic model. Therefore the method is not suitable for the acoustic problem.

3.5.4 Subband method III: Reformulating $\mathbf{R}_{\varphi\varphi}$ and $\underline{\mathbf{R}}_{y\varphi}$ in the frequency domain.

The expression for the matrix $\mathbf{R}_{\varphi\varphi}$ and the vector $\mathbf{R}_{y\varphi}$ (3-4a and 3-4b) can also directly be represented in the frequency domain. The elements of $\mathbf{R}_{\varphi\varphi}$ and $\mathbf{R}_{y\varphi}$ are typically of the form:

$$\sum_{n=0}^{N-1} y_i[n] f_i[n-r] \qquad r = 0 \ldots\ldots \max(P,Q)$$

Where $f_i[n]$ is either $u_i[n]$ or $y_i[n]$. $y_i[n]$ in the above expression can be replaced by the IDFT (inverse discrete Fourier transform, [19]) of $Y_i\left(e^{j\Omega}\right)$, the DFT of $y_i[n]$. This results in:

$$\sum_{n=0}^{N-1} \tfrac{1}{N} \sum_{k=0}^{N-1} Y_i[k] e^{j\left(\frac{2\pi}{N}\right)kn} f_i[n-r] = \sum_{n=0}^{N-1} \tfrac{1}{N} \left(\sum_{k=0}^{N-1} Y_i^*[k] e^{-j\left(\frac{2\pi}{N}\right)kn} \right)^* f_i[n-r]$$

Because the expression has to be real ($y_i[n]$ is real), the above expression is equal to:

$$\tfrac{1}{N} \sum_{n=0}^{N-1} \sum_{k=0}^{N-1} Y_i^*[k] e^{-j\left(\frac{2\pi}{N}\right)kn} f_i[n-r]$$

$$\Leftrightarrow \tfrac{1}{N} \sum_{k=0}^{N-1} Y_i^*[k] \sum_{n=0}^{N-1} f_i[n-r] e^{-j\left(\frac{2\pi}{N}\right)kn}$$

The sum $\sum_{n=0}^{N-1} f_i[n-r] e^{-j\left(\frac{2\pi}{N}\right)kn}$ can be approximated by its DFT:

$$\sum_{n=0}^{N-1} f_i[n-r] e^{-j\left(\frac{2\pi}{N}\right)kn} = \sum_{m=-r}^{N-1-r} f_i[m] e^{-j\left(\frac{2\pi}{N}\right)k(m+r)}$$

$$f_i[n] = 0 \quad \forall n \le -1$$

$$\Rightarrow \sum_{m=0}^{N-1-r} f_i[m] e^{-j\left(\frac{2\pi}{N}\right)k(m+r)}$$

In the case of the acoustic impulse responses and the associated synthetic model, the impulse responses are all damped. Also, if P is small (P<<N) the energy in the 'tail'

of the impulse response of the model is much smaller than the energy in the 'head'. Under this condition the following approximation may be made:

$$\sum_{m=0}^{N-1-r} f_i[m]e^{-j\left(\frac{2\pi}{N}\right)k(m+r)} \approx \sum_{m=0}^{N-1} f_i[m]e^{-j\left(\frac{2\pi}{N}\right)k(m+r)} = F_i[k]e^{-j\left(\frac{2\pi}{N}\right)kr}$$

Thus, the elements of $\mathbf{R}_{\varphi\varphi}$ and $\underline{\mathbf{R}}_{y\varphi}$ can be approximated by:

$$\sum_{n=0}^{N-1} y_i[n]f_i[n-r] \approx \frac{1}{N}\sum_{k=0}^{N-1} Y_i[k]F_i[k]e^{-j\left(\frac{2\pi}{N}\right)kr}$$

When a subband approach is chosen for this problem, the range *k=0....N-1*, can be cut into S subbands. P can then be kept very small, so that the approximation is justified.

Approach

The same approach is chosen as with the previous method. The results are also similar. A *RME* of 70.59 % with the tested synthetic model.

3.6 Results

From the previous paragraph it is clear that, although a lot of effort was invested in finding a suited method for identification of a high order system as a room, the investigated subband methods are not good enough. None of the subbands methods is capable of finding a *RME* of 100% when a synthetic model is used without the addition of noise.

From the in paragraph 3.3. discussed methods, only the Prony method is economically enough with it's usage of computer memory and computer power. Used on the impulse responses imp1, imp2, imp3, imp4, imp5, and imp6 it is capable of finding a *RME* of around 96 %. The results can be found in chapter 5.

4. Kautz filters

4.1 Introduction

IIR filters can be implemented in numerous ways. Based on one set of poles several complete different realizations can be thought of.

Kautz filters possess some nice properties, commonly found in FIR filters, in fact, the tapped-delay line can be considered a special case of a Kautz filter bank. Kautz filters are based on Kautz functions. These functions are damped orthogonalized oscillations defined on the positive axis. In paragraph 4.2, some properties of Kautz functions are described. Later on, in Chapter 5, it becomes clear that the Prony method yield complex conjugated pole pairs. Paragraph 4.3 discusses the Kautz filter bank, build out of complex conjugated sections in advance.

4.2 Kautz functions

In the continuous time domain, the exponential functions $\exp(p_i t)$ are linearly independent if $p_i \neq p_j$ for $i \neq j$. Complex-valued parameters are allowed as long as $\Re\{p_i\}<0$, since only in that case they belong to $L^2(0, \infty)$ [15].

When these functions are used as a base in $L^2(0, \infty)$, they have to be orthogonalized. This can be done with the aid of a Gram-Schmidt procedure. These orthogonalized exponential functions are now called Kautz functions. In the remainder of this chapter they will be denoted by $\phi_i(t)$, i=0,1,2,3....

The Gram-Schmidt procedure in the time domain lead to all-pass sections in the Laplace domain:

$$\Phi_i(s) = a_i \frac{\sqrt{-(p_i + p_i^*)}}{s - p_i} \prod_{j=0}^{i-1} \frac{s + p_j^*}{s - p_j} \quad |a_i| = 1 \text{ and } \Re\{p_i\} < 1$$

The Kautz functions can be generated as the impulse responses of the following filter bank:

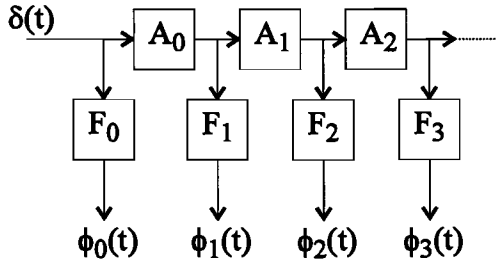

Figure 4-1: *General Kautz filter bank*

In this filter bank, A_i represent the all-pass sections and F_i represent the filter sections. The continue Kautz functions have also a discrete counterpart. The discrete Kautz functions are defined in the Z-domain by:

$$\Psi_i(z) = a_i\sqrt{1-p_i p_i^*}\,\frac{z}{z-p_i}\prod_{j=0}^{i-1}\frac{1-zp_j^*}{z-p_j} \quad |a_i| = 1 \text{ and } |p_i| < 1$$

The orthonormality property of $\psi_i[n]$ comes to expression in the following inner product (window function $w[n]$=1):

$$\langle \psi_i, \psi_j \rangle = \sum_{n=0}^{\infty} \psi_i[n]\psi_j^*[n] = \delta_{ij}$$

These functions can constitute a complete orthonormal basis in $\ell^2(0, \infty)$ if the following condition is met:

$$\sum_{i=0}^{\infty}\left(1-|p_i|\right) = \infty$$

A Kautz series meeting this condition can describe an arbitrary function $h[n]$ on $\ell^2(0, \infty)$. A truncated Kautz series is able to approximate an arbitrary function $h[n]$ on $\ell^2(0, \infty)$.The expansion $h[n]$ reads:

$$h[n] = \sum_{i=0}^{\infty} c_i\psi_i[n] \tag{1-4}$$

The orthonormality of the Kautz functions assures that the coefficients c_i can be determined with a inner product:

$$c_i = \langle h, \psi_i \rangle = \sum_{n=0}^{\infty} h[n]\psi_j^*[n] = \frac{1}{2\pi j}\oint H(z)\Psi_j^*(z)\frac{d}{dz} \tag{2-4}$$

The function $h[n]$ can be considered as an impulse response of the 'filter bank' in Figure 4-1, when weights are incorporated and a adder, in the outputs of the filters F_i. For complex conjugated sectionssuch a filter can be found in Figure 4-2, and will be called a Kautz filter bank.

It is important to note that this Kautz filter bank is not unique. There are N! ways to order the poles in the Kautz bank, stemming from N! orders to perform the Gram-Schmidt method.

The expansion in Kautz functions can be considered as a signal transform. Hence, the energy E contained in the impulse response can be expressed with the Parseval relation:

$$E = \sum_{n=0}^{\infty} h[n]h^*[n] = \sum_{i=0}^{N} |w_i|^2 ,$$

4.3 The Kautz filter bank

The room impulse response is real. Therefore poles can only be present as real or as complex conjugated poles. These complex conjugated poles have to be kept together in the filter bank. Figure 4-2 pictures such Kautz filter bank with complex conjugated poles.

Let's first assume that the poles can be chosen fixed and there exists a set of poles describing all the variations which can take place in a room. In this way, only the coefficients $w_{1\Phi}$ - $w_{N\Phi}$ and $w_{1\Psi}$ - $w_{2\Psi}$ have to be adapted.

There are algorithms to adapt the positions of the poles as well (in real time), but they have some nasty properties. For example, an adaptation of the pole location of the first filter section, alters the current contents of the memory element of this filter. It takes a while before this alteration reaches the last filter section. During this time it is impossible to alter this pole again, because the effect of the first alteration still isn't known. In [21] a derivation is made in order to find a gradient expression for adapting poles.

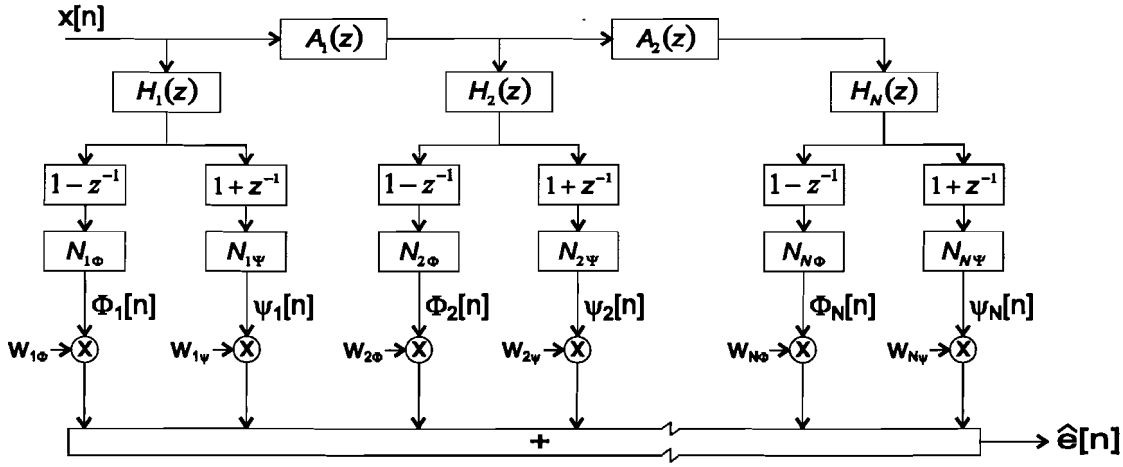

Figure 4-2: *Kautz filter bank*

$$H_i(z) = \frac{1}{(1-z_i z^{-1})(1-z_i^* z^{-1})} \qquad A_i(z) = \frac{(z_i - z^{-1})(z_i^* - z^{-1})}{(1-z_i z^{-1})(1-z_i^* z^{-1})}$$

$$N_{i\Phi} = \sqrt{\frac{(1-z_i)(1-z_i^*)(1-z_i z_i^*)}{2}} \qquad N_{i\Psi} = \sqrt{\frac{(1+z_i)(1+z_i^*)(1-z_i z_i^*)}{2}}$$

Figure 4-2 depicts such a (complex conjugated) Kautz bank. This Kautz bank is again built out of all pass sections $H_i(z)$ and filter sections $F_i(z)$. The filter blocks $N_{i\Phi}$ and $N_{i\Psi}$ in the filter outputs Φ_i and Ψ_i are normalizing factors. In addition to the orthonormality property, the Kautz filter bank has the attractive energy conservation property. When a signal enters the i^{th} filter all pass stage, the energy content of the signal, is the same as at the input of the first filter all pass stage.

[23,24] have studied the possibilities of what they call Fixed Pole Adaptive Filters, similar to the Kautz bank in Figure 4-2. They determine the modeling capabilities, describe ways of selecting the appropriate poles and state that under certain excitation conditions on the filter input, global convergence with several adaptation algorithms is guaranteed.

[22] States that when a priori knowledge can be used to select N parameters for the all-pass sections, LMS (Least Mean Square) adaptation used in conjunction with the Kautz filter bank can outperform LMS applied to the tapped-delay line. This conclusion was drawn by investigation the rate of convergence and the steady state weight fluctuations.

The filter bank reduces to the FIR filter when all poles z_i are chosen zero. The filter bank reduces to a Laguerre filter when all poles are chosen equal and real. [23,24] Refer to the Kautz bank as the complex version of a Laguerre filter bank.

As one can observe, the Kautz filter bank offers some nice properties. These properties can be exploited, but much depends on the modeling method used to find the location of the poles of the Kautz bank.

The adaptation process is not considered in this report. When a Kautz filter bank is actually used for echo cancellation, this adaptation process can add a considerable amount of noise to the result. How well a Kautz filter bank performs in contrast to its FIR counterpart, depends on the noise added in the adaptation in both realizations. [22] Suggest that when a Kautz bank can be used, and 'consumes' less coefficients than the tapped-delay line, faster convergence and therefore better tracking oft varying room conditions should be possible.

5. Results

5.1 Introduction

In chapter 3 several modeling methods were tested and investigated for their suitability to model acoustic impulse responses. The conclusion was that although the iterative method was better, the demands on computer power and memory were too large to use this method. This was also concluded in the introduction of 3 for the balanced realization. The developed subband methods didn't meet their expatiation. The only method left to model such a large system was the Prony method.

In this chapter the Prony method is used to find a model. The room impulse responses (Appendix I) contain dead time. This dead time can perhaps best be modeled with a tapped-delay line. The impulse responses from this tapped-delay line are orthogonal on each other and on the impulse responses of the following Kautz sections. The impulse responses of Appendix I are therefore shortened, i.e. the first 70 samples are thrown away.

In paragraph 5.2 the results of the Prony method are discussed. Furthermore, in paragraph 5.3, the pole-set found in paragraph 5.2 is used to test the performance of this pole-set on each of the impulse responses and the performance in comparison to the FIR filter bank. To implement a Kautz filter in the future in a commercial application, no extensive measurements and calculations can be carried out for a room. In paragraph 5.3 finally, the performance of a fixed raster for the poles are compared with the performance of the pole-set found by the Prony method.

Throughout the chapter the term suppression is used. With this term is meant the maximum obtainable suppression. Suppression losses due to adaptation are not considered.

5.2 Applying the Prony method

For experimenting purposes, 8 comparable impulse responses were present. In order to use all the information present in these 8 impulse responses, they were added together. In this way, a set of poles is created which has the capability of modeling all measured 8 situations in the room.

When using the Prony method, it is possible to assign the half of the available coefficients to the MA part and the other half to the AR part. The order of the AR part is then: 2048-70=1978/2= 989. When using the Matlab roots command, this leads to 989 poles, from which 844 are stable and the rest is in-stable.

It is now possible to use a model reduction method suggested by [20]. This method uses the fact that given a set of N poles, these poles can be ordered on N! different ways. A Kautz bank is a non-unique representation.

All poles are put into a initial Kautz bank in a random fashion. In [20] a method is discussed which searches the pole from which the corresponding weight has the largest magnitude. This pole is taken out of the initial Kautz bank and put in to the first section of the Kautz bank. The remaining poles follow this first pole. The weights are recalculated. From the remaining poles the next pole is selected according to the same principle, and so on, until the set of remaining poles reduces to zero. In [20] is also pointed out that this is a sub-optimal method. The resulting pole set is called the overall pole-set.

The radia of the poles which are found can now be plotted in a figure. This is done in Figure 5-1.

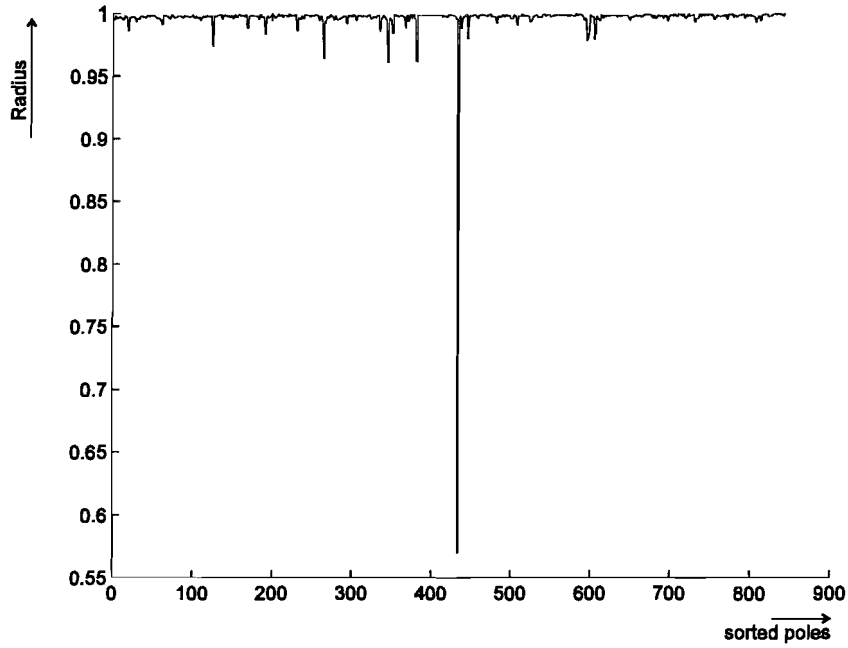

Figure 5-1: *Radia of the poles (imaginary part greater than 1)*

In, Figure 5-1 one can observe that all the poles have (with a few exceptions) a radius coinciding with the reverberation time.

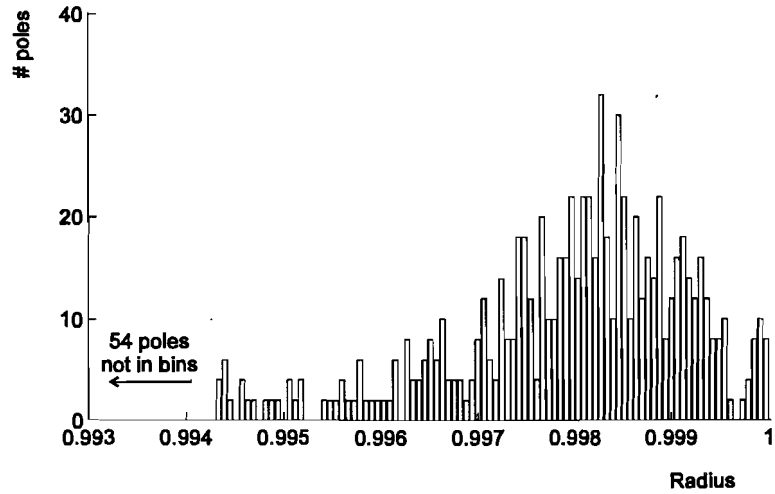

Figure 5-2: *Histogram, amount of radia per radia bin*

This is also demonstrated in the histogram of Figure 5-2. The mean radius is 0.9961 and the perhaps more representing medium radius is 0.9981. The mean radius does not entirely coincide with the reverberation time (radius 0,9983), but this can be expected when looking at the severe exception present in Figure 5-1. On the other hand, the medium radius does coincide with the reverberation time.

More curious is the distribution of the angle of the poles. Remember the plot of Figure 2.2. In this plot the modes became more dense when the frequency approached the 4 [kHz] bandwidth frequency. One expects to observe a similar effect after locating the poles (which can show some coherence with the modes) with a Prony method. This is however not the case, as illustrated in Figure 5-3.

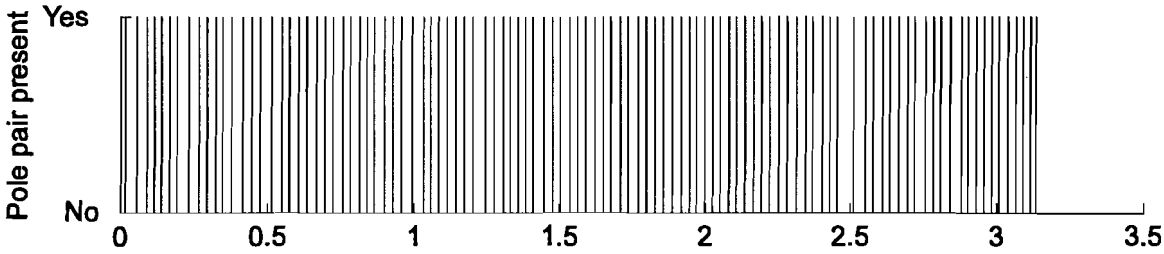

Figure 5-3: *Angle (sorted ascending) of the poles (imaginary part greater than one), decimated a factor 4 by taking the median value of each following 4 poles)*

It is however very well possible that poles which almost have the same angle, and thus have impulse responses which have almost the same frequencies, when entered in a second order filter section, are substituted by one pole. If this happens for multiple poles in the 'dense area' then it may very well be possible that a lot of poles here, are substituted by one or a few other poles in the same area.

When investigating Figure 5-3, it seems that the Prony model yields a kind of subband model, where each pole takes 'care' of a certain small frequency subband. This idea stems from the fact that the a Kautz bank is built from an all-pass bank and several almost equally spaced band filters, from which the room impulse response is reconstructed (see Chapter 4).

5.3 Evaluating the performance of the Kautz filter bank

The *RME* of the Kautz bank, can be plotted against a certain number of Kautz sections in the with the method described in [20] sorted order. Each extra Kautz section will cumulate to a higher *RME*, as can be observed in Figure 5-4.

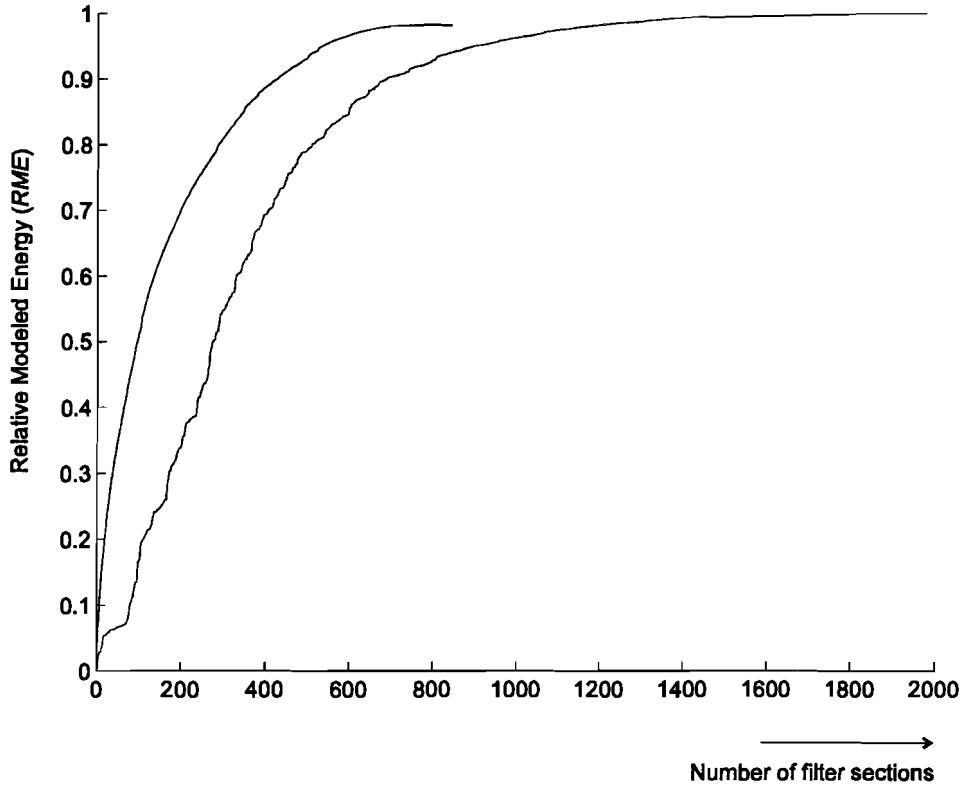

Figure 5-4: *RME against number of filter sections, left: Kautz, right tapped-delay*

What also can be noticed from Figure 5-4 is that with less sections a higher *RME* can be reached with a Kautz filter bank than with a tapped-delay line. When the number of sections increases, this advantage disappears, until finally (around 1200 sections, if the Kautz plot is extrapolated) the tapped-delay line performs better than the Kautz bank.

Filter under variable room conditions

Data from some variable room conditions are available. The opportunity arises to enter the sorted poles in a Kautz filter bank, and determine the weights for each available impulse response (Appendix I). The square of these weights represent the *RME*. Subtracting this *RME* from 100 %, and plotting these values logarithmically against the number of filter sections gives a good impression how many filter sections are necessary for each impulse response to reach a certain suppression. When using all 844 poles the following table can be derived for the suppression:

Table 5-1: *RME and suppression based on the overall pole-set*

	imp1	imp2	imp3	imp4	imp5	imp6
RME %	96.13	96.68	95.67	95.79	95.17	95.56
Suppression [dB]	14.12	14.79	13.63	13.76	13.16	13.53

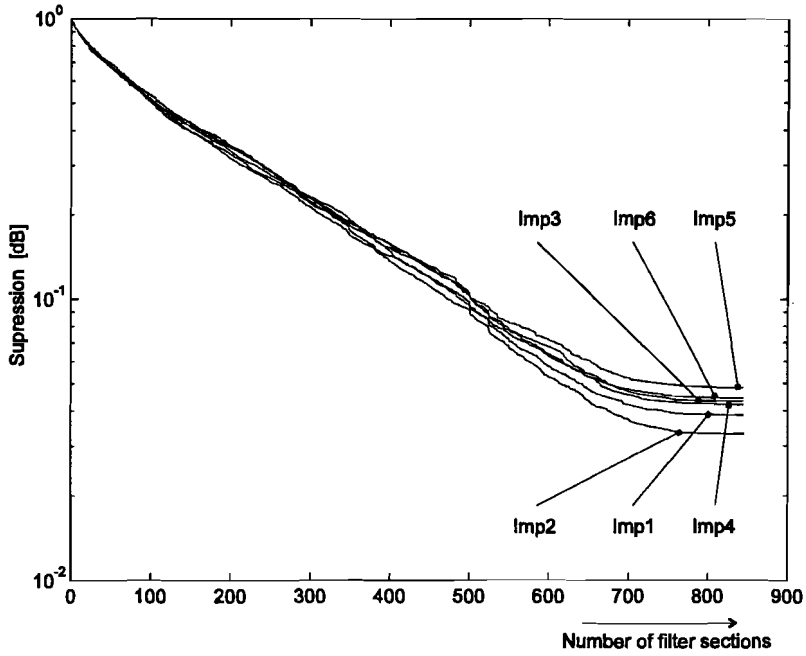

Figure 5-5: *Number of filter sections against suppression*

Looking at Table 5-1 and Figure 5-5 one can see that impulse response imp2 scores best, with the highest suppression. This can be expected, since imp2 was repeated with imp2b, and both were used to determine the overall pole-set (see paragraph 5.1). Both are virtually equal (Appendix I).

None of the plots in Figure 5-4 reaches the desired suppression level of 20 [dB]. The tapped-delay line with 2048 coefficients is capable of reaching this 20 [dB].

5.4 Fixed pole-set

As mentioned in the introduction of this chapter, in commercial applications it is often not possible to carry out extensive calculations and measurements, in order to locate the system poles. Even if it were possible, these calculations and measurements have to be carried out when large pieces of for example furniture are moved.

There are two approaches to such a fixed pole model. The first is distributing the poles according to the results of the Prony modeling method. I.e. a linear distribution along the range 0-p and all the poles placed on a radius coinciding with the median value of the roots found by the Prony method. The angles are then located according to the MatLab commando:

```
anglelin=linspace(0.001,pi-0.001,422);
```

The other is placing the poles according to the physical model, with a more dense distribution toward the bandwidth. To assure that poles are present also in the lower frequency range, one half of the poles is distributed logarithmic and the other half is distributed linear.

anglelog=[logspace(0.001,pi-0.001,211),linspace(0.001,pi-0.001,211)]

Both angle sets are used to find complex conjugated poles. The weights are determined by means of taking the inner product with the added impulse responses (paragraph 5.2).The results are plotted in Figure 5-6.

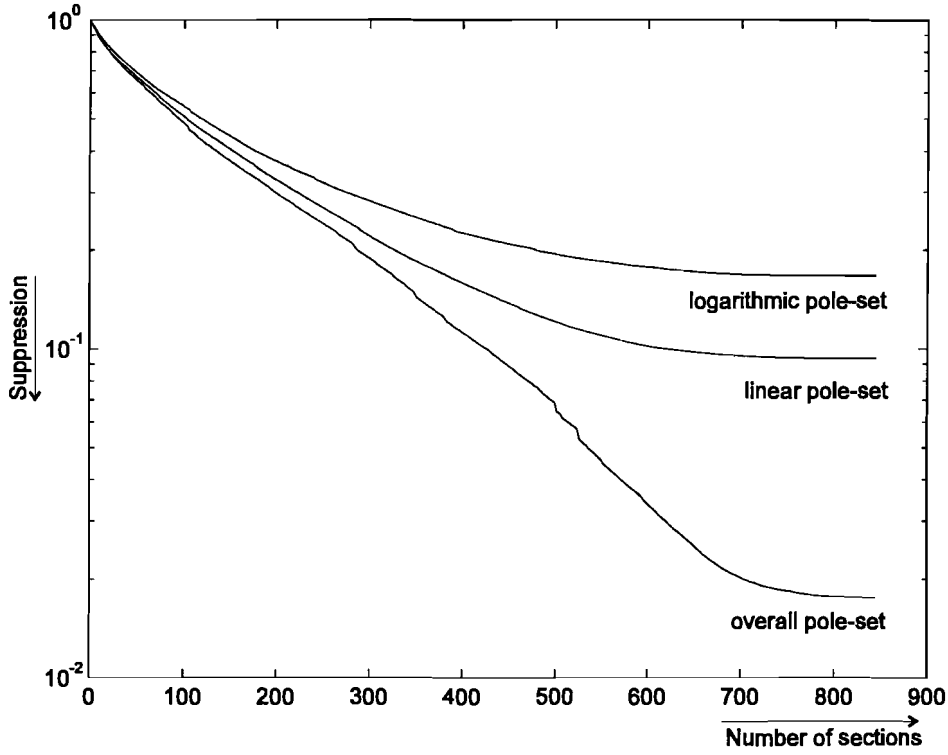

Figure 5-6: *Performance of 2 different fixed pole-sets against overall pole-set*

Clearly a good identification is necessary in order to obtain sufficient suppression. At 844 poles, an *RME* of 98.24 % with the overall pole set on the added impulse responses is achieved. This in contrast to the linear pole-set which achieves an *RME* of 90.64 % and the logarithmic pole-set which achieves an *RME* of 83.29 %.

This can only mean that a linear distribution of the angles is preferred above the logarithmic distribution of the angles, which is expected according to the physical model of Chapter 2.

6. Discussion

Concluding from the results (Chapter 5) it seems that a suppression of 14 - 15 [dB] on all impulse responses can be reached. These results are obtained when a Prony method is used to find the poles of the system. The poles are almost all placed on a radius coinciding with the reverberation time.

Although it seems that the poles are found on a more or less constant radius, each pole representing a small subband, replacing this pole set with a pole set where poles are placed equidistantly at constant radius does yield a worse suppression. Replacing the pole set with a logarithmically distributed pole set according to Chapter 5 also not improves this result.

The above conclusions suggest that a good identification of the system (LEMS) is necessary, and perhaps the desired suppression of 20 - 30 [dB] can be reached when using a better system identification procedure. Generating a synthetic model and testing several identification methods with this synthetic model suggest that there are better methods to find these poles. For example in Chapter 3 is demonstrated that the tested iterative Prony method "scores" better on the synthetic model than the "standard" Prony method. Unfortunately, this method makes a too large demand on computing power, and couldn't be used for this high-order problem.

Also, too less data was available on the noise present in the measurements. If the noise level in the data is too high, the modeling methods are of course not capable of finding a model with sufficient suppression.

When the found poles describe the LEMS properly (enough suppression over the majority of possible room variations), and sufficient coefficient reduction can be achieved, the idea of using an IIR structure to model the LEMS becomes attractive. In Chapter 4 already is mentioned that a coefficient reduction can lead to faster adaptation of the filter structure with the suppression remaining the same. This leads to better and faster tracking conditions, i.e. the capability of the filter to adapt to changing room conditions.

Further research

In the future it is perhaps possible to develop identification methods specially dedicated to this problem which use restrictions, and therefore could reduce the amount of needed calculations and memory. A Suggestion for these restrictions is including limitations on the radius in an identification method. See for example figure 5.2. The probability of selecting a good pole decreases according to a certain probability density function, with the medium value at a radius coinciding with the reverberation time. Such a probability density function can be included in a cost- or error criterion.

Another suggestion can be limiting the amount of poles per subband. The influence of a certain pole on a subband is calculated in Paragraph 3.5.1. A similar approach can be used here. Decrease the probability a pole is located near another by using its influence on a certain subband as probability criterion. Try to find a probability density function that fits this problem and use this probability density function again in the cost criterion.

With good identification methods it is perhaps possible to develop some rules of thumb for the location of the poles. In this way, using an IIR filter bank can be included in commercial applications without extensive calculations and measurements on the room in advance

To judge the modeling methods it is vital to know how large the contribution of the noise is to the room impulse responses. Therefore, more knowledge has to be gathered on this noise.

References

[1] Hänsler, E.
THE HANDS-FREE TELEPHONE PROBLEM - AN ANNOTATED BIBLIOGRAPHY.
Signal Processing, Vol. 27, 1992, P. 259-271 Elsevier

[2] Hänsler, E.
THE HANDS-FREE TELEPHONE PROBLEM - A SECCOND ANNOTATED BIBLIOGRAPHY UPDATE.
Internal publication: Institut für Netzwerk- und Signaltheorie, Technische Hochschule Darmstadt, Merckstrasse 25, D-64283 Darmstadt, Germany.

[3] Kerkhof, Leon M. van de, and Wil J.W. Kitzen
TRACKING OF A TIME-VARYING ACOUSTIC IMPULSE RESPONSE BY AN ADAPTIVE FILTER.
IEEE Transactions on Signal Processing, Vol. 40, No. 6, 1992, P. 1285-1294.

[4] Hänsler, E.
THE HANDS-FREE TELEPHONE PROBLEM: AN ANNOTATED BIBLIOGRAPHY UPDATE
Internal publication: Institut für Netzwerk- und Signaltheorie, Technische Hochschule Darmstadt, Merckstrasse 25, D-64283 Darmstadt, Germany, July 7 1994.

[5] Von Zitzewitz, A.
CONSIDERATIONS ON ACOUSTIC ECHO CANCELLING BASED ON REAL TIME EXPERIMENTS,
'SIGNAL PROCESSING V: THEORIES AND APPLICATIONS', proceedings of EUSIPCO-90, fith European Signal Processing Conference, September 18-21, 1990, (editors: Torres, L; Enrique Masgrau and Miguel A. Lagunas), Elsevier, 1990, P. 1987-1990.

[6] Gudvangen, S and S.J.Flockton.
MODELLING OF ACOUSTIC TRANSFER FUNCTIONS FOR ECHO CANCELLERS,
IEE Proceedings of Vis. Image Signal Process., Vol. 142, No. 1, February 1995, P. 47-51.

[7] Gudvangen, S and S.J.Flockton.
COMPARISON OF POLE-ZERO AND ALL-ZERO MODELLING OF ACOUSTIC TRANSFER FUNCTIONS,
Electronics letters, Vol. 28, No.21, 8th October 1992.

[8] Mboup, M. and Madeleine Bonnet.
ON THE ADEQUATENESS OF IIR ADAPTIVE FILTERING FOR ACOUSTIC ECHO CANCELLATION
'SIGNAL PROCESSING VI: THEORIES AND APPLICATIONS', 1992, (editors: J. Vanderwalle; R. Boite; M. Moonen and A. Oosterinck), Elsevier Science Publishers, 1992, P. 111-114.

[9] Oliveira e Silva T.
KAUTZ FILTERS
(English translation of a work submitted to Prémio Científfico IBM 94, original in Portuguese), September 27, 1994 - Revised November 7, 1994.

[10] Muller Helmut A. and Lothar Cremer
PRINCIPLES AND APPLICATIONS OF ROOM ACOUSTICS
transl. by Theodore J. Schultz. - London : Applied Science Publications, 1982. - 2 dl. Transl. from: Die wissenschaftlichen Grundlagen der Raumakustik, 1978. - ISBN 0-85334-113-3, 0-85334-114-1

[11] Philip M. Morse and K. Uno Ingard.
THEORETICAL ACOUSTICS
Princeton : Princeton University Press, 1986. - XIX, 927 p. First print.: 1968. - ISBN 0-691-08425-4, 0-691-02401-4 (International series in pure and applied physics).

[12] Ford, R.D.
INTRODUCTION TO ACOUSTICS
Amsterdam : Elsevier, 1970. - IX, 154 p. - ISBN 0-444-20078-9

[13] Ziomek, Lawrence J.
ACOUSTIC FIELD THEORY AND SPACE-TIME SIGNAL PROCESSING
Boca Raton, Florida: CRC Press, Inc, 1995, 692 p. ISBN 0-8493-9455-4

[14] Nouri, Mohammad Mehdinejad; Nobuhiro Miki and Nobuo Nagai
ARMA MODEL ORDER ESTIMATION BASED ON THE SVD OF THE DATA MATRIX
Journal of the Acoustical Society, Japan [E], Vol. 15, Iss. 6, p. 383-92, 1994

[15] Den Brinker, A.C. and M.J. Bastiaans.
DICTAAT VAN HET COLLEGE: MODERNE SIGNAALTRANSFORMATIES
Eindhoven University of Technology department of Electrical Engineering, March 1995, internal publication.

[16] Backx, A.C.P.M. and A.J.W. van den Boom
DICTAAT VAN HET COLLEGE: TOEGEPASTE SYSTEEM ANALYSE DEEL II
Eindhoven University of Technology department of Electrical Engineering, Juni 1994, internal publication.

[17] Therrien, Charles W, and Carlos H. Velasco
AN ITERATIVE PRONY METHOD FOR ARMA SIGNAL MODELING
IEEE Transactions on Signal Processing, Vol. 43, No.1, January 1995

[18] K. Steiglitz and L.E.Mcbride
A TECHNIQUE FOR THE IDENTIFICATION OF LINEAR SYSTEMS
IEEE Transactions on Automatic Control, Vol. AC-10, p. 461-464, October 1996.

[19] A.W.M van den Enden and N.A.M. Verhoeckx
DIGITALE SIGNAALBEWERKING
Overberg (the Netherlands), Delta Press B.V. 1987, 379 p., First print, ISBN 90 6674 722 6

[20] Den Brinker, A.C.
MODEL REDUCTION BY KAUTZ FILTERS
Proc. VVI Europ.S.P.Conf. (EUSIPCO), Trieste Italy, Sept. 10-13 1996, Vol II, p. 515-518.

[21] Friedman, David H.
ON APPROXIMATING AN FIR FILTER USING DISCRETE ORTHONORMAL EXPONENTIALS
IEEE Transactions on Acoustics, Speech and Signal processing, vol. ASSP-29, No. 4, August, 1981

[22] Belt, H.J.W. and H.J.Butterweck
CASCADED ALL-PASS SECTIONS FOR LMS ADAPTIVE FILTERING
Proc. VIII Euro.S.P.Conf. (EUSIPCO), Trieste, Italy, Sept. 10-13, 1996, Vol. III, p. 1219-1222.

[23] Zimmermann, Zergio and Geoffrey A. Williamson
PERFORMANCE PROPERTIES OF FIXED POLE ADAPTIVE FILTERS
Proceedings 1993 IEEE International Symposium on Circuits and Systems p. 56-9, Vol. 1, 1993

[24] Williamson, Geoffrey A. and Sergio Zimmermann
GLOBALLY CONVERGENT ADAPTIVE IIR FILTERS BASED ON FIXED POLE LOCATIONS
IEEE Transactions on Signal Processing, Vol. 44, No 6, June 1996

[25] M.J. Bastiaans
GABOR'S EXPANSION OF A SIGNAL INTO GAUSSIAN ELEMENTARY SIGNALS
Proc. IEEE 68, 538-539 (1980)

[26] M.J. Bastiaans
GABOR'S SIGNAL EXPANSION AND DEGREES OF FREEDOM OF A SIGNAL
Opt. Acta 29 1223-1229 (1982)

[27] D. Gabor
THEORY OF COMMUNICATION
J. Inst. Elec. Eng. 93 (III), 429-457 (1946)

Appendix I

Data acquisition

In this report use is made of measurements in a room. These measurements are room impulse responses, the inverse Fourier transform of the RTF in different situations. The impulse responses are obtained by exciting the room with a Pseudo Binary Random Noise Sequence (PBRNS).

The room is excited with a signal $u[n]$. The registered output signal is $y[n]$. The room impulse response is given by $h[n]$. The cross correlation function $\Phi_{uy}[t]$ of the two discrete variables $u[n]$ and $y[n]$ is defined by:

$$\Phi_{uy}[t] = \lim_{N\to\infty} \frac{1}{N} \sum_{n=-N}^{N} \left(u[n]+\mu_u\right)\left(y[t+n]+\mu_y\right)$$

with μ_u the mean of $u[n]$ and μ_y the mean of $y[n]$.

The output signal $y[n]$ can is given by the following convolution:

$$y[n] = \sum_{p=0}^{\infty} h[p]u[n-p]$$

Substituting this expression in the expression for the cross correlation function $\Phi_{uy}[t]$ and assuming that μ_u and μ_y are both zero yields:

$$\Phi_{uy}[t] = \lim_{N\to\infty} \frac{1}{N} \sum_{n=-N}^{N} u[n] \sum_{p=0}^{\infty} h[p]u[n+t-p]$$

$$\Leftrightarrow \lim_{N\to\infty} \frac{1}{N} \sum_{p=0}^{\infty} h[p] \sum_{n=-N}^{N} u[n]u[t-p+n]$$

$$\Leftrightarrow \sum_{p=0}^{\infty} h[p]\Phi_{uu}[t-p]$$

Now remember that u[n] was a PBRNS signal. This signal is filtered in such a way that the power density spectrum is flat and the signal resembles a zero mean white noise signal. In that case the autocorrelationfunction $\Phi_{uu}[n] = \delta[n]$. Hence, the above expression reduces to:

$$\Phi_{uy}[t] = h[t]$$

Table A-1: *Description of the measured impulse responses*

measurement	description	sample frequency
direct	The impulse response is measured, with the microphone pointing directly to the source.	10 [kHz]
diffuse	The impulse response is measured, with the microphone pointing to the walls (away from the microphone).	10 [kHz]
imp01a	A test subject sitting behind a terminal	8 [kHz]
imp01b	The test subject stood up, walked around and sat down again behind his terminal, after this, the measurement was repeated.	8 [kHz]
imp02a	The test subject has moved 50 [cm] to another position.	8 [kHz]
imp02b	imp02 is repeated to test the reproducibility of this measurement.	8 [kHz]
imp03	The test subject has moved for around 3 [m], still sitting down.	8 [kHz]
imp04	The test subject has moved again for around 50 [cm], relative to imp03.	8 [kHz]
imp05	The test subject is standing straight, on the position of imp04	8 [kHz]
imp06	The test subject moved for around 2 [m], standing straight.	8 [kHz]

Testing the reproducibility of the impulse response measurements

For testing the reproducibility of the impulse responses the impulse responses imp02 and imp02b can be used. However before these impulse responses can be used, there has to be checked if they start at the same moment. This is the case, as can be seen in Figure A0-1.

Also, we are able to define a quantity which expressed how much imp02a differs from imp02b. This is done by calculating the energy in the difference between imp02a and imp02b and relating this to the energy in imp02a or imp02b.

$$J = \frac{\sum_{n=0}^{N-1}\left(imp02a[n] - imp02b[n]\right)^2}{\sum_{n=0}^{N-1}\left(imp02a[n]\right)^2} * 100\%$$

Applying this leads to $J=0.4773$ %. This percentage can also be related to measuring and background noise. Too less data is available to make a good noise estimation, however an impression can be obtained from the above expression:

$$10\log\left(\frac{1}{0.004773}\right) = 23.21 \text{ [dB]}$$

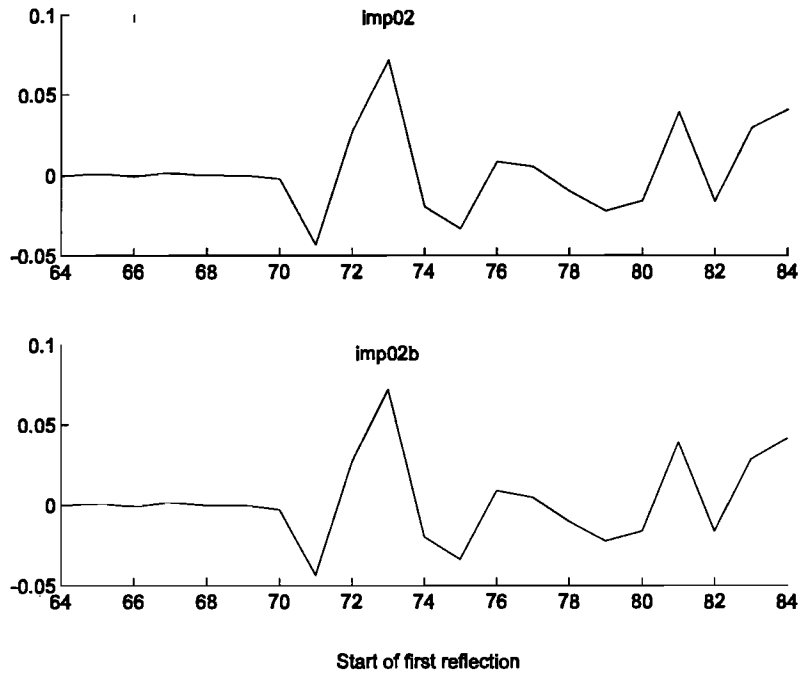

Figure A0-1: *Testing the starting point of both impulse responses*

Determining the reverberation time

The reverberation time is defined as the time at which the energy in the signal is down to 60 [dB] beneath the total energy present in the signal. This is a very strict norm, something which can also be concluded from Figure A0-2. There is simply not enough data available to express the reverberation time in a figure. The last samples would simply disappear in the noise. Also care has to be taken of the first 80 samples, which consist out of dead time, i.e. the time it takes for the first reverberation to reach the microphone.

However, to get an impression of the reverberation time, it is possible to extrapolate the available data. This can best be done by estimating the slope on the reliable part op the data (the mid section). In doing so, we find at -60 [dB] the time of τ_{60} =0.51 [s],. In this reverberation time is also included the dead time. This dead time is estimated around 80 samples at 8 [kHz], corresponding to 0.01 [s]. So the total reverberation time $\tau_r \approx 0.5$ [s].

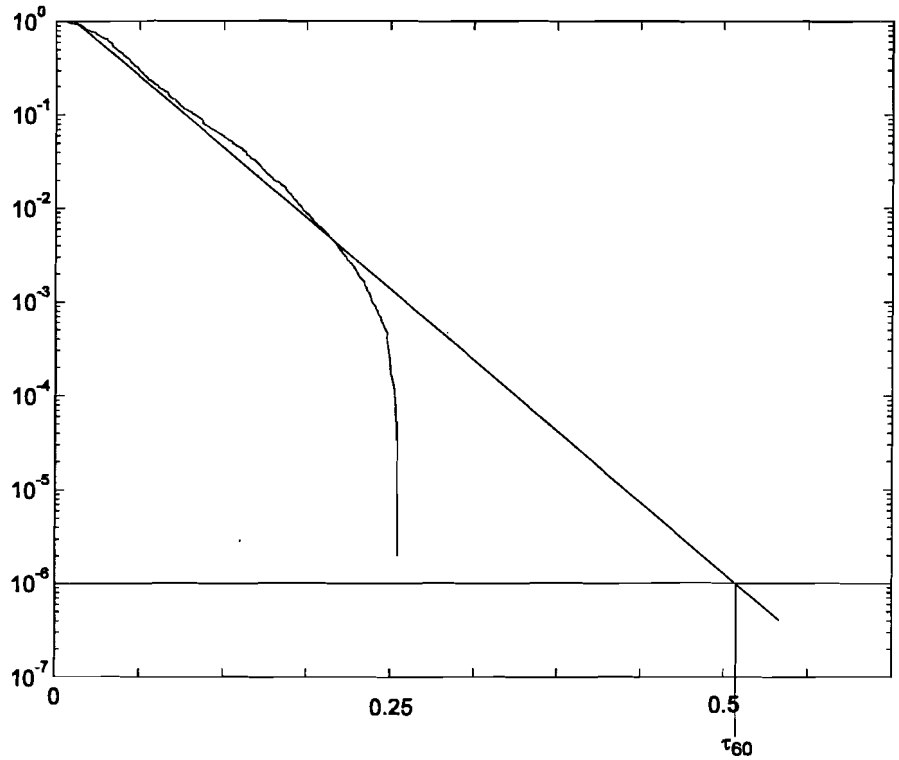

Figure A0-2 *The log of the energy present after t seconds relative to the total energy.*

Appendix II

A

Result of applying the Prony method, the iterative Prony method and the Steiglitz-McBride method to the synthetic model of paragraph 3.2. The model generates 512 samples. The damping is chosen such that the model decays enough in these 512 samples. This way, it is almost not possible for the methods to generate non stable poles.

		Relative Modeled Energy [%]		
Noise level	Approximation order	Prony Method	Iterative Prony Method	Steiglitz-McBride
2	20	84.31	84.66	84.34
	22	92.32	92.32	92.93
	24	81.88	83.57	81.87
	26	99.55	99.56	99.56
	28	99.60	89.94	99.59
4	20	79.08	79.78	79.07
	22	50.93	50.93	50.93
	24	61.31	63.23	61.00
	26	91.01	91.24	90.97
	28	83.93	84.21	83.93
6	20	64.17	66.07	64.76
	22	76.44	76.86	76.48
	24	76.22	77.70	76.73
	26	97.80	97.78	97.76
	28	97.30	98.01	98.02
8	20	52.63	52.79	52.19
	22	58.63	60.64	58.84
	24	70.53	72.41	70.70
	26	72.72	70.67	72.57
	28	78.84	78.90	78.73
10	20	64.02	65.17	64.05
	22	72.51	73.21	73.15
	24	83.52	84.10	63.68
	26	73.23	74.25	73.20
	28	69.51	69.61	69.43
12	20	58.41	58.33	58.25
	22	64.00	67.00	64.53
	24	74.60	75.21	74.51
	26	73.94	74.10	73.86
	28	89.90	89.93	89.37
14	20	60.33	60.35	59.59
	22	69.42	69.23	69.08
	24	63.39	58.54	63.10

	26	76.10	77.07	76.10
	28	75.02	75.64	73.86
16	20	60.72	61.88	60.22
	22	42.09	40.77	42.09
	24	76.51	76.66	76.40
	26	80.03	79.64	79.60
	28	68.39	69.55	67.46
18	20	44.30	46.07	44.55
	22	50.83	50.75	49.06
	24	59.94	54.06	54.75
	26	58.86	60.34	85.50
	28	79.78	79.06	79.51
20	20	70.04	71.07	68.66
	22	70.04	71.67	68.66
	24	70.25	68.95	69.28
	26	61.88	62.18	60.95
	28	62.14	63.22	61.95

B

Calculation 5 times repeated for each method, synthetic model based on 20 poles

	Relative Modeled Energy [%]		
Noise level	Prony Method	Iterative Prony Method	Steiglitz-McBride
2	54.31	54.74	54.27
	78.31	78.31	78.29
84.05		84.48	83.99
	71.05	72.88	70.98
	69.64	70.72	70.06
	66.67	68.10	66.63
4	81.27	81.21	81.30
	88.81	89.09	89.15
	55.08	58.10	55.09
	83.61	84.89	83.61
	90.61	90.49	90.51
6	50.90	52.77	45.28
	64.72	59.89	64.64
	67.46	69.06	67.04
	63.83	65.27	63.85
	60.02	61.14	60.00
8	54.67	56.53	54.28
	39.42	42.22	40.87
	71.41	64.43	71.21
	64.40	66.22	64.49
	69.49	70.38	69.31
10	58.99	59.99	59.25
	41.60	43.96	41.38

	51.84	53.88	51.41
	60.64	52.51	60.52
	47.57	47.19	46.15
12	60.79	62.59	60.27
	53.62	53.75	53.42
	34.91	47.19	44.96
	70.04	67.43	69.35
	71.46	71.98	71.01
14	70.67	70.99	70.52
	49.02	49.16	48.91
	71.46	71.98	71.01
	49.02	49.16	48.90
	71.46	71.98	71.01
16	56.89	57.58	56.04
	51.84	51.29	51.09
	33.92	36.01	32.86
	57.09	59.45	55.85
	69.84	70.32	69.49
18	58.61	60.66	58.68
	53.38	53.08	55.11
	56.83	58.41	56.68
	54.42	55.36	50.28
	64.31	64.51	63.13
20	59.78	60.19	58.56
	60.29	61.11	58.58
	47.04	47.44	47.24
	33.74	33.22	30.63
	52.37	47.97	50.10

Appendix III

This algorithm is based on the separation of the real and imaginary part of a root vector $\underline{\mathbf{r}}$. A root r_i is given by:

$$r_i = \Re\{r_i\} + j\,\Re\{r_i\}$$

From this expression a root vector $\underline{\mathbf{r}}$ can be built. In this root vector, the real and imaginary part are separated, so the derivative can be taken of an expression with respect to the real part respectively the imaginary part.

For the gradient expression can be derived:

$$\underline{\mathbf{f}}_i \triangleq \begin{pmatrix} 0 & 1 & 2r_i & 3r_i^2 & \cdots & (N-1)r_i^{N-2} \end{pmatrix}^T c_i$$

$$\mathbf{F} = \begin{pmatrix} \underline{\mathbf{f}}_1 & \underline{\mathbf{f}}_2 & \cdots & \underline{\mathbf{f}}_3 \end{pmatrix}$$

$$\frac{\partial\, \underline{\mathbf{e}}}{\partial\, \Re\{r_i\}} = \frac{\partial\, \mathbf{R}}{\partial\, \Re\{r_i\}}\underline{\mathbf{c}} = \underline{\mathbf{f}}_i$$

$$\frac{\partial\, \underline{\mathbf{e}}}{\partial\, \Im\{r_i\}} = \frac{\partial\, \mathbf{R}}{\partial\, \Im\{r_i\}}\underline{\mathbf{c}} = j\underline{\mathbf{f}}_i$$

$$\frac{\partial\, Q}{\partial\, \Re\{r_i\}} = \underline{\mathbf{e}}^h \frac{\partial\, \mathbf{R}}{\partial\, \Re\{r_i\}}\underline{\mathbf{c}} + \underline{\mathbf{c}}^h \frac{\partial\, \mathbf{R}}{\partial\, \Re\{r_i\}}\underline{\mathbf{e}} = 2\Re\left\{\underline{\mathbf{f}}_i^h \underline{\mathbf{e}}\right\}$$

$$\frac{\partial\, Q}{\partial\, \Im\{r_i\}} = j\underline{\mathbf{e}}^h \underline{\mathbf{f}}_i - j\underline{\mathbf{f}}_i^h \underline{\mathbf{e}} = 2\Im\left\{\underline{\mathbf{f}}_i^h \underline{\mathbf{e}}\right\}$$

$$\Rightarrow \underline{\mathbf{g}} = 2\begin{pmatrix} \Re\{\mathbf{F}^h \underline{\mathbf{e}}\} \\ \Im\{\mathbf{F}^h \underline{\mathbf{e}}\} \end{pmatrix}$$

For the Hessian can be derived:

$$\underline{\mathbf{s}}_i \triangleq \begin{pmatrix} 0 & 0 & 2 & 6r_i & 12r_i^2 & \cdots & (N-1)(N-2)r_i^{N-2} \end{pmatrix}^t c_i$$

$$\mathbf{S} = \begin{pmatrix} \underline{\mathbf{s}}_1 & \underline{\mathbf{s}}_2 & \cdots & \underline{\mathbf{s}}_N \end{pmatrix}$$

$$\mathbf{H}=\begin{pmatrix}\dfrac{\partial}{\partial\Re\{r_k\}}\begin{pmatrix}\dfrac{\partial Q}{\partial\Re\{r_i\}} & \dfrac{\partial Q}{\partial\Im\{r_i\}}\end{pmatrix}\\ \dfrac{\partial}{\partial\Im\{r_k\}}\begin{pmatrix}\dfrac{\partial Q}{\partial\Re\{r_i\}} & \dfrac{\partial Q}{\partial\Im\{r_i\}}\end{pmatrix}\end{pmatrix}=\begin{pmatrix}\dfrac{\partial}{\partial\Re\{r_k\}}\left(\underline{\mathbf{e}}^h\underline{\mathbf{f}}_i+\underline{\mathbf{f}}_i^h\underline{\mathbf{e}} & j\left(\underline{\mathbf{e}}^h\underline{\mathbf{f}}_i-\underline{\mathbf{f}}_i^h\underline{\mathbf{e}}\right)\right)\\ \dfrac{\partial}{\partial\Im\{r_k\}}\left(\underline{\mathbf{e}}^h\underline{\mathbf{f}}_i+\underline{\mathbf{f}}_i^h\underline{\mathbf{e}} & j\left(\underline{\mathbf{e}}^h\underline{\mathbf{f}}_i-\underline{\mathbf{f}}_i^h\underline{\mathbf{e}}\right)\right)\end{pmatrix}$$

$$k=1.....P$$

$$i=1.....P$$

$$\frac{\partial\,\underline{\mathbf{f}}_i}{\partial\,\Re\{r_k\}}=\underline{\mathbf{s}}_i\delta_{ik}$$

$$\frac{\partial\,\underline{\mathbf{f}}_i}{\partial\,\Im\{r_k\}}=j\underline{\mathbf{s}}_i\delta_{ik}$$

This expression is obtained by applying the chain rule. δ_{ik} is the Kronecker delta function.

$$H=\begin{pmatrix}\left(\underline{\mathbf{e}}^h\underline{\mathbf{s}}_i\delta_{ik}+\underline{\mathbf{f}}_k^h\underline{\mathbf{f}}_i+\underline{\mathbf{f}}_i^h\underline{\mathbf{f}}_k+\underline{\mathbf{s}}_i^h\underline{\mathbf{e}}\delta_{ik}\right) & j\left(\underline{\mathbf{e}}^h\underline{\mathbf{s}}_i\delta_{ik}+\underline{\mathbf{f}}_k^h\underline{\mathbf{f}}_i-\underline{\mathbf{f}}_i^h\underline{\mathbf{f}}_k-\underline{\mathbf{s}}_i^h\underline{\mathbf{e}}\delta_{ik}\right)\\ j\left(\underline{\mathbf{e}}^h\underline{\mathbf{s}}_i\delta_{ik}-\underline{\mathbf{f}}_k^h\underline{\mathbf{f}}_i+\underline{\mathbf{f}}_i^h\underline{\mathbf{f}}_k-\underline{\mathbf{s}}_i^h\underline{\mathbf{e}}\delta_{ik}\right) & -\left(\underline{\mathbf{e}}^h\underline{\mathbf{s}}_i\delta_{ik}-\underline{\mathbf{f}}_k^h\underline{\mathbf{f}}_i-\underline{\mathbf{f}}_i^h\underline{\mathbf{f}}_k+\underline{\mathbf{s}}_i^h\underline{\mathbf{e}}\delta_{ik}\right)\end{pmatrix}$$

$$\Leftrightarrow H=\begin{pmatrix}2\Re\left\{\underline{\mathbf{f}}_i^h\underline{\mathbf{f}}_k\right\}+2\Re\left\{\underline{\mathbf{s}}_i^h\underline{\mathbf{e}}\delta_{ik}\right\} & 2\Im\left\{\underline{\mathbf{f}}_i^h\underline{\mathbf{f}}_k\right\}-2\Im\left\{\underline{\mathbf{s}}_i^h\underline{\mathbf{e}}\delta_{ik}\right\}\\ -2\Im\left\{\underline{\mathbf{f}}_i^h\underline{\mathbf{f}}_k\right\}+2\Im\left\{\underline{\mathbf{s}}_i^h\underline{\mathbf{e}}\delta_{ik}\right\} & 2\Re\left\{\underline{\mathbf{f}}_i^h\underline{\mathbf{f}}_k\right\}-2\Re\left\{\underline{\mathbf{s}}_i^h\underline{\mathbf{e}}\delta_{ik}\right\}\end{pmatrix}$$

$$\Leftrightarrow H=2\begin{pmatrix}\Re\left\{\mathbf{F}^h\mathbf{F}+\mathrm{diag}\left(\mathbf{S}^h\underline{\mathbf{e}}\right)\right\} & \Im\left\{\mathbf{F}^h\mathbf{F}-\mathrm{diag}\left(\mathbf{S}^h\underline{\mathbf{e}}\right)\right\}\\ -\Im\left\{\mathbf{F}^h\mathbf{F}-\mathrm{diag}\left(\mathbf{S}^h\underline{\mathbf{e}}\right)\right\} & \Re\left\{\mathbf{F}^h\mathbf{F}-\mathrm{diag}\left(\mathbf{S}^h\underline{\mathbf{e}}\right)\right\}\end{pmatrix}$$

$$\underline{\mathbf{x}}=\begin{pmatrix}x_1 & x_2 & \cdots & x_N\end{pmatrix}^T \qquad \mathrm{diag}(\underline{\mathbf{x}})=\begin{pmatrix}x_1 & 0 & \cdots & 0\\ 0 & x_2 & & \vdots\\ \vdots & & \ddots & 0\\ 0 & \cdots & 0 & x_N\end{pmatrix}$$

Appendix IV

$$\underline{\mathbf{R}}_{Y\varphi} = \begin{pmatrix} \int_{\Omega_2}^{\Omega_1} \left| \frac{\sum_{r=0}^{N-1} y[r] e^{-jr\Omega}}{\sum_{p=0}^{P} a_{p,i} e^{-jp\Omega}} \right|^2 e^{-j\Omega} d\Omega \\ \int_{\Omega_2}^{\Omega_1} \left| \frac{\sum_{r=0}^{N-1} y[r] e^{-jr\Omega}}{\sum_{p=0}^{P} a_{p,i} e^{-jp\Omega}} \right|^2 e^{-j2\Omega} d\Omega \\ \vdots \\ \int_{\Omega_2}^{\Omega_1} \left| \frac{\sum_{r=0}^{N-1} y[r] e^{-jr\Omega}}{\sum_{p=0}^{P} a_{p,i} e^{-jp\Omega}} \right|^2 e^{-jP\Omega} d\Omega \\ -\int_{\Omega_2}^{\Omega_1} \frac{\sum_{r=0}^{N-1} y[r] e^{-jr\Omega}}{\left| \sum_{p=0}^{P} a_{p,i} e^{-jp\Omega} \right|^2} d\Omega \\ -\int_{\Omega_2}^{\Omega_1} \frac{\sum_{r=0}^{N-1} y[r] e^{-jr\Omega}}{\left| \sum_{p=0}^{P} a_{p,i} e^{-jp\Omega} \right|^2} e^{-j\Omega} d\Omega \\ \vdots \\ -\int_{\Omega_2}^{\Omega_1} \frac{\sum_{r=0}^{N-1} y[r] e^{-jr\Omega}}{\left| \sum_{p=0}^{P} a_{p,i} e^{-jp\Omega} \right|^2} e^{-jQ\Omega} d\Omega \end{pmatrix}$$

$$\mathbf{R}_{\varphi\varphi} = \begin{pmatrix} \begin{pmatrix} \mathbf{R}_{\varphi\varphi}^{(1)} \end{pmatrix} & \begin{pmatrix} \mathbf{R}_{\varphi\varphi}^{(2)} \end{pmatrix} \\ \begin{pmatrix} \mathbf{R}_{\varphi\varphi}^{(3)} \end{pmatrix} & \begin{pmatrix} \mathbf{R}_{\varphi\varphi}^{(4)} \end{pmatrix} \end{pmatrix} .$$

$$\mathbf{R}_{\varphi\varphi}^{(1)} = \begin{pmatrix} \int_{\Omega_0}^{\Omega_1} \left| \frac{\sum_{r=0}^{N-1} y[r]e^{-jr\Omega}}{\sum_{p=0}^{P} a_{p,i}e^{-jp\Omega}} \right|^2 d\Omega & \int_{\Omega_0}^{\Omega_1} \left| \frac{\sum_{r=0}^{N-1} y[r]e^{-jr\Omega}}{\sum_{p=0}^{P} a_{p,i}e^{-jp\Omega}} \right|^2 e^{j\Omega} d\Omega & \cdots & \int_{\Omega_0}^{\Omega_1} \left| \frac{\sum_{r=0}^{N-1} y[r]e^{-jr\Omega}}{\sum_{p=0}^{P} a_{p,i}e^{-jp\Omega}} \right|^2 e^{j(P-1)\Omega} d\Omega \\ \int_{\Omega_0}^{\Omega_1} \left| \frac{\sum_{r=0}^{N-1} y[r]e^{-jr\Omega}}{\sum_{p=0}^{P} a_{p,i}e^{-jp\Omega}} \right|^2 e^{-j\Omega} d\Omega & \int_{\Omega_0}^{\Omega_1} \left| \frac{\sum_{r=0}^{N-1} y[r]e^{-jr\Omega}}{\sum_{p=0}^{P} a_{p,i}e^{-jp\Omega}} \right|^2 d\Omega & & \vdots \\ \vdots & & \ddots & \vdots \\ \int_{\Omega_0}^{\Omega_1} \left| \frac{\sum_{r=0}^{N-1} y[r]e^{-jr\Omega}}{\sum_{p=0}^{P} a_{p,i}e^{-jp\Omega}} \right|^2 e^{-j(P-1)\Omega} d\Omega & \int_{\Omega_0}^{\Omega_1} \left| \frac{\sum_{r=0}^{N-1} y[r]e^{-jr\Omega}}{\sum_{p=0}^{P} a_{p,i}e^{-jp\Omega}} \right|^2 e^{-j(P-2)\Omega} d\Omega & \cdots & \int_{\Omega_0}^{\Omega_1} \left| \frac{\sum_{r=0}^{N-1} y[r]e^{-jr\Omega}}{\sum_{p=0}^{P} a_{p,i}e^{-jp\Omega}} \right|^2 d\Omega \end{pmatrix}$$

$$\mathbf{R}_{\varphi\varphi}^{(2)} = \begin{pmatrix} -\int_{\Omega_0}^{\Omega_1} \frac{\sum_{r=0}^{N-1} y[r]e^{-jr\Omega}}{\left| \sum_{p=0}^{P} a_{p,i}e^{-jp\Omega} \right|^2} e^{-j\Omega} d\Omega & -\int_{\Omega_0}^{\Omega_1} \frac{\sum_{r=0}^{N-1} y[r]e^{-jr\Omega}}{\left| \sum_{p=0}^{P} a_{p,i}e^{-jp\Omega} \right|^2} d\Omega & \cdots & -\int_{\Omega_0}^{\Omega_1} \frac{\sum_{r=0}^{N-1} y[r]e^{-jr\Omega}}{\left| \sum_{p=0}^{P} a_{p,i}e^{-jp\Omega} \right|^2} e^{j(Q-1)\Omega} d\Omega \\ -\int_{\Omega_0}^{\Omega_1} \frac{\sum_{r=0}^{N-1} y[r]e^{-jr\Omega}}{\left| \sum_{p=0}^{P} a_{p,i}e^{-jp\Omega} \right|^2} e^{-j2\Omega} d\Omega & -\int_{\Omega_0}^{\Omega_1} \frac{\sum_{r=0}^{N-1} y[r]e^{-jr\Omega}}{\left| \sum_{p=0}^{P} a_{p,i}e^{-jp\Omega} \right|^2} e^{-j\Omega} d\Omega & & \vdots \\ \vdots & \vdots & & \vdots \\ -\int_{\Omega_0}^{\Omega_1} \frac{\sum_{r=0}^{N-1} y[r]e^{-jr\Omega}}{\left| \sum_{p=0}^{P} a_{p,i}e^{-jp\Omega} \right|^2} e^{-jP\Omega} d\Omega & -\int_{\Omega_0}^{\Omega_1} \frac{\sum_{r=0}^{N-1} y[r]e^{-jr\Omega}}{\left| \sum_{p=0}^{P} a_{p,i}e^{-jp\Omega} \right|^2} e^{-j(P-1)\Omega} d\Omega & \cdots & -\int_{\Omega_0}^{\Omega_1} \frac{\sum_{r=0}^{N-1} y[r]e^{-j(P-Q-1)\Omega}}{\left| \sum_{p=0}^{P} a_{p,i}e^{-jp\Omega} \right|^2} d\Omega \end{pmatrix}$$

$$\mathbf{R}_{\varphi\varphi}^{(3)} = \begin{pmatrix} -\int_{\Omega_0}^{\Omega_1} \frac{\sum_{r=0}^{N-1} y[r]e^{-jr\Omega}}{\left|\sum_{p=0}^{P} a_{p,i}e^{-jp\Omega}\right|^2} e^{j\Omega} d\Omega & -\int_{\Omega_0}^{\Omega_1} \frac{\sum_{r=0}^{N-1} y[r]e^{-jr\Omega}}{\left|\sum_{p=0}^{P} a_{p,i}e^{-jp\Omega}\right|^2} e^{j2\Omega} d\Omega & \cdots & -\int_{\Omega_0}^{\Omega_1} \frac{\sum_{r=0}^{N-1} y[r]e^{-jr}}{\left|\sum_{p=0}^{P} a_{p,i}e^{-jp\Omega}\right|^2} e^{jP\Omega} d\Omega \\ -\int_{\Omega_0}^{\Omega_1} \frac{\sum_{r=0}^{N-1} y[r]e^{-jr\Omega}}{\left|\sum_{p=0}^{P} a_{p,i}e^{-jp\Omega}\right|^2} d\Omega & -\int_{\Omega_0}^{\Omega_1} \frac{\sum_{r=0}^{N-1} y[r]e^{-jr\Omega}}{\left|\sum_{p=0}^{P} a_{p,i}e^{-jp\Omega}\right|^2} e^{j\Omega} d\Omega & & \vdots \\ \vdots & \vdots & & \vdots \\ -\int_{\Omega_0}^{\Omega_1} \frac{\sum_{r=0}^{N-1} y[r]e^{-jr\Omega}}{\left|\sum_{p=0}^{P} a_{p,i}e^{-jp\Omega}\right|^2} e^{-j(Q-1)\Omega} d\Omega & -\int_{\Omega_0}^{\Omega_1} \frac{\sum_{r=0}^{N-1} y[r]e^{-jr\Omega}}{\left|\sum_{p=0}^{P} a_{p,i}e^{-jp\Omega}\right|^2} e^{-j(Q-2)\Omega} d\Omega & \cdots & -\int_{\Omega_0}^{\Omega_1} \frac{\sum_{r=0}^{N-1} y[r]e^{-j\Omega}}{\left|\sum_{p=0}^{P} a_{p,i}e^{-jp\Omega}\right|^2} e^{-j(Q-P)\Omega} d\Omega \end{pmatrix}$$

$$\mathbf{R}_{\varphi\varphi}^{(e)} = \begin{pmatrix} \int_{\Omega_0}^{\Omega_1} \frac{1}{\left|\sum_{p=0}^{P} a_{p,i}e^{-jp\Omega}\right|^2} d\Omega & \int_{\Omega_0}^{\Omega_1} \frac{1}{\left|\sum_{p=0}^{P} a_{p,i}e^{-jp\Omega}\right|^2} e^{j\Omega} d\Omega & \cdots & \int_{\Omega_0}^{\Omega_1} \frac{1}{\left|\sum_{p=0}^{P} a_{p,i}e^{-jp\Omega}\right|^2} e^{jQ\Omega} d\Omega \\ \int_{\Omega_0}^{\Omega_1} \frac{1}{\left|\sum_{p=0}^{P} a_{p,i}e^{-jp\Omega}\right|^2} e^{-j\Omega} d\Omega & \int_{\Omega_0}^{\Omega_1} \frac{1}{\left|\sum_{p=0}^{P} a_{p,i}e^{-jp\Omega}\right|^2} d\Omega & & \vdots \\ \vdots & \vdots & \ddots & \vdots \\ \int_{\Omega_0}^{\Omega_1} \frac{1}{\left|\sum_{p=0}^{P} a_{p,i}e^{-jp\Omega}\right|^2} e^{-jQ\Omega} d\Omega & \int_{\Omega_0}^{\Omega_1} \frac{1}{\left|\sum_{p=0}^{P} a_{p,i}e^{-jp\Omega}\right|^2} e^{-j(Q-1)\Omega} d\Omega & \cdots & \int_{\Omega_0}^{\Omega_1} \frac{1}{\left|\sum_{p=0}^{P} a_{p,i}e^{-jp\Omega}\right|^2} d\Omega \end{pmatrix}$$